Università degli Studi di Cagliari

PHD DEGREE

in Industrial Engineering

Cycle XXXIII

TITLE OF THE PHD THESIS

On the Robust Control and Optimization Strategies for Islanded Inverter-Based Microgrids

Scientific Disciplinary Sector

ING-INF/04 – Automatica

PhD Student: Milad Gholami

Supervisor Prof. Alessandro Pisano

Final exam: Academic Year 2019 – 2020

Thesis defence: April 2021 Session

UNIVERSITÀ DEGLI STUDI DI CAGLIARI

Abstract

Faculty of Engineering and Architecture
Department of Electrical and Electronic Engineering (DIEE)

Doctor of Philosophy

On the Robust Control and Optimization Strategies for Islanded Inverter-Based Microgrids

by Milad GHOLAMI

In recent years, the concept of Microgrids (MGs) has become more popular due to a significant integration of renewable energy sources (RESs) into electric power systems. Microgrids are small-scale power grids consisting of localized grouping of heterogeneous Distributed Generators (DGs), storage systems, and loads. MGs may operate either in autonomous islanded mode or connected to the main power system. Despite the significant benefits of increasing RESs, many new challenges raise in controlling MGs. Hence, a three layered hierarchical architecture consisting of three control loops closed on the DGs dynamics has been introduced for MGs. The inner loop is called Primary Control (PC), and it provides the references for the DG's DC-AC power converters. In general, the PC is implemented in a decentralized way with the aim to establish, by means of a droop control term, the desired sharing of power among DGs while preserving the MG stability. Then, because of inverter-based DGs have no inertia, a Secondary Control (SC) layer is needed to compensate the frequency and voltage deviations introduced by the PC's droop control terms. Finally, an operation control is designed to optimize the operation of the MGs by providing power setpoints to the lower control layers.

This thesis is mainly devoted to the design of robust distributed secondary frequency and voltage restoration control strategies for AC MGs to avoid central controllers and complexity of communication networks. Different distributed strategies are proposed in this work: (i) Robust Adaptive Distributed SC with Communication delays (ii) Robust Optimal Distributed Voltage SC with Communication Delays and (iii) Distributed Finite-Time SC by Coupled Sliding-Mode Technique. In all three proposed approaches, the problem is addressed in a multi-agent fashion where the generator plays the role of cooperative agents communicating over a network and physically coupled through the power system. The first approach provides an exponentially converging voltage and frequency restoration rate in the presence of both, model uncertainties, and multiple time-varying delays in the DGs's communications. This approach consist of two terms: 1) a decentralized Integral Sliding Mode Control (ISMC) aimed to enforce each agent (DG) to behaves as reference unperturbed dynamic; 2) an ad-hoc designed distributed protocol aimed to globally, exponentially, achieves the frequency and voltage restoration while fulfilling the power-sharing constraints in spite of the communication delays. The second approach extends the first one by including an optimization algorithm to find the optimal control gains and estimate the corresponding maximum delay tolerated by the controlled system. In the third approach, the problem of voltage and frequency restoration as well as active power sharing are solved in finite-time by exploiting delay-free communications among DGs and considering model uncertainties. In

this approach, for DGs with no direct access to their reference values, a finite-time distributed sliding mode estimator is implemented for both secondary frequency and voltage schemes. The estimator determines local estimates of the global reference values of the voltage and frequency for DGs in a finite time and provides this information for the distributed SC schemes.

This dissertation also proposes a novel certainty Model Predictive Control (MPC) approach for the operation of islanded MG with very high share of renewable energy sources. To this aim, the conversion losses of storage units are formulated by quadratic functions to reduce the error in storage units state of charge prediction.

Acknowledgements

First of all, I would like to express my deep and sincere gratitude to my primary supervisor Prof. **Alessandro Pisano** for the continuous support of Ph.D program and research, for his patience, motivation, enthusiasm, and immense knowledge. His guidance helped me in all the time of research and writing of this thesis. Thanks a lot, Prof. Pisano.

Secondly, I wish to show my deep appreciation to my secondary supervisor Prof. **Elio Usai** for providing the necessary information regarding my scientific research. Thanks a lot, Prof. Usai.

I am highly indebted to Dr. **Alessandro Pilloni**, who is an excellent co-supervisor and friend. You provided me everything needed to start a Ph.D at Automatic Control Group, Cagliari University. You are aware that, without your help, probably, I would not have started and completed research on this topic. Thanks, Alessandro.

My sincere thank also goes to Prof. **Jörg Raisch**, for allowing me to pursue my Ph.D program at the Microgrids Group, TU Berlin as a Ph.D exchange. I highly appreciate you for supporting me throughout my Ph.D program at TU Berlin. Thanks a lot, Prof. Raisch.

In addition, a big thanks to Dr. **Christian A. Hans** helped me to develop my scientific research on the new topics of control of microgrids during my visiting period at Technical University Berlin.

Besides my advisors, I would like to thank my thesis evaluators: Prof. **Thierry Floquet** and Prof. **Gian Paolo Incremona**, for their encouragement and insightful comments.

Finally, I want to appreciate the support and love of my family: my parents and my wife for supporting me throughout my life.

Contents

List of Figures

List of Tables

List of Abbreviations

DG	**D**istributed **G**eneration
DER	**D**istributed **E**nergy **R**esource
RES	**R**enewable **E**nergy **S**ource
ESS	**E**nergy **S**torage **S**ystem
PV	**P**hotovoltaics
WT	**W**ind **T**urbine
MG	**M**icro**G**rid
PCC	**P**oint of **C**ommon **C**oupling
PC	**P**rimary **C**ontrol
SC	**S**econdary **C**ontrol
TC	**T**ertiary **C**ontrol
DA	**D**istributed **A**veraging
PI	**P**roportional **I**ntegral
DT	**D**istributed **T**racking
SMC	**S**liding **M**ode **C**ontrol
RBF	**R**adial **B**asis **F**unction
NN	**N**eural **N**etwork
MPC	**M**odel **P**redictive **C**ontrol
LMI	**L**inear **M**atrix **I**nequality
ISMC	**I**ntegral **S**liding **M**ode **C**ontrol
OPF	**O**ptimal **P**ower **F**low
SOCP	**S**econd **O**rder **C**one **p**rogram

List of Symbols

$\mathbb{C}$	Set of complex numbers
$\mathbb{R}$	Set of real numbers
$\mathbb{R}_{<0}$	Set of negative real numbers
$\mathbb{R}_{>0}$	Set of positive real numbers
$\mathbb{N}$	Set of natural numbers
$\mathbb{B} = \{0, 1\}$	Set of Boolean numbers
A'	Transpose of a square matrix A
δ_i	Voltage phase angle of the i-th DG
ω_i	Angular frequency of the i-th DG
v_i	Voltage magnitude of the i-th DG
k_{P_i}	Droop coefficient
k_{Q_i}	Droop coefficient
ω_{n_i}	Frequency SC action
v_{n_i}	Voltage SC action
ω_0	Frequency set-point
v_0	Voltage set-point
P_i^m	Measured active power injection at DG i
Q_i^m	Measured reactive power injection at DG i
P_i	Active power injection at DG i
Q_i	Reactive power injection at DG i
$\mathcal{V}$	Set of DGs
$\mathcal{E}^e$	Set of power lines
Y_{ij}	Line admittance between agent "i" and "j"
G_{ij}	Line conductance between agent "i" and "j"
B_{ij}	Line susceptance between agent "i" and "j"
$\mathcal{N}_i^c$	Set of neighboring DGs connected to DG i
$\mathcal{L}^c$	Laplacian matrix of $\mathcal{G}_N^c$
$\mathcal{L}_{N+1}^c$	Laplacian matrix of $\mathcal{G}_{N+1}^c$
$\hat{s}_i(t)$	Desired sliding manifold of frequency SC
$\hat{k}_{ij}(t)$	Adaptive gains of frequency SC
$\hat{m}_i$	Local discontinuous control gain
$\tau_{ij}(t)$	Time-varying communication delay
$\mathcal{T}(t)$	Set of delays affecting the communication of between each DG and the leader (node 0)
$\mathcal{S}(t)$	Set of delays affecting the communication between each of the N DGs to another DG
$\tau_l^\star, \sigma_g^\star$	A-priori known bounds of the communication delays
d_l, d_g	A-priori known bounds of the time derivative of communication delays
$\hat{e}_i$	Frequency error of the i-th DG
$\tilde{s}_i(t)$	Desired sliding manifold of voltage SC
$\tilde{k}_{ij}(t)$	Adaptive gains of voltage SC
$\tilde{m}_i$	Local discontinuous voltage control gain
$\tilde{e}_i$	Voltage error of the i-th DG
$\tilde{k}_{ij}$	Constant gains of voltage SC

$\hat{u}_i$	Frequency SC
$\tilde{u}_i$	Voltage SC
$\bar{u}_i$	Active power SC
e_i^{ω}	Frequency error of the i-th DG
e_i^{P}	Active power error of the i-th DG
k_i^{ω},η^{ω}	Constant voltage control gains
k_i^{P},η^{P}	Constant active power control gains
$\mathcal{V}_T$	Set of conventional units
$\mathcal{V}_S$	Set of storage units
$\mathcal{V}_R$	Set of renewable energy storage units
$\mathcal{V}_L$	Set of loads
x	State vector
v	Control input vector
w	Uncertain external input
w_d	Load
w_r	Maximum possible renewable infeed under weather conditions
$\bar{q}$	Vector of auxiliary variables
u	Power setpoints of units
u_t	Power setpoints of storage units
u_s	Power setpoints of storage units
u_r	Power setpoints, i.e., maximum power, of renewable units
p	Power of units
p_t	Power of conventional generators
p_s	Power of storage units
p_r	Power of renewable units
P_e	Power of transmission lines
$\tilde{x}$	Forecast of the sate of charge

Dedicated to my wife

Chapter 1

Introduction

1.1 Concept of Microgrids

1.1.1 Why microgrids?

Electric power systems have been playing a key role in technological advances, infrastructure development, and economic growth since their invention [1]. Conventional power systems typically use fossil fuels (for example, coal, natural gas, or oil) nuclear and hydro power plants [2]. Unfortunately, the performance of most of them leads to a significant increase in greenhouse gas emissions. Hence in recent years, researchers have been encouraged on how to reduce greenhouse gas emissions and fossil fuel consumption in the area of power systems. One of the effective ways to reduce greenhouse gas emissions is by replacing conventional generators with Renewable Energy Sources (RES) [3], for example Photo-Voltaic (PV) power plants or Wind Turbines (WT). Most renewable energy sources are relatively small-sized in terms of generation power and therefore often connected to the power system at the medium and low voltage levels, and typically interfaced to the network via AC inverters. To facilitate the integration of a sizeable number of renewable Distributed Generation (DG) units, the concept of Microgrids (MGs) has become increasingly popular [4, 5, 6].

A microgrid is a small-scale power system, generally consisting of conventional generators, RESs, Energy Storage Sources (ESSs) and loads interconnected by transmission lines [7, 8, 9]. MGs can be typically operated in grid-connected or island mode. In grid-connected mode, the MG is electrically coupled with a transmission network via the Point of Common Coupling (PCC). In case of failures, it can be disconnected from the transmission network and operated as an islanded MGs. Small power systems that do not have a connection to a transmission network due to their geographical location, e.g., islands or rural areas, also fall into the class of islanded MGs. In islanded operation, all fluctuations of renewable generation and load must be covered locally by adapting the power of the remaining units. Maintaining this local power equilibrium makes the islanded operation particularly challenging.

1.2 Hierarchical control of MGs

Designing a suitable microgrid control is of special significance for stable and economically efficient performance. The microgrid control system adjusts voltage and frequency for either operating modes, satisfactorily shares the load among DGs, controls the power flow between the microgrids and the main grid, and optimizes the microgrid operating cost. In grid-connected mode, frequency synchronization and voltage support are provided by the main grid, which has synchronous generators and large rotating inertia reserves. When disturbances and faults occur, a microgrid

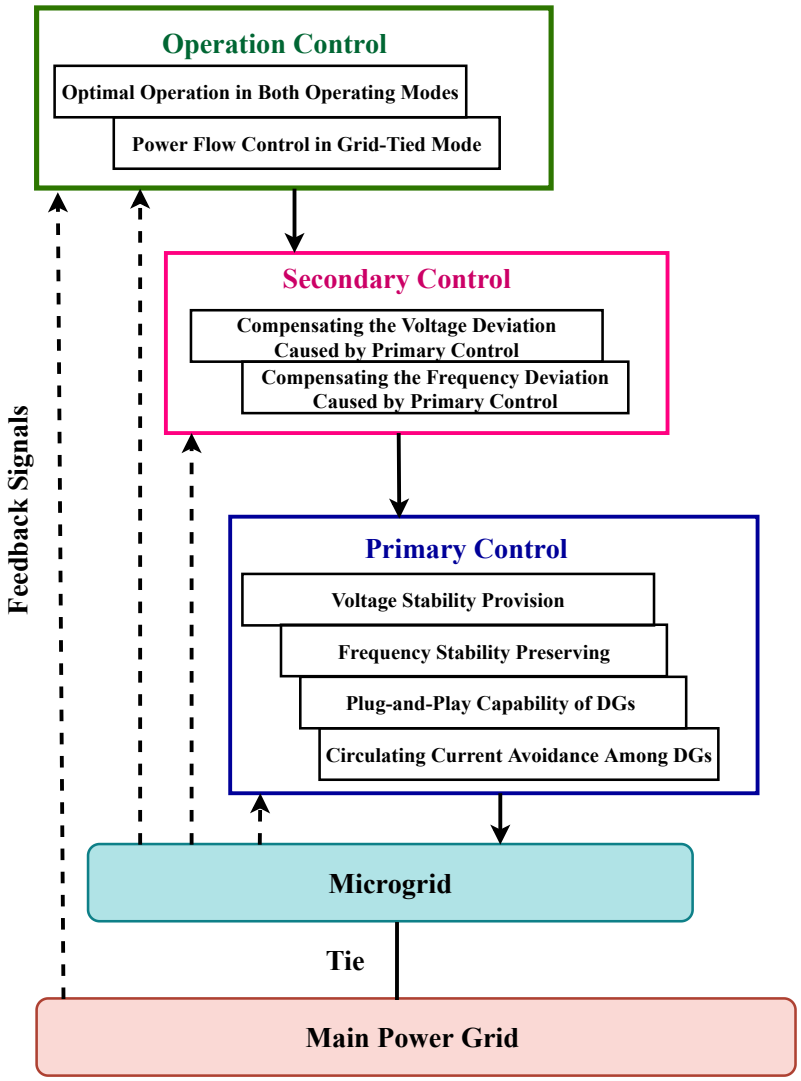

FIGURE 1.1: The hierarchical control system of MGs.

can switch to islanded operation. In this mode, the microgrid can supply power support for critical loads in the event of upstream network power outages. In islanded mode, control systems must synchronize frequency and voltage to the setpoint values and restore pre-fault power conditions. Transients should be set when switching between modes [10, 11, 5].

These operational needs are met in current microgrids through a hierarchical control structure [12, 13, 14]. The hierarchical control system of MGs has been recently standardized into three levels, namely, primary, secondary, and operation controls (see Figure 1.1) that operate in different timescales.

1.3 Primary control (PC) of MGs

1.3.1 Why Primary Control?

As depicted in Figure 1.1, the lowest control layer is referred to as primary control. This control layer typically operates on a fast time-scale (in the range of tens of milliseconds to seconds). The task of PC layer is to enforces the MG's stability while

establishing the power sharing among DGs, as well as perform plug-and-play functionalities [10, 15]. This control layer is often designed in a decentralized way by means of a droop control term [5]. This control is an autonomous control that rely on the physical coupling of the units via the electrical lines and do not require intercommunication links between the DGs. Primary controls, however, may cause the frequency and voltage amplitudes of MGs deviate from the setpoint values [14, 16]. Therefore, Secondary control can be used to compensate these deviations.

1.4 Secondary Control (SC) of MGs

1.4.1 Why Secondary Control?

The SC layer is located above the PC. This layer typically operates on a timescales from seconds to minutes and compensates the unavoidable deviations of the DG's output voltages and frequencies from the expected set-points [10, 17]. Furthermore, it can be used to achieve active power sharing [14]. However, optimizing the performance of MGs using these control layers is very difficult. For operations that are economically and environmentally significant, it is usually necessary to act on changing states of charge of storage units as well as changing load and available infeed from renewable sources. In addition, it is desired to include optional bounds of the units in the MGs. Unfortunately, realizing these aims using primary and secondary control is difficult. Therefore, an operation control layer is often considered on top of them.

1.5 Operation control of MGs

1.5.1 Why operation control?

The high level is usually called operation control or energy management, which in many publications is also referred to as tertiary control (TC). This layer typically operates on a timescale from minutes to fractions of hours. The goal of this control is to optimize the operation of the MGs by providing power setpoints to the lower control layers. The power setpoints of units are normally obtained by solving optimization problems that contain a cost function along with a set of constraints that represent the MG behavior [18]. As the share of RES increases, it becomes difficult to predict the stored energy over an entire day. Since the dispatch of units extremely rely on the stored energy and the forecast of the available renewable power, it is hard to achieve a meaningful operation schedule for MGs with a high share of RES over a prediction horizon of, for example, one day. Hence, [19, 20, 21] combined optimal dispatch and schedule to form a single optimal operation control layer.

Various the operation control approaches are designed based on the Model Predictive Control (MPC). Indeed, MPC is employed in the operation control of MG to predict the system behavior into the future using forecasts of renewable infeed and load as well as the current measurement of the state of charge.

1.6 Literature Review

1.6.1 Secondary Control Strategies

The conventional SC to solve the restoration problem in MGs employs a centralized control approach which gathers all the information of the individual DGs and then

transmits the control command to each DG [22, 23, 24, 25, 26, 27]. However, the current trend is to discourage centralized strategies [28] which bring disadvantages such as latency and delays due to all-to-one communication; the need of costly central computing and communication units; limited scalability and reliability of the power system due to single-point failures.

In the literature also decentralized approaches have been proposed. Worth to mention, for instance [26, 29], where second-order sliding-mode control strategies are proposed, respectively, to regulate voltages while compensating the effects of load variations, nonlinearities, and model uncertainties, and for the robust load frequency control and economic dispatch of power in partitioned power networks. A decentralized secondary frequency control is reported in [30], where the stability and optimal frequency regulation is confirmed using an LQR optimal solution. Authors in [31] also propose a switched secondary frequency restoration, in which the control scheme switches between two configurations by a time-dependent protocol. Moreover, estimation-based decentralized secondary control approaches are introduced in [32, 33, 34] to control voltage and frequency of microgrids.

On the other hand, although decentralized approach works satisfactorily in most of today's power systems, in accordance with [35], strategies that employ only local information may become unfeasible in future power system developments, for which, due to the large penetration of renewable power generation which increases power fluctuations, more flexibility in the control system is needed.

To overcome these limitations, multi-agent consensus-based controllers have been proposed to take advantage of their inherent scalability and flexibility features [36], in order to address the frequency regulation while minimizing generation costs (economic dispatch) [37, 17] or the SC restoration problems [38, 39, 40, 41, 42, 43, 13]. Additionally, multi-agent based distributed approaches can more easily deal with packet loss and/or latency in communication as compared to the centralized solutions [44].

In [38] the secondary distributed voltage and frequency restoration task is addressed. However, due to the requirement of all-to-all communication among DGs, its communication overhead was significantly greater than that of the centralized strategies [24]. Furthermore, no formal stability analysis was presented. Among the existing investigations, references [39]-[13] appear to be the more closely related to the present research. An overview of the main features of these existing proposals as well as the main improvements provided by the results presented in this chapter are explained hereinafter, separately for the frequency and the voltage restoration problems.

Review of Frequency SCs

Based on a Distributed Averaging Proportional Integral (DA-PI) scheme, [39] first proposed the use of the consensus paradigm to restore the frequencies in an islanded MG modeled in terms of coupled Kuramoto oscillators. A consensus-based Distributed Tracking (DT) approach, is proposed in [40]. Both papers [39, 40] also implement active power sharing functionalities, but the corresponding approached only possess local exponential stability properties. Additionally, in [39] the frequency setpoint must be constant and globally known to all DGs. The approach in [40] allows to arbitrarily modify the steady-state frequency value of the MG by only acting on a particular virtual DG, referred to as "leader", which directly communicates only

with a small portion of DGs. This feature is particularly useful during islanded operation when more active power is required [45], or to seamlessly transfer the MG from islanded to grid-connected mode [46].

Review of voltage SCs

DA-PI and DT solutions have also been employed in the SC layer for voltage restoration purposes. The DA-PI approach in [41] is only capable of providing a tuneable compromise between the adverse tasks of voltage restoration and reactive power sharing accuracy to arbitrarily affect the restoration voltages. Other solutions can be found in [47, 48, 49]. DT schemes such as those in [40], [42]-[13] focus on the exact voltage restoration problem only, disregarding the reactive power sharing issue.

A commonly used approach is to convert the voltage restoration problem into a linear DT consensus problem by using feedback linearization techniques. Then, after linearization, voltage restoration can be achieved by using different DT consensus strategies, such as power fractional finite-time consensus control [40], linear proportional-derivative based consensus [42], and sliding-mode (SM) based adaptive neural networks [43]. Worth also to mention [13], where the agent-based concepts are combined with that of virtual impedance to perform the SC objectives. It is worth remarking that all these works had the full information requirements on the DGs models and parameters. However, MGs are complex systems subjected to disturbances, uncertainties, and changes in the operating conditions. Thus [14] proposed two continuous sliding-mode control (SMC) protocols, aimed to restore both the DG's frequencies and voltage, in the case of undirected communication among agents, thus introducing the concept of robustness in the SC layer design.

Feedback linearization techniques yield the underlying requirement of a perfectly known MG mathematical model which is rather unrealistic in practical power system scenarios, due to the presence of unmodelled dynamics, parameter uncertainties, abrupt modifications of the power demand, and the presence of nonsmooth nonlinearities introduced by the PWM-based power converters, thus making the performance of the control system prone to these uncertainties. Furthermore feedback linearization may also yield numerical problems (e.g., due to the online computation of nonlinear coordinate transformations or high-order Lie derivatives) that can compromise the effectiveness of the whole control system. For these reasons, in this work some robust distributed secondary control strategies whose design is completely model-free and robust against system uncertainties.

1.6.2 Challenges in secondary control of islanded MGs

The challenges in secondary control of islanded MGs in this thesis are divided into two parts.

Challenge in communication delays

Although all the mentioned strategies rely on communication networks, none of them takes into account the presence of neither delays nor asynchronous communications that may, as discussed in [50] destabilize the power-system. Hence, more recently the design of SCs subjected to communication delays attracted many researchers. For instance, a local stability conditions based on a small-signal analysis of the frequency SC, under a constant communication delay among agents, is discussed in [51]. On the other hand [52], through the stochastic differential equation

theory, discussed the stability conditions of a stochastic distributed frequency SC under a single, time-varying, communication delay. Lastly it is also worth mentioning the voltage SCs proposed, resp, in [53, 54] under the assumption of a single constant communication delay, and [55, 56] in the case of multiple constant delays. Finally, note that all these strategies consider only constant single/multiple delays, or single time-varying delays, and that none of them consider model uncertainties. Thus, one of the core question of this thesis is "how to solve the problem of voltage and frequency restoration in droop-controlled inverter-based islanded microgrids with multiple time-varying delays and model uncertainties"?

Challenge in solving the problem of restoration in finite-time

It is worth noting that, most of the secondary control-related works studied the frequency/voltage regulation and active power sharing with the asymptotically convergence speed. To accelerate the convergence speed, a finite-time frequency synchronization method and a finite-time approximate consensus strategy were, respectively, proposed in [57] and [58], where the voltage and reactive power control are not considered. Additionally, in [59] and [60], finite time frequency regulation strategies with bounded control inputs are proposed in autonomous microgrids, however, their voltage control algorithms are asymptotically convergent. A sliding mode controller based on a distributed Radial Basis Function Neural Network (RBF-NN) is suggested in [61] which only focuses on restoring the output voltage of all DGs to a reference value. Moreover, secondary restoration schemes for voltage and frequency control is proposed in [62] based on sliding mode controller. However, the problem of establishing active power-sharing is not guaranteed. In [17], feedback linearization techniques combined with a Lipschitz continuous distributed tracking controller is proposed to achieve the SC aims in a finite time. It is worthwhile to note that the underlying requirement of the exact knowledge of the MG mathematical model and parameters for feedback linearization purposes is rather unrealistic in practical scenarios. Therefore, the second challenge in designing SCs is "how to restore the DG's voltages and frequencies to the desired values in a finite time under parameters uncertainties and unexpected load variations"?

1.6.3 Operation Control Strategies

Several control schemes have been reported for the operation of islanded MGs. These approaches according to the way they handle uncertainties can be categorised as: (i) certainty equivalence, wherein a forecast in the form of the mean value is fully reliable, (ii) worst-case, where no possibility information is presumed, (iii) risk-neutral stochastic, where a forecast probability distribution is fully reliable, and (iv) risk-averse, where uncertainties in the forecast probability distribution are considered. The last section of this work focuses on designing a novel certainty equivalence model predictive.

In this context, a two-stage operation control algorithm is recorded in [63], that includes a schedule and a dispatch layer. By using genetic algorithms, a day ahead schedule for MGs is also designed in [64]. To dispatch generators of islanded MGs, an energy management approach is proposed in [65] by adapting power setpoints and droop gains of the units. Furthermore, a method is provided in [66] to schedule islanded MGs. Additionally, [67] proposes an operation controller based on a rolling horizon strategy. Another operation control is introduced in [68] to address an energy management problem for deterministic forecasts of load and renewable

generation. Furthermore, in [69, 70, 71, 72] MPC approaches for the operation of islanded MGs are reported.

Although all the mentioned strategies are promising, most models are limited to one of the following: (i) They do not consider a possible limitation of infeed from RES [68, 65, 63, 66, 69, 70]. (ii) The dynamics of the storage units are not modeled [65]. (iii) The formulations do not include storage dynamics with power conversion losses [65, 68, 63, 66, 69, 70, 71, 72]. (iv) It is not assumed that conventional units can be turned on and off [65, 63]. (v) They do not explicitly model the power flow over a transmission network [68, 65, 63, 66, 69, 70]. Additionally, the authors in [65, 71, 72] only take into account power sharing of grid-forming units. Thus motivated, we extend the works in [71, 72] by including the conversion losses model in the proposed controller in order to reduce the prediction error in the storage units.

1.6.4 Challenge in operation control of islanded MGs

The challenge of designing operation control in this thesis is how to reduce the error in storage units state of charge prediction by including the conversion losses model?

1.7 Thesis Contribution

To address the mentioned challenges in the previous subsection regarding secondary control, this thesis proposes distributed secondary strategies for AC MGs. Three different distributed strategies are studied and introduced in this work: (i) Robust Adaptive Distributed SC with Communication delays (ii) Robust Optimal Distributed Voltage SC with Communication Delays and (iii) Distributed Finite-Time SC by Coupled Sliding-Mode Technique. As mentioned in Section 1.6.2, most of the existing time-delay tolerant MG control protocols are linear. Thus, because of a MG is a strongly nonlinear system, all those approaches can only provide stability feature in the local sense under additional model approximation or linearization procedures. Moreover, it is worth mention that, all these strategies consider only a single constant/time-varying delay and multiple constant delays per link. Thus motivated, we propose (i) Robust Adaptive Distributed SC and (ii) Robust Optimal Distributed Voltage SC under multiple communication delays and nonlinear model uncertainties. The first approach consist of two terms: 1) a discontinuous integral sliding mode control term aimed to reject the local uncertain terms; 2) a linear distributed consensus control term aimed to globally, exponentially, restores the DG's frequencies and voltages to the expected values while preserving the power sharing among DGs despite the multiple communication delays. The second approach develops the first one by introducing an optimization algorithm to find the optimal control gains and estimate the allowable upper bound for communication delays. Apart from these two approaches, this thesis proposes the third approach to solve the problem of voltage and frequency restoration as well as active power sharing in finite-time by exploiting delay-free communications among DGs and considering model uncertainties. In this approach, for each DG with no access to the information about the SC's setpoints, the finite-time distributed estimators are employed to provide an estimate of the SC's setpoints for the distributed SC schemes. Lyapunov analysis is employed to verify the associated stability and fast convergence time of the proposed controller.

In addition, to solve the operation control mentioned challenges in the previous subsection, this thesis designs a certainty model predictive control (MPC) approach

for the operation of islanded MG with very high share of renewable energy sources. To this aim, the conversion losses of storage units are modelled by quadratic functions to reduce the error in storage units state of charge prediction.

1.8 Publications

Many of the results presented in this work are based on existing publications. To all of the them, the author of this thesis has made substantial contributions.

- A. Pilloni, M. Gholami, A. Pisano, and E. Usai, "*Distributed optimal secondary frequency restoration control under network-induced time-varying communication delays*", Automatica, under review in 2021.
- M. Gholami, A. Pilloni, A. Pisano, and E. Usai, "*Robust distributed secondary voltage restoration control of AC Microgrids under multiple communication delays*", Energies, 2021, 14(4), 1165.
- A. Pilloni, M. Gholami, A. Pisano, and E. Usai, "*On the robust distributed secondary control of islanded inverter-based microgrids*," in Variable-Structure Systems and Sliding-Mode Control. Springer, 2020, pp. 309–357.
- M. Gholami, A. Pisano, S. M. Hosseini, and E. Usai, "*Distributed finitetime secondary control of islanded microgrids by coupled sliding-mode technique*", in 2020 IEEE 25th International Conference on Emerging Technologies and Factory Automation (ETFA). IEEE, 2020, pp. 454– 461.
- M. Gholami, A. Pisano, and E. Usai, "*Robust Distributed Optimal Secondary Voltage Control in Islanded Microgrids with Time-Varying Multiple Delays*", in 2020 IEEE 21st Workshop on Control and Modeling for Power Electronics (COMPEL). IEEE, 2020, pp. 1-8.
- M. Gholami, M. Hajimani, Z. A. Z. Sanai Dashti, and A. Pisano, "*Distributed robust finite-time non-linear consensus protocol for highorder multi-agent systems via coupled sliding mode control*," in 2019 6th International Conference on Control, Instrumentation and Automation (ICCIA). IEEE, 2019, pp. 1–6.
- M. Gholami, A. Pilloni, A. Pisano, Z. A. S. Dashti, and E. Usai, "*Robust consensus-based secondary voltage restoration of inverter-based islanded microgrids with delayed communications*," in 2018 IEEE Conference on Decision and Control (CDC). IEEE, 2018, pp. 811–816.
- M. Gholami, A. Pilloni, A. Pisano, and E. Usai, "*On the robust distributed control of inverter-based microgrids*," 5th International Conference on Electrical, Electronic and Computing Engineering, IcETRAN 2018, Palić, Serbia, June 11 – 14, 2018.

1.9 Thesis Outline

This dissertation is structured as six chapters with a common conclusion. The main contents of each chapter are summarized in the following.

Chapter 2: Preliminaries

In Chapter 2, preliminaries on notation and graph theory are provided. Then, some useful properties from other authors are outlined for later use. Moreover, the model of islanded MGs for designing SCs and operation control are introduced.

Chapter 3: Robust Adaptive Distributed SC

In Chapter 3, novel robust adaptive distributed frequency and voltage SCs in the presence of both, model uncertainties, and multiple time-varying delays in the DGs's communications are proposed. There, the main theorems as well as the stability and convergence features of the resulting closed-loop systems are investigated. Then the performance and effectiveness of the proposed SCs are verified by simulating it on a nonlinear inverter-based MG. Finally, a summary and concluding remarks are provided.

Chapter 4: Robust Distributed Optimal Voltage SC

Chapter 4 outlines a novel distributed voltage SC scheme under communication delays and model uncertainties with constant control gains. Furthermore, by developing an optimization algorithm, the net gains of the proposed control are tuned and optimized. Then, the voltage secondary restoration features, and the closed loop stability of the microgrid, in spite of the communication delays are demonstrated through a Lyapunov-Krasovskii analysis and the use of Linear Matrix Inequalities. An upper bound for the time-delay tolerated by the system is also provided by linear matrix inequalities. Finally, simulation results confirm the effectiveness of the proposed control strategy.

Chapter 5: Distributed Finite-Time SC

This chapter proposes a novel distributed secondary control protocol based on the sliding-mode approach, which not only guarantees the exact finite-time restoration among voltages and frequencies of an inverter-based islanded microgrid, but also preserves the active power sharing among distributed generations (DGs). Then, Lyapunov analysis is used to verify the associated stability and fast convergence time of the proposed SCs. Simulation results are also presented and analyzed to confirm the effectiveness of the proposed approach. Finally, conclusions are collected at the end of the chapter.

Chapter 6: Operation Control

In Chapter 6, a novel certainty equivalence MPC approach for the operation of islanded MG is proposed. The model of an islanded MG with uncertain renewable generation and loads with very high share of RES is firstly derived. Then, the operating costs of the MG is quantified. Lastly, the properties of the resulting certainty equivalence MPC in a numerical case study is illustrated.

Chapter 2

Preliminaries

This chapter is structured as follows. In Section 2.1 some basics on notation are given. After that, in Section 2.2 for later use we present some useful properties of other literatures. Next, in Section 2.3 the preliminaries of graph theory is illustrated. Furthermore, a nonlinear modeling of the inverter-based MG for SC purposes are introduced. Finally, in Section 2.4 a model of an islanded MG for designing operation control is discussed.

2.1 Mathematical Preliminaries and notations

The sets of complex, real, strictly positive and negative real numbers are denoted by $\mathbb{C}$, $\mathbb{R}$, $\mathbb{R}_{<0}$ and $\mathbb{R}_{>0}$, respectively. Moreover, the set of nonpositive real numbers is $\mathbb{R}_{\leq 0}$ and the set of positive real numbers including 0 is $\mathbb{R}_{\geq 0}$. The set of natural number is $\mathbb{N}$ and the set of nonnegative integers is $\mathbb{N}_0$. Furthermore, the set of Boolean numbers is $\mathbb{B} = \{0, 1\}$. For $d \in \mathbb{N}$ and a column vector of $x \in \mathbb{R}^d$, let x' be its transpose. Given a matrix A, its transpose is denoted by A', while its hermitian (complex conjugate) transpose is A^H and let $\|A\|_2$ be Euclidean norm. The Matrix A is also non-negative (psd), denoted by $A \succeq 0$, if A is Hermitian and $z^H A z \succeq 0$ for all $z \in \mathbb{C}^n$. The trace of a matrix A is specified by $tr(A)$. Given a complex number z, its real part is denoted by $\mathrm{Re}(z)$ while the imaginary part of a complex number z is denoted by $\mathrm{Im}(z)$. Additionally, given a scalar a, its absolute value is defined by $|a|$. Finally, the sign operator $\mathrm{sign}(a)$ is understood in the Filippov sense [73], such that, $\mathrm{sign}(a) = 1$ if $a > 0$, -1 if $a < 0$, otherwise it is $\mathrm{sign}(a) \in [-1, 1]$. I_n denotes the n-dimensional identity matrix, and by 1_n and 0_n respectively the all 1, and all 0, n-dimensional column vectors.

2.2 Useful Properties

For later use, the following useful properties are exploited:

Theorem 2.2.1 *(Lyapunov-Krasovskii Stability Theorem [44]). Consider the retarded functional differential equation:*

$$\begin{aligned} \dot{x} &= f(t, x_t), && t \geq 0 \\ x(t_0 + s) &= \phi(s), && s \in [-h, 0] \end{aligned} \tag{2.1}$$

where $h > 0$ is the delay, $\phi \in \mathcal{C}([-h, 0], \mathbb{R}^n)$ is the functional initial condition, and $x_t \in \mathcal{C}([-h, 0], \mathbb{R}^n)$ is the system' state, with $x_t(s) = x(t + s)$. Suppose that $f : \mathbb{R}_{\geq 0} \times \mathcal{C}([-h, 0], \mathbb{R}^n) \mapsto \mathbb{R}^n$ in (2.1) maps $\mathbb{R}_{\geq 0} \times$ (bounded sets of $\mathcal{C}([-h, 0], \mathbb{R}^n)$ into a bounded sets of $\mathbb{R}^n$, and that u, v, $w : \mathbb{R}_{\geq 0} \mapsto \mathbb{R}_{\geq 0}$ are are strictly positive functions, where additionally $u(s)$ and $v(s)$ are positive for $s > 0$, and $u(0) = v(0) = 0$. Assume further that

there exists a continuous differentiable functional $V : \mathbb{R} \times \mathcal{C}([-h, 0], \mathbb{R}^n) \mapsto \mathbb{R}_{>0}$ *such that:*

$$u\left(\|\phi(0)\|_2\right) \leq V(t,\phi) \leq v\left(\|\phi\|_2\right) \quad , \quad \dot{V}(t,\phi) \leq -w(\|\phi(0)\|_2), \tag{2.2}$$

then the trivial solution of (2.1) is uniformly stable. If $w(s) > 0$ *for* $s > 0$*, then it is uniformly asymptotically stable. In addition, if* $\lim_{s\to\infty} u(s) = +\infty$ *then it is globally uniformly asymptotically stable.* ■

Lemma 2.2.1 ([74]) *Let* $a(t), b(t) \in \mathbb{R}^n$ *and* $\psi \in \mathbb{R}^{n\times n}_{>0}$ *the following inequalities are in force:*

$$|2a(t)'b(t)| \leq a(t)'\psi a(t) + b(t)'\psi^{-1}b(t). \tag{2.3}$$

Moreover, let $h \in \mathbb{R}$ *and* $\bar{h}$ *be maximum value assumed by a time delay, then:*

$$-2a(t)' \int_{t-h(t)}^{t} \dot{b}(s)ds \leq \bar{h}a(t)'\psi^{-1}a(t) + \int_{t-h(t)}^{t} \dot{b}(s)\psi\dot{b}(s)ds. \tag{2.4}$$

■

Lemma 2.2.2 ([75, Lemma 2.1]) *Let* $x \in \mathbb{R}^n$*,* B *be any positive definite symmetric matrix, i.e.* $B = B' \succ 0$*, and* $h > 0$*, the Jensen inequality for the integral terms is:*

$$-\int_0^h x(s)'Bx(s)ds \leq -\frac{1}{h}\left(\int_0^h x(s)ds\right)' B \left(\int_0^h x(s)ds\right) \tag{2.5}$$

■

Lemma 2.2.3 ([76]) *The Schur complement lemma converts a class of convex nonlinear inequalities that appears regularly in control problems to an LMI. The convex nonlinear inequalities are:*

$$R(x) < 0, \qquad Q(x) - S(x)R(x)^{-1}S(x)' < 0, \tag{2.6}$$

where $Q(x) = Q(x)'$*,* $R(x) = R(x)'$*, and* $S(x)$ *depend affinely on* x*. The Schur complement lemma converts this set of convex nonlinear inequalities into the equivalent LMI:*

$$\begin{bmatrix} Q(x) & S(x) \\ S(x)' & R(x) \end{bmatrix} < 0. \tag{2.7}$$

■

Theorem 2.2.2 *Let* $M_1 \in \mathbb{R}^{n\times n}$ *be a negative symmetric matrix and* $M_2 \in \mathbb{R}^{n\times n}$ *be a positive symmetric definite matrix, and then let* $\tau \in \mathbb{R}_{>0}$ *be a positive constant. If the following relation is satisfied:*

$$M_1 + \tau M_2 < 0$$

then it yields:

$$M_1 + \xi M_2 < 0 \quad \forall\, \xi\ (0, \xi_m],$$

where

$$\xi_m = \frac{\|M_1\|_2}{\|M_2\|_2}.$$

■

Proof of Theorem 2.2.1 *Let $X \in \mathbb{R}^n$ and let $M \in \mathbb{R}^{n\times n}$, then:*

$$M < 0 \quad \Leftrightarrow \quad X'MX < 0 \quad \forall X \neq 0 \tag{2.8}$$

According to (2.8), we can write:

$$X'(M_1 + \xi M_2)X = X'M_1X + \xi X'M_2X < 0 \tag{2.9}$$

By denoting ${\lambda_{max}}^{M_1} < 0$ and ${\lambda_{max}}^{M_2} > 0$ be the maximum eigenvalues of M_1 and M_2, (2.9) can be recast as follows:

$$X'M_1X + \xi X'M_2X \leq ({\lambda_{max}}^{M_1} + \xi {\lambda_{max}}^{M_2})\|X\|_2^2 \tag{2.10}$$

it follows that:

$$\begin{aligned} {\lambda_{max}}^{M_1} + \xi {\lambda_{max}}^{M_2} < 0 \quad &\Rightarrow \quad \xi {\lambda_{max}}^{M_2} < -{\lambda_{max}}^{M_1} \\ \xi < -\frac{{\lambda_{max}}^{M_1}}{{\lambda_{max}}^{M_2}} &= \frac{|{\lambda_{max}}^{M_1}|}{|{\lambda_{max}}^{M_2}|} \end{aligned} \tag{2.11}$$

Since M_1 and M_2 are negative and positive symmetric matrices, respectively and $\|M\| = {\lambda_{max}}^{M}$, we can thus rewrite (2.11) as follows:

$$\xi < \frac{\|M_1\|_2}{\|M_2\|_2}. \tag{2.12}$$

This concludes the proof. ■

Lemma 2.2.4 ([77, 78, 79]) *If there exists a positive definite continuous function $V(x(t)) : U \to \mathbb{R}_{>0}$, such that $\dot{V}(x(t)) + \rho(V(x(t)))^{\delta} \leq 0$, where $\rho > 0$ and $\delta \in (0, 1)$, for the following system:*

$$\dot{x}(t) = f(x(t)), \quad f(0) = 0, \quad x(t) \in \mathbb{R}^n \tag{2.13}$$

where $f(\cdot) : \mathbb{R}^n \to \mathbb{R}^n$ is a continuous function, then $V(x)$ converges to zero in a finite time. The finite convergence time $\bar{T}$ satisfies $\bar{T} \leq (V(x(0))^{1-\delta}/\rho(1-\delta))$. ■

2.3 MG Modeling for SC Design

A MG is a geographically distributed power system consisting of DGs and loads physically connected by power lines. The DG control units exchange information for monitoring and control purposes over a communication infrastructure, as shown for instance in Figure 2.1.

2.3.1 Distributed generator model

An inverter-based DG includes a 3-ph power converter which DC side is connected to a dc power source (e.g., photovoltaic panels [80], fuel cell system [81] or a wind turbine [40]), while the AC side is connected to the 3-phase power grid by the series of the coupling and the output filters, see Figure 2.2. A more detailed DG's modelization can be found in [14]. Here, as done in [40, 82], we refer to the next simplified representation:

$$\dot{\delta}_i(t) = \omega_i(t) = \omega_{n_i}(t) - k_{P_i} \cdot P_i^m(t) \tag{2.14}$$

$$k_{v_i} \cdot \dot{v}_i(t) = -v_i(t) + v_{n_i}(t) - k_{Q_i} \cdot Q_i^m(t), \quad i = 1, \ldots, N. \tag{2.15}$$

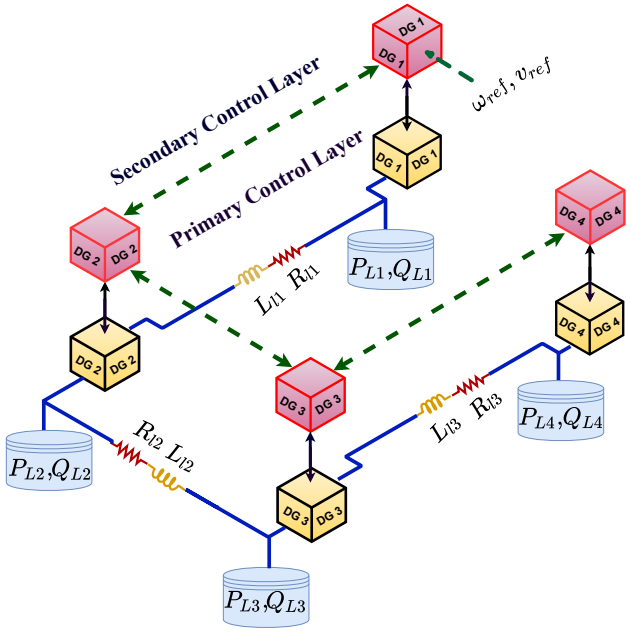

FIGURE 2.1: An islanded MG with four DGs and four loads equipped with a leader-follower SC architecture.

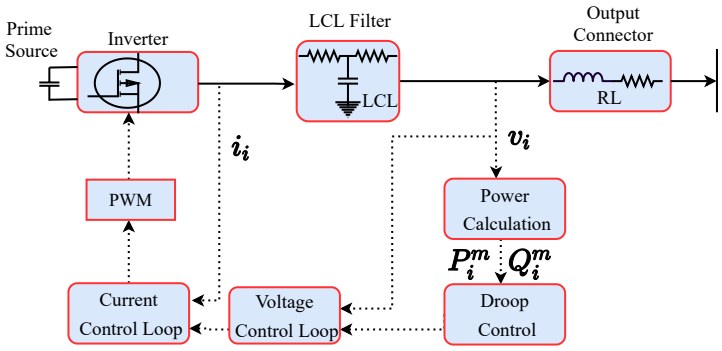

FIGURE 2.2: Primary control block diagram of an inverter-based DG.

where $\delta_i(t)$, and $\omega_i(t)$ represent the voltage phase angle, and the angular frequency expressed in rad/sec of the i-th DG, and $v_i(t)$ is its voltage magnitude expressed in $\mathrm{V_{RMS}}$ (per phase rms). N denotes the number of DGs. Then, $k_{v_i} \in \mathbb{R}_{>0}$ is the voltage control gain, and $k_{P_i} \in \mathbb{R}_{>0}$ and $k_{Q_i} \in \mathbb{R}_{>0}$ are the droop PC's coefficients, selected to meet the power sharing specifications among DGs. $\omega_{n_i}(t)$ and $v_{n_i}(t) \in \mathbb{R}$ are, respectively, the frequency and the voltage SC action which play the role of references for the PC layer. If the SC is inactive, their values correspond to the nominal set-points $\omega_{n_i}(t) = \omega_0 = 2\pi \cdot 50\mathrm{Hz}$ and $v_{n_i}(t) = v_0 = 220\mathrm{V_{RMS}}$(per phase rms) $\equiv 310\mathrm{V_{ph-0}}$. Let τ_{P_i} and $\tau_{Q_i} \in \mathbb{R}_{>0}$ be the time-constants of two low-pass filters, $P_i^m(t)$ and $Q_i^m(t)$ denote the filtered measurements of the instantaneous active and reactive power flows $P_i(t)$ and $Q_i(t)$ such that:

$$\tau_{P_i} \cdot \dot{P}_i^m(t) = -P_i^m(t) + P_i(t) \tag{2.16}$$

$$\tau_{Q_i} \cdot \dot{Q}_i^m(t) = -Q_i^m(t) + Q_i(t) \tag{2.17}$$

2.3.2 MG's Network Models

Since graphs enable the description of both the electrical couplings among DGs through the transmission lines, and the interaction among the DGs' local controllers over a communication infrastructure, preliminary definitions on graph theory are now introduced.

Graph theory

A directed graph (or *digraph*) $\mathcal{G}_{\mathcal{N}}(\mathcal{V}, \mathcal{E}, \mathcal{A})$ is a mathematical tool to describe pairwise mutual interactions between objects, usually referred to as *agents*. $\mathcal{V} = \{1, \dots, N\}$ denotes the agent's set. $\mathcal{E} \subseteq \{\mathcal{V} \times \mathcal{V}\}$ is the edges's set. $\mathcal{A} = [a_{ij}] \in \mathbb{C}^{N \times N}$ is the adjacency matrix of $\mathcal{G}_{\mathcal{N}}$, with weight $a_{ij} = 1$ if agent i communicates with agent j $(i, j) \subseteq \mathcal{E}$, $a_{ij} = 0$ otherwise. $\mathcal{N}_i = \{j \in \mathcal{V} : (i, j) \in \mathcal{E}\}$ is the neighbor's set of agent i. Information on $\mathcal{G}_N$ is also encoded by the following matrix which is called *Laplacian matrix*:

$$\mathcal{L} = \mathcal{B} - \mathcal{A} \quad : \quad \mathcal{L} \cdot 1_N = 0_N.$$

where $\mathcal{B} = \text{diag}\{b_1, \dots, b_n\}$, with $b_i = \sum_{j=1}^{N} \alpha_{ij}$, $\forall\, i = 1, 2, \dots, N$. $\mathcal{N}_i = \{j \in \mathcal{V} : (i, j) \in \mathcal{E}\}$ denotes the set of neighbors of agent "i". We define a "*directed path*" in $\mathcal{G}_N$, a possible alternating sequence of agents and edges over $\mathcal{G}_N$ with both endpoints of an edge appearing adjacent to it in the sequence. A di-graph is weakly connected if, by replacing all directed edges with undirected edges, the resulting graph has not disconnected nodes. A di-graph is strongly connected if it is possible to reach any node starting from any other node by traversing edges in the direction(s) in which they point.

If $\mathcal{G}$ is weakly connected, then $\text{rank}\{\mathcal{L}\} = N - 1$. Moreover, $\mathcal{L}$ has a simple zero eigenvalue. In addition, let $\lambda_2(\mathcal{L})$ be the smallest nonzero eigenvalue of the symmetric-part of $\mathcal{L}$, namely of $\frac{1}{2}(\mathcal{L} + \mathcal{L}^\intercal)$, and let $\varepsilon \in \mathbb{R}^N$ be any vector such that $1_N^\intercal \varepsilon = 0$ then, if $\mathcal{G}_N$ is strongly connected, the next property holds:

$$-\lambda_2(\mathcal{L}) \cdot \|\varepsilon\|_2^2 \leq -\varepsilon' \mathcal{L} \varepsilon. \tag{2.18}$$

An agent i is a root node for $\mathcal{G}_N$, namely it is "*globally reachable*", if it can be reached from any other agent by traversing a directed path. If $\mathcal{G}_N$ admit a root node, then it is also weakly connected.

In our modelization the agent set $\mathcal{V}$ will denote the set of DGs operating over the MG, which cardinality, without loss of generality, is equal to N, namely $\text{card}\{\mathcal{V}\} = N$. Now, we are going to distinguish between the graph $\mathcal{G}_N^e$ representing the interactions among DGs at the electrical level, and $\mathcal{G}_N^c$ which describes the interactions at the communication level among the DGs' SCs.

Electrical network model

To derive the MG's electrical model, let us first notice that the MG's nodes coincides with the DGs connection ports, see e.g. Figure 2.1, and that, the DGs are electrically coupled through the transmission lines. Thus, the electric power network can be described by a di-graph $\mathcal{G}_N^e(\mathcal{V}, \mathcal{E}^e, \mathcal{A}^e)$ which vertex set consists of the set of DGs, namely $\mathcal{V} = \{1, 2, \dots, N\}$. Let $\imath = \sqrt{-1}$ be the imaginary unit, and let $Y_{ij} = G_{ij} + \imath \cdot B_{ij}$ be the line admittance between node "i" and "j", where the terms G_{ij} and B_{ij} denote, resp., the line conductance and susceptance, the couplings among DGs

consists of complex weights $Y_{ij} \in \mathbb{C}$, such that $\mathcal{A}^e = [Y_{ij}] \in \mathbb{C}^{N\times N}$. Clearly, if node "$i$" and "$j$" are not connected $Y_{ij} = 0$ and thus $(i,j) \notin \mathcal{E}$. Let us further note that $B_{ij} > 0$ implies that its inductive component is dominant.

By means of the power flows equations, and under the common assumption that the inverters' output admittances are purely inductive and dominates any resistive effect [47]-[82], namely, $Y_{ik} \approx \imath \cdot B_{ik}\ \forall\ i,k \in \mathcal{V}$, it results that the active and reactive powers at node "i" due to the coupling lines among generators are:

$$\hat{P}_i(t) = \sum_{k\in\mathcal{N}_i^e} v_i(t)v_k(t)B_{ik}\sin(\delta_i(t) - \delta_k(t)) \tag{2.19}$$

$$\hat{Q}_i(t) = v_i^2 B_{ii} + \sum_{k\in\mathcal{N}_i^e} v_i(t)v_k(t)B_{ik}\cos(\delta_i(t) - \delta_k(t)) \tag{2.20}$$

Furthermore, in order to consider also the presence of local loads $(P_{Li}(t), Q_{Li})(t)$ connected at the DG's output port, we further define $(P_i(t), Q_i(t))$ as:

$$P_i(t) = P_{Li}(t) + \hat{P}_i(t) \tag{2.21}$$

$$Q_i(t) = Q_{Li}(t) + \hat{Q}_i(t) \tag{2.22}$$

where $P_{Li}(t) = P_{1i}v_i(t)^2 + P_{2i}v_i(t) + P_{3i}$, and $Q_{Li} = Q_{1i}v_i(t)^2 + Q_{2i}v_i(t) + Q_{3i}$ shows the power-flows load behavior under varying voltage conditions in accordance with the ZIP load power-flow modelization. There, the pairs of parameters (P_{ki}, Q_{ki}), with $k = 1,2,3$, describe the active and reactive power flows absorbed by the i-th load at, resp., constant impedance (Z) that are (P_{1i}, Q_{1i}), constant current (I) that are (P_{2i}, Q_{2i}), and constant power (P) that are (P_{3i}, Q_{3i}). Worth also to remark that the ZIP load modelization is widely accepted in power generation, see for instance [40, 83, 84]. That's because it completely describes the power flows absorbed by an electrical load throughout its operation by means of only 6 parameters, while meeting the constraints of the power system load flow analysis paradigm [85]. Worth also to mention that in the literature there exists simple automated measurement-based identification procedures for the identification of the ZIP load parameters, see [86, 87]. Combining (2.14) to (2.22), the overall dynamical MG model is obtained.

Communication network model

Since we assume each DG provided with communication facilities for SC purposes, the communication network is assumed to be modelled by a directed, weakly connected di-graph $\mathcal{G}_N^c = (\mathcal{V}, \mathcal{E}^c, \mathcal{A}^c)$, which vertex set $\mathcal{V} = \{1, ..., N\}$ is the same used to model the electrical network, but now the nodes play the role of agents. The edge set $\mathcal{E}^c$ collects instead all the available links among the local communication interfaces embedded within each local controller. It further results that $\mathcal{N}_i^c = \{j|(i,j) \in \mathcal{E}^c\}$ and $\mathcal{A}^c = [\alpha_{ij}] \in \mathbb{R}^{N\times N}$ is real and non-negative, where $\alpha_{ij} = 1$ if $(i,j) \in \mathcal{E}^c$, namely if DG i can receive data delivered by DG j, otherwise $\alpha_{ij} = 0$.

Let "0" be an additional virtual node/agent in the augmented communication graph $\mathcal{G}_{N+1}^c$, in the remainder node "0" is considered as the "*virtual leader*" which provides the frequency and voltage set-points ω_0 and $v_0 \in \mathbb{R}$ to the SC layer. Similarly with the related literature [14, 88, 17, 82, 89, 90, 91], node 0 is assumed to be globally reachable on $\mathcal{G}_{N+1}^c$, namely 0 is a root node for $\mathcal{G}_{N+1}^c$. Let $\mathcal{L}^c$ and $\mathcal{L}_{N+1}^c$ be the Laplacian matrices associated with, resp., $\mathcal{G}_N^c$ and $\mathcal{G}_{N+1}^c$. Because of $\mathcal{G}_N^c$ is assumed connected, and 0 is a root node for $\mathcal{G}_{N+1}^c$, then $\text{rank}(\mathcal{L}^c) = N-1$, $\text{rank}(\mathcal{L}_{N+1}^c) = N$. Moreover, both $\mathcal{L}^c$ and $\mathcal{L}_{N+1}^c$ have a simple zero eigenvalue.

Before presenting our final compact model let us made the next reasonable assumption.

Assumption 2.3.1 *Consider a MG described by (2.14)-(2.22). We assume the active and reactive powers (2.21), (2.22) to be bounded-in-magnitude according to* $|P_i(t)| \leq \Pi^P$, $|Q_i(t)| \leq \Pi^Q$, $\forall\, i \in \mathcal{V}$, Π^P, $\Pi^Q \in \mathbb{R}_{>0}$. *Due to (2.16), (2.17), it follows that the time derivatives of the measured powers are uniformly bounded as well.* ■

Remark 2.3.1 *Assumption 2.3.1 is justified because the power flowing in the lines and/or absorbed by the load is bounded everywhere due to: a) the passive behaviour of loads and lines; b) the bounded operating range of the DC-AC power-converters due to their physical limits; c) the presence of protection apparatus and the inner voltage and current PC. This, keeps the power flows within pre-specified ranges as discussed for instance in [14, 82, 92].* ■

For designing SCs, we now express the MG model in terms of the next augmented state form, obtained by time-differentiating (2.14) and (2.15) as follows:

$$\dot{\omega}_i(t) = \dot{\omega}_{n_i}(t) + \dot{\tilde{w}}_i(t) \tag{2.23}$$

$$\begin{bmatrix} \dot{v}_i(t) \\ \ddot{v}_i(t) \end{bmatrix} = \bar{A}_i \cdot \begin{bmatrix} v_i(t) \\ \dot{v}_i(t) \end{bmatrix} + \bar{B}_i \cdot \dot{v}_{n_i}(t) + \begin{bmatrix} 0 \\ \dot{\tilde{w}}_i(t) \end{bmatrix}, \tag{2.24}$$

with

$$\bar{A}_i = \begin{bmatrix} 0 & 1 \\ 0 & -\frac{1}{k_{v_i}} \end{bmatrix}, \quad \bar{B}_i = \begin{bmatrix} 0 \\ \frac{1}{k_{v_i}} \end{bmatrix}, \quad \forall\, i \in \mathcal{V}.$$

where

$$\hat{w}_i(t) = -k_{Pi} \cdot P_i^m(t) \quad , \quad \tilde{w}_i(t) = -\frac{k_{Qi}}{k_{v_i}} \cdot Q_i^m(t) \tag{2.25}$$

play as physical unknown perturbations accounting parameter uncertainties, unmodelled dynamics, chances in the MG working-point, etc. In the remainder of the thesis, and according to the input dynamic extension principle, $\dot{\omega}_{n_i}(t)$ in (2.23), and $\dot{v}_{n_i}(t)$ in (2.24) will be used as the control signals. By doing this, we shall be able to define such signals in a discontinuous manner while having $\omega_{n_i}(t)$ and $v_{n_i}(t)$ continuous, thus well-suited to safely fed the DGs' inner control loops. Finally, $\omega_i(t)$ in (2.23), and $v_i(t)$ and $\dot{v}_i(t)$ in (2.24) express the state signals and need to be controlled by the SC control signals.

Let us further note that from Assumption 2.3.1, and due to the uniform boundedness of the stable first-order filters (2.16)-(2.17), it results that the time derivatives of the measured powers are uniformly bounded as well in accordance with the next relations:

$$|\dot{P}_i^m(t)| \leq \frac{2\Pi_i^P}{\tau_{P_i}} \quad , \quad |\dot{Q}_i^m(t)| \leq \frac{2\Pi_i^Q}{\tau_{Q_i}}, \quad \forall \quad i \in \mathcal{V}. \tag{2.26}$$

From (2.26), and thanks to (2.14)-(2.15), also $\dot{\hat{w}}_i(t)$ and $\dot{\tilde{w}}_i(t)$ meet boundedness restrictions. In particular, after straightforward computations, on the basis of the physical limits of the generators, it results that:

$$\exists \quad \Gamma_i^P = \frac{2k_{P_i}\Pi_i^P}{\tau_{P_i}} \in \mathbb{R}_{>0} \quad : \quad |\dot{\hat{w}}_i(t)| \leq \Gamma_i^P, \tag{2.27}$$

$$\exists \quad \Gamma_i^Q = \frac{2k_{Q_i}\Pi_i^Q}{k_{v_i}\tau_{Q_i}} \in \mathbb{R}_{>0} \quad : \quad |\dot{\tilde{w}}_i(t)| \leq \Gamma_i^Q. \tag{2.28}$$

2.4 MG Modeling for Operation Control Design

The microgrid model that is extracted in this thesis for designing an operation control includes a grouping of conventional generator, storage renewable energy storage units, and loads connected to each other by transmission lines. Figure 2.3 depicts a basic MG, consisting of all these components. The electrical connection among units and loads due to power lines can be modelled by a di-graph $\mathcal{G}_N^e(\mathcal{V}, \mathcal{E}^e)$, where $\mathcal{V} = \{1, \ldots, N\}$ represents the set of agents and $\mathcal{E}^e \subseteq \{\mathcal{V} \times \mathcal{V}\}$ is the set of edges (transmission lines) between two distinct agents. In this manuscript, we consider that the set of agents includes four subsets $\mathcal{V}_T$, $\mathcal{V}_S$, $\mathcal{V}_R$ and $\mathcal{V}_L$, wherein these letters denote, respectively, the sets of conventional, energy storage, renewable units, and loads. We also denote by $\mathcal{Y}_{ij} = G_{ik} + \imath \cdot B_{ij} \in \mathbb{C}$ the admittance line between i-th agent and j-th agent, wherein G_{ij} and B_{ij} show the line conductance and susceptance between i-th agent and j-th agent. If no connection between i-th agent and j-th agent exists, $G_{ij} = B_{ij} = 0$. Given the linear constraint functions on the units and the loads

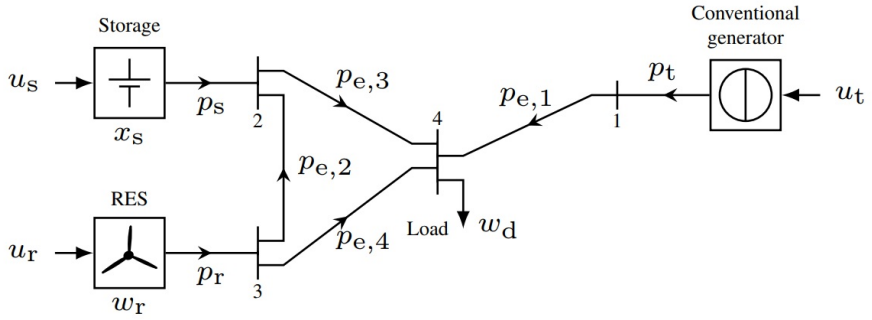

FIGURE 2.3: MG used for operation control as a running example.

in Chapter 6, th dynamic model of the MG can be described by:

$$x(k) + B\bar{q}(k) - x(k+1) = 0, \tag{2.29a}$$

$$H_1 \cdot x(k+1) \leq h_1, \tag{2.29b}$$

$$H_2 \cdot \begin{bmatrix} v(k)' & \bar{q}(k)' & w(k)' \end{bmatrix}' \leq h_2, \tag{2.29c}$$

$$G \cdot \begin{bmatrix} v(k)' & \bar{q}(k)' & w(k)' \end{bmatrix}' = g, \tag{2.29d}$$

where $k \in \mathbb{N}_0$ is time index, $x(k) \in \mathbb{R}^S_{\geq 0}$ with $S \in \mathbb{N}$ is the state vector with initial value $x_0 \in \mathbb{R}^S_{\geq 0}$. In fact, this vector is included of entries $x_i(k)$ that represent the stored energy of unit $i \in \mathbb{N}_{[1,S]}$. $\bar{q}(k) \in \mathbb{R}^Q$ is referred to as a vector of $Q \in \mathbb{N}$ auxiliary variables. And also, $v(k) = [u(k)' \ \delta_t(k)']'$ states the vector of control inputs, wherein $u(k) \in \mathbb{R}^U$ is denoted as the vector of real-valued control inputs of all $U \in \mathbb{N}$ units and $\delta_t(k) \in \{0,1\}^T$ is defined to be the vector of $T \in \mathbb{N}$ Boolean inputs. We have also collected the uncertain external inputs of the model in the vector $w(k) \in \mathbb{R}^W$, $W \in \mathbb{N}$. Let $B \in \mathbb{R}^{S \times Q}$ in (2.29a) and H_1, h_1 in (2.29b) be appropriate dimensions. Furthermore, we consider in (2.29c), H_2 and h_2, respectively, as a matrix and a vector of appropriate dimensions that reflect inequality constraints. Likewise, in (2.29d) G is a matrix and g a vector of appropriate dimensions that reflect equality constraints. In more detail, the real-valued control inputs are the power setpoints of the units $u(k) = [u_t(k)' \ u_s(k)' \ u_r(k)']'$ where $u_t(k)' \in \mathbb{R}^T_{\geq 0}$ is related with the conventional units, $u_s(k)' \in \mathbb{R}^S$ with the storage units and $u_r(k) \in \mathbb{R}^R_{\geq 0}$ with the renewable

units such as wind turbines and PV power plants. Regarding to the storage and conventional generators, $u_s(k)$ and $u_t(k)$ represent desired power values. For RES, $u_r(k)$ represents an upper limit on the weather dependent power infeed. Hence, $u_r(k)$ is their maximum admissible.

Furthermore, for each conventional generator will be considered a Boolean control input $\delta_{t,i}(k) \in \{0,1\}$. This input shows whether generator $i \in \mathbb{N}_{[1,T]}$ is active ($\delta_{t,i}(k) = 1$) or Inactive ($\delta_{t,i}(k) = 0$). The Boolean variables of all conventional generators are gathered in the vector δ_t. The uncertain external input is also collected in the vector $w(k) = [w_r(k)' \; w_t(k)']'$, where $w_r(k)$ is the maximum infeed under weather conditions of all renewable units and $w_t(k)$ includes all loads.

In Chapter 6, we will extract a control-oriented MG model of the form (2.29).

Chapter 3

Robust Adaptive Distributed SC under Delayed communications and Model Uncertainties

3.1 Introduction

In the previous chapter (see Section 2.3), the model of an islanded MG for design SC was derived. Based on this model, an adaptive SC strategy for the asymptotic restoration of the frequencies and the voltages of the AC islanded microgrid is presented in this chapter. The problem is addressed in a multi-agent fashion where the distributed generators play the role of agents subject to model uncertainties and unknown load variation. Moreover, multiple time-varying delays affects the communication links. Robustness against a class of agent's uncertainties and load variations is obtained by means of an integral sliding mode term in the control protocol.

The chapter is organized as follows: Section 3.2 presents the contributions of this chapter as well as the problem statement. A novel adaptive distributed frequency SC is designed in Section 3.3. Then, the secondary restoration features, and the closed loop stability of the microgrid, in spite of the communication delays are demonstrated through a Lyapunov-Krasovskii analysis and the use of LMIs. After that, a novel adaptive distributed voltage SC is proposed in Section 3.4 where the performance of the proposed control system is analyzed by Lyapunov tools. Then, in Section 3.5 the effectiveness of the proposed SCs is verified by computer simulations. Finally, in Section 3.6 some concluding remarks are outlined.

3.2 Main Contributions and Problem Statement

The main contribution of this chapter consists of two novel multi-agent robust consensus SCs, one for the frequency, and one for the voltage, capable to satisfy, globally, and asymptotically, the SC objectives in the presence of both, model uncertainties, and multiple time-varying delays in the DGs's communications. Each SC consists of two terms. The first is a local Integral Sliding Mode Control (ISMC) such that each DG tracks a given reference unperturbed dynamic. Then, taking inspiration by [93], [94] where the adaptive synchronization of high-order linear systems with time-varying multiple delays is studied, an ad-hoc adaptive time-delay consensus protocol is designed to guarantee both the frequency and voltage SC restoration, while preserving the expected sharing of power among DGs. A delay-dependent stability criterion is also provided by combining the Lyapunov –Krasovskii method with the Linear Matrix Inequality (LMI) approach. Lastly, it is worth noting that, although SMCs have discontinuous control actions, thus suffering from the so-called

chattering effect, our SCs yield only discontinuous time derivatives. Thus, the actual control can safely be used to fed the inner PC layer.

In the absence of a SC layer, all the DG's frequencies and output voltages deviate from their reference values. Following [39, 40], it is known that relation (2.14) along with the constraints $k_{P_i} P_i^m = k_{P_k} P_k^m \; \forall \; i, k \in \mathcal{V}$, enforces a steady-state ("ss") frequency synchronization condition depending on the active power flowing in the MG and on the droop coefficients, such that,

$$\lim_{t\to\infty} \omega_i(t) = \omega_{i,ss} = \omega_0 - \frac{\sum_{k=1}^{n} P_k^m}{\sum_{k=1}^{n} \frac{1}{k_{P_k}}} \quad \forall \quad i = 1, \ldots, N \tag{3.1}$$

Similarly, due to (2.15), the steady-stage voltages deviate from v_0. It follows that the two main tasks of the SC layer are:

1. Restore the frequencies and voltages of each DG to their reference values, i.e.,

$$\omega_{i,ss} = \omega_0 \qquad \forall \; i \in \mathcal{V} \tag{3.2}$$
$$v_{i,ss} = v_0 \quad \forall \; i \in \mathcal{V} \tag{3.3}$$

2. Guarantee the active power sharing ratio, i.e.,

$$\frac{P_{i,ss}^m}{P_{k,ss}^m} = \frac{k_{P_k}}{k_{P_i}} \; \forall \; i, k \in \mathcal{V} \tag{3.4}$$

3.3 Frequency secondary controller design

Strategies ranging from centralized to completely decentralized have been suggested to achieve the aforementioned SC purpose. However, centralized approaches conflict with the MG paradigm of autonomous management [41]. On the other hand, decentralized strategies appear to be unfeasible by using only local information [95]. As such, the communication between DGs has been identified as the key ingredient in achieving these goals while avoiding a centralized architecture. In accordance with the DT paradigm, and similarly to [40], [42], [43] and [13], we assume that at least one DG may receive the information on the SC set-points (ω_0, v_0) dispatched by the virtual leader (referred to as node "0"). Thus, node zero is globally reachable on $\mathcal{G}_{N+1}^c$. Furthermore, we assume $\mathcal{G}_N^c$ to be a directed connected graph.

Notice that consider oriented communications is an important difference with respect to the know robust SC strategies such as [14, 41] where they were instead simply undirected. Moreover, in contrast with [88, 14, 17, 89, 90, 91] and [39, 40, 41, 42, 13], but similarly to [51, 53, 54, 55, 52, 56], communications are assumed potentially affected by delays due to packet losses and/or communication latency. However, with respect to the above mentioned works, here the communications are subjected to multiple time-varying delays. We also assume that the DGs may only communicate according to the communication topological graph $\mathcal{G}_N^c$ described in Chapter 2.

Thanks to the droop characteristic (2.14), and according to (3.1), the condition to achieve the frequency restoration (3.2) while preserving desired power sharing capability (3.4) is:

$$\lim_{t\to\infty} \omega_{n_i}(t) = \lim_{t\to\infty} \omega_{n_k}(t) \quad \forall \; i, \; k \in \mathcal{V}. \tag{3.5}$$

In fact, except from special cases, see for instance [95], achieving the frequency synchronization without guaranteeing (3.5) destroys the power sharing property established by the PC [40, 41, 95]. Achieving condition (3.2) subject to (3.5) is a more involved problem that cannot be solved by using standard consensus-based synchronization algorithms. Thus motivated, we propose the following adaptive frequency SC strategy by taking into account delayed communications among DGs:

$$\dot{\omega}_{n_i}(t) = \dot{\hat{u}}_i(t) - \hat{m}_i \cdot \text{sign}(\hat{s}_i(t)) \tag{3.6}$$

where $\hat{s}_i(t)$ is the desired sliding manifold designed as follows:

$$\hat{s}_i(t) = \omega_i(t) + \hat{z}_i(t) \tag{3.7}$$

$$\dot{\hat{z}}_i(t) = -\dot{\hat{u}}_i(t), \quad \hat{z}_i(0) = -\omega_i(0), \tag{3.8}$$

and

$$\begin{aligned}\dot{\hat{u}}_i(t) = &-\sum_{j=0}^{N} \alpha_{ij}\hat{k}_{ij,1}(t)\left[\omega_i(t-\tau_{ij}(t)) - \omega_j(t-\tau_{ij}(t))\right] \\ &-\sum_{j=1}^{N} \alpha_{ij}\hat{k}_{ij,2}(t)\left[\hat{u}_i(t-\tau_{ij}(t)) - \hat{u}_j(t-\tau_{ij}(t))\right],\end{aligned} \tag{3.9}$$

where α_{ij} models the presence/absence of a communication link between the i-th and j-th DG over $\mathcal{G}^c_{N+1}$, whereas $\tau_{ij}(t)$ shows the time-varying communication delay associated with that communication, assumed to be measurable. Moreover, $\hat{m}_i$ is the local discontinuous control gain. Finally $\hat{k}_{ij,1}(t)$, $\hat{k}_{i0}(t)$ and $\hat{k}_{ij,2}(t) \in \mathbb{R}_{>0}$ denote adaptive gains whose update rules are:

$$\dot{\hat{k}}_{ij,1}(t) = \hat{\zeta}_{ij,1} \cdot |\omega_i(t-\tau_{ij}(t)) - \omega_j(t-\tau_{ij}(t))|^2 \tag{3.10}$$

$$\dot{\hat{k}}_{i0,1}(t) = \hat{\zeta}_{i0,1} \cdot |\omega_i(t-\tau_{i0}(t)) - \omega_0(t-\tau_{i0}(t))|^2 \tag{3.11}$$

$$\dot{\hat{k}}_{ij,2}(t) = \hat{\zeta}_{ij,2} \cdot |\hat{u}_i(t-\tau_{ij}(t)) - \hat{u}_j(t-\tau_{ij}(t))|^2. \tag{3.12}$$

with $\hat{\zeta}_{ij,1}$, $\hat{\zeta}_{i0,1}$ and $\hat{\zeta}_{ij,2} \in \mathbb{R}_{>0}$ and $\hat{k}_{ij,1}(0) > 0$, $\hat{k}_{i0,1}(0) > 0$ and $\hat{k}_{ij,2}(0) > 0$.

Remark 3.3.1 *Since DGs share information through a communication infrastructure, due to communication noise, packet collisions, communication errors and others, it may happen the receiver has to wait another beacon interval before receiving the next update. The above consideration leads to the need of running the controller based on outdated information and that τ_{ij} is measurable to correctly correlate the available data for feedback purposes. Thus following [93, 94], we consider that $\tau_{ij}(t)$ is measurable. Note that adding the time-stamp within packets is inexpensive because of most of the standard communication protocols already includes, at least at the MAC ISO/OSI layer this information [96]. On the other hand, communication protocols used to include the data-packet timestamp, thus the requirement of measurable delays is costless [96]. Once the delay is measured by means of local buffers each controller is enabled to retrieve its own state at that time, and performs (3.9).*

Remark 3.3.2 *The design of (3.6)-(3.12) follows from [73, Algorithm 1]. In particular, the term $\hat{u}_i(t)$ in (3.9) is designed ad-hoc to solve the SC objectives (3.2), (3.4) in a distributed way, in the case the agents (DGs) were simply modeled by ideal integrator-type, thus by assuming $\hat{w}_i(t) \equiv 0$. Then, the discontinuous term in (3.6) is designed to account the presence of the electrical, and possibly uncertain, couplings among the DGs due to the presence of the transmission lines and the local loads in (2.16)-(2.22), and thus in the case of non-zero*

$\hat{w}_i(t)$ terms in (2.25). Differently from [73, Algorithm 1], here the term $\hat{u}_i(t)$ accounts also the presence of communication delays, that is a step beyond the design of ISMC-based distributed controllers. No te that the design is based on a distributed implementation of the Integral Sliding Mode Control (ISMC) paradigm [97].

Before presenting the operating assumptions on the delays, let us first introduce the following compact notation, used also in [93, 94]. We indicate with $\mathcal{T}(t) = \{\tau_1(t), \tau_2(t), \dots, \tau_q(t)\}$ the set of delays affecting the communication of between each DG and the leader (node 0), and such that

$$\tau_l(t) = \tau_{i0}(t), \ \ \forall\, i : (i,0) \in \mathcal{E}^c_{N+1},\ l = 1,2,\dots,q. \tag{3.13}$$

Analogously, we indicate with $\mathcal{S}(t) = \{\sigma_1(t), \sigma_2(t), \dots, \sigma_m(t)\}$ the collection of delays affecting the communication between each of the N DGs to another DG where

$$\sigma_g(t) = \tau_{ij}(t), \ \ \forall\, (i,j) \in \mathcal{G}^c_N, \ \ \forall\, g = 1,2,\dots,m. \tag{3.14}$$

Note that the indexes $m \leq N(N-1)$ and $q \leq N$ equal their maximum values only if $\mathcal{G}^c_{N+1}$ is a complete graph, and all the delays, for a given time t, are different. The common assumption of slowly-varying, bounded delays, is now made [98], [99].

Assumption 3.3.1 *Let a-priori known bounds $\tau_l^\star, \sigma_g^\star,\ d_l, d_g \in \mathbb{R}_{>0}$ exist such that the communication delays $\tau_l \in \mathcal{T}(t)$ and $\sigma_g \in \mathcal{S}(t)$ over the communication topology $\mathcal{G}^c_{N+1}$ satisfies:*

$$\begin{array}{l} \tau_{i0}(t) \in [0, \tau_l^\star), \quad |\dot{\tau}_{i0}(t)| \leq d_l < 1, \quad \forall\, t \geq 0,\ \forall\, \tau_{i0} \in \tau_l,\ l = 1,2,\dots,q \\ \tau_{ij}(t) \in [0, \sigma_g^\star), \quad |\dot{\tau}_{ij}(t)| \leq d_g < 1, \quad \forall\, t \geq 0,\ \forall\, \tau_{ij} \in \sigma_g,\ g = 1,2,\dots,m. \end{array} \tag{3.15}$$

Before presenting the first main result of this chapter the following Lemma is provided.

Lemma 3.3.1 *Let $\hat{A}_{i0} = -\alpha_{i0}\hat{k}_{i0,1}(t)$, $\hat{A}_{ij}(t) = -\alpha_{ij}\hat{k}_{ij,1}(t)$, $\hat{\mathcal{A}}_{ij}(t) = -\alpha_{ij}\hat{k}_{ij,2}(t) \in \mathbb{R}$, and let*

$$A_l(t) = \begin{pmatrix} A_{l(1,1)} & 0 & \dots & 0 \\ 0 & A_{l(2,2)} & \dots & \vdots \\ \vdots & \vdots & \ddots & \vdots \\ 0 & \dots & \dots & A_{l(N,N)} \end{pmatrix} \in \mathbb{R}^{N\times N}, \tag{3.16}$$

with diagonal blocks such that ($i = 1,\dots,N$; $l = 1,\dots,q$)

$$A_{l(i,i)}(t) \ : \ \begin{cases} \hat{A}_{i0}(t) & \text{if } l = i\ \tau_l = \tau_{il}, \\ 0 & \text{otherwise}, \end{cases} \tag{3.17}$$

Then, let define Matrices $\hat{A}_g(t) \in \mathbb{R}^{N\times N}$ and $\hat{\mathcal{A}}_g(t) \in \mathbb{R}^{N\times N}$ with entries, resp.,

$$\hat{A}_{g(r,y)}(t) \ : \ \begin{cases} \hat{A}_{ij}(t) & \text{if } \sigma_g = \tau_{ij},\ i \neq j,\ r = y = i \\ -\hat{A}_{ij}(t) & \text{if } \sigma_g = \tau_{ij},\ i \neq j,\ r = i,\ y = j \\ 0 & \text{otherwise} \end{cases} \tag{3.18}$$

$$\hat{\mathcal{A}}_{g(r,y)}(t) \ : \ \begin{cases} \hat{\mathcal{A}}_{ij}(t) & \text{if } \sigma_g = \tau_{ij},\ i \neq j,\ r = y = i \\ -\hat{\mathcal{A}}_{ij}(t) & \text{if } \sigma_g = \tau_{ij},\ i \neq j,\ r = i,\ y = j \\ 0 & \text{otherwise} \end{cases} \tag{3.19}$$

with $r, y = 1, 2, \dots, N$. Assume $\mathcal{G}_N^c$ connected and undirected, and node 0 in $\mathcal{G}_{N+1}^c$ globally reachable. Then $\hat{\Phi}(t) = \sum_{l=1}^{q} A_l(t) + \sum_{g=1}^{m} \hat{A}_g(t)$, as in (3.28), is Hurwitz, $\forall\ t \geq 0$. Moreover, let $\xi \in \mathbb{R}^n$ be any vector such that $1'\xi = 0$, and let $\hat{\Phi}_2(t) = \sum_{g=1}^{m} \hat{\mathcal{A}}_g(t) \preceq 0$, then it results that $\xi' \left(\hat{\Phi}_2(t)' + \hat{\Phi}_2(t)\right) \xi \leq \lambda_2 \|\xi\|_2^2 < 0$, where $\lambda_2 < 0$ is the second greater non-zero eigenvalue of the symmetric part of $\hat{\Phi}_2(t)$.

Proof of Lemma 3.3.1 *Let $\hat{\Phi}_{(r,y)}(t)$ be the (r, y) entry of matrix $\hat{\Phi}(t)$. Because of (3.17), (3.18) and (3.19), we can observe that $-\hat{\Phi}(t)$ is weakly diagonally dominant, namely $|\hat{\Phi}_{(r,r)}(t)| \geq \sum_{y \neq r} |\hat{\Phi}_{(r,y)}(t)|$, $\forall\ r = 1, 2, \dots, N$, $t \geq 0$. Thus, the eigenvalues of $-\hat{\Phi}(t)$, have non-negative real part $\forall\ t \geq 0$. Now, to prove that $\hat{\Phi}(t)$ is Hurwitz we are going to simply show that its inverse exists. Let us first define the vector $b = -(\hat{A}_{10}, \hat{A}_{20}, \dots, \hat{A}_{N0})' \in \mathbb{R}^N$ and the matrices*

$$\mathcal{B} = -\sum_{l=1}^{q} A_l(t) = -\begin{pmatrix} \hat{A}_{10}(t) & 0 & \dots & 0 \\ 0 & \hat{A}_{20}(t) & \dots & \vdots \\ \vdots & \vdots & \ddots & \vdots \\ 0 & \dots & \dots & \hat{A}_{N0}(t) \end{pmatrix}$$

$$\mathcal{L}^c \equiv -\sum_{g=1}^{q} \hat{\mathcal{A}}_g(t) \quad , \quad \mathcal{L}_{N+1}^c = \left(\begin{array}{c|c} 0 & 0_N' \\ \hline b & \mathcal{L}^c \end{array}\right).$$

It can be easily shown that $\mathcal{L}^c$ and $\mathcal{L}_{N+1}^c$ are the Laplacian matrices, resp., of $\mathcal{G}_N^c$ and of $\mathcal{G}_{N+1}^c$, with non-negative weights $-A_{ij}$. Moreover, because of $\mathcal{G}_N^c$ is connected and because of node 0 is a root node on $\mathcal{G}_{N+1}^c$ it results that $\text{rank}\{\mathcal{L}^c\} = N - 1$, $\text{rank}\{\mathcal{L}_{N+1}^c\} = \text{rank}\{[b,\ \mathcal{L}_N^c]\} = N$. Now, let us define $x = 1_N \cdot x_0$, with $x_0 \in \mathbb{R}$. Because of $\mathcal{L}^c 1_N = 0_N$, the following continued equality holds

$$\mathcal{L}^c x = 0_N \quad \Longrightarrow \quad \mathcal{L}^c x + \mathcal{B} 1_n \cdot x_0 = \mathcal{B}^c 1_N \cdot x_0 \quad \Longrightarrow \quad (\mathcal{L}^c + \mathcal{B})\, x = -\hat{\Phi}(t) x = \mathcal{B} 1_n \cdot x_0.$$

Thus, according to $-\hat{\Phi}(t) = \mathcal{B} + \mathcal{L}^c$, it yields there exists $\hat{\Phi}(t)^{-1}$ with $\text{rank}\{\hat{\Phi}(t)\} = N$, and lastly the eigenvalues of $\hat{\Phi}(t)$ have negative real part for all $t \geq 0$.

By similar consideration, it results that the matrix $-\hat{\Phi}_2(t) = \mathcal{L}^c$ corresponds to the Laplacian matrix of the graph which topology is encoded by $\mathcal{G}_N^c$ and with non-negative weights $-\hat{\mathcal{A}}_{ij}$. Thus because of $\mathcal{G}_N^c$ is assumed connected and undirected, then by means of property (2.18), we can straightforwardly derive that $\xi' \hat{\Phi}_2(t) \xi \leq \lambda_2(\hat{\Phi}_2(t)) \|\xi\|_2^2 < 0$ holds. This conclude the proof.

Theorem 3.3.1 *Consider a microgrid of N DGs, which frequency dynamics (2.23) are under the adaptive frequency SC (3.6)-(3.12). Let Assumption 2.3.1 and Assumption 3.3.1 be satisfied. Let the communication topology among DGs be described by a connected, and undirected graph $\mathcal{G}_N^c(\mathcal{V}, \mathcal{E}^c)$, with weight $\alpha_{ij} = 1$, if $(i, j) \in \mathcal{E}^c$, 0 otherwise. Let node 0 be globally reachable on $\mathcal{G}_{N+1}^c$. Let Ω be the so-called average disagreement matrix*

$$\Omega = I_N - \frac{1}{N} 1_N 1_N' \succeq 0 \tag{3.20}$$

where by Lemma 3.3.1, results that:

$$\lambda_2(t) = \max_{\text{eig} \neq 0} \left\{ \sum_{g=1}^{m} \hat{A}_g(t)' + \sum_{g=1}^{m} \hat{\mathcal{A}}_g(t) \right\} < 0, \quad \hat{\Phi}(t) = \sum_{l=1}^{q} A_l(t) + \sum_{g=1}^{m} \hat{A}_g(t) \prec 0 \quad \forall t \geq 0. \tag{3.21}$$

Let there exist $\hat{m}_i > \Gamma_i^P = 2k_{P_i}\Pi_i^P/\tau_{P_i}$, *and positive definite matrices* $\hat{P}$, $\hat{Q}_l$, $\hat{Q}_g$, $\hat{\mathcal{Q}}_g$, $\hat{R}_g$, $\hat{\mathcal{R}}_g$, $\hat{W}_l$, $\hat{W}_g$, $\hat{\mathcal{W}}_g \in \mathbb{R}^{N\times N}$ *such that the following LMIs holds:*

$$\hat{P}\hat{\Phi}(t)' + \hat{P}\hat{\Phi}(t) \prec \sum_{l=1}^{q}\hat{Q}_l + \sum_{g=1}^{m}\hat{Q}_g + \sum_{g=1}^{m}\sigma_g^\star\hat{R}_g \tag{3.22}$$

$$\lambda_2(t)I_N \prec \hat{\eta}\sum_{g=1}^{m}\hat{\mathcal{Q}}_g + \sum_{g=1}^{m}\sigma_g^\star\hat{\mathcal{R}}_g \tag{3.23}$$

$$-(1-d_l)\hat{Q}_l \prec \hat{\eta}\left(A_l(t)'\hat{H}_1A_l(t) + \Omega' A_l(t)'\hat{M}_1\Omega A_l(t)\right) \tag{3.24}$$

$$-(1-d_g)\hat{Q}_g \prec \hat{\eta}\left(\hat{A}_g(t)'\hat{H}_1\hat{A}_g(t) + \Omega'\hat{A}_g(t)'\hat{M}_1\Omega\hat{A}_g(t)\right) \tag{3.25}$$

$$-(1-d_g)\hat{\mathcal{Q}}_g \prec \hat{\eta}\left(\hat{\mathcal{A}}_g(t)'\hat{H}_1(t)\hat{A}_g(t) + \hat{\mathcal{A}}_g(t)'\hat{M}_1(t)\hat{A}_g(t)\right) \tag{3.26}$$

where $\hat{\eta} > 0$, *and*

$$\hat{H}_1 = \sum_{g=1}^{m}\sigma_g^\star\hat{W}_g + \sum_{l=1}^{q}\tau_l^\star\hat{W}_l \succ 0 \quad , \quad \hat{M}_1 = \sum_{g=1}^{m}\sigma_g^\star\hat{\mathcal{W}}_g \succ 0, \tag{3.27}$$

and by Lemma 3.3.1, results that:

$$\lambda_2(t) = \max_{\text{eig}\neq 0}\left\{\sum_{g=1}^{m}\hat{A}_g(t)' + \sum_{g=1}^{m}\hat{\mathcal{A}}_g(t)\right\} < 0, \quad \hat{\Phi}(t) = \sum_{l=1}^{q}A_l(t) + \sum_{g=1}^{m}\hat{A}_g(t) \prec 0 \quad \forall t \geq 0. \tag{3.28}$$

Then, the frequency SC objectives (3.2) and (3.5) are verified, and the adaptive gains $\hat{k}_{ij,1}$,$\hat{k}_{i0,1}$, *and* $\hat{k}_{ij,2}$ *asymptotically converge to some positive constants* $\hat{k}^\star_{ij,1}$, $\hat{k}^\star_{i0,1}$ *and* $\hat{k}^\star_{ij,2}$, *for all* i *and* $j \in \mathcal{V}$.

Proof of Theorem 3.3.1 Let us substitute Equations (3.6) into Equation (2.23) as

$$\dot{\omega}_i(t) = \dot{\hat{u}}_i(t) - \hat{m}_i\cdot\text{sign}(\hat{s}_i(t)) + \dot{\hat{w}}_i(t) = \dot{\hat{u}}_i(t) + \dot{\hat{s}}_i(t), \tag{3.29}$$

$$\dot{\hat{s}}_i(t) = \dot{\hat{w}}_i(t) - \hat{m}_i\cdot\text{sign}(\hat{s}_i(t)). \tag{3.30}$$

For a differential equation with discontinuous right-hand side as (3.30), in the remainder, the resulting solution $\hat{s}_i(t)$ will be understood in the so-called Filippov sense. Namely, as the solution of an appropriate differential inclusion, the existence of which is guaranteed (owing on certain properties of the associated set-valued map) and for its absolute continuity is satisfied. The reader is referred to [73] for a comprehensive account of the necessary notions of non-smooth analysis.

Given that, and because of Assumption 2.3.1, and (2.27), $\|\dot{\hat{w}}(t)\| \leq \Gamma_i^P$, and $\hat{m}_i > \Gamma_i^P$, and $\hat{z}_i(0) = -\omega_i(0)$, by differentiating the following candidate Lyapunov functional:

$$\hat{V}(t) = \frac{1}{2}\sum_{i=1}^{N}\hat{s}_i(t)^2, \tag{3.31}$$

along the trajectories of (3.30), after straightforwards computations, it results that:

$$\begin{aligned}\dot{\hat{V}}(t) = \sum_{i=1}^{N}\hat{s}_i(t)\cdot\dot{\hat{s}}_i(t) &\leq \sum_{i=1}^{N}\left|\hat{s}_i(t)\cdot\dot{\hat{w}}_i(t)\right| - \hat{m}_i\left|\hat{s}_i(t)\right| \\ &\leq -\sum_{i=1}^{N}\left(\hat{m}_i - \Gamma_i^P\right)\cdot\left|\hat{s}_i(t)\right| \prec 0 \qquad \forall\, t \geq 0.\end{aligned} \tag{3.32}$$

From this, one concludes that, except for points of Lebesgue measure zero (that can be disregarded in accordance with the Filippov Theory [73]), the condition $\hat{s}_i(t) = \dot{\hat{s}}_i(t) = 0$ is time-invariant for all $t \geq 0$. Now, by letting $s_i = \dot{s}_i = 0$ into (3.29), and by substituting (3.9), the following closed-loop dynamic takes place:

$$\begin{aligned}\dot{\omega}_i(t) = &-\sum_{j=0}^{N} \alpha_{ij} \cdot \hat{k}_{ij,1}(t)(\omega_i(t-\tau_{ij}(t)) - \omega_j(t-\tau_{ij}(t))) \\ &-\sum_{j=1}^{N} \alpha_{ij} \cdot \hat{k}_{ij,2}(t)(\hat{u}_i(t-\tau_{ij}(t)) - \hat{u}_j(t-\tau_{ij}(t))).\end{aligned} \tag{3.33}$$

The point now is to find which conditions (3.33) have to met in order to achieve the control objectives (3.2) and (3.1). Up to now, we found that (2.23) is degenerated into $\dot{\omega}_i(t) = \dot{\hat{u}}_i(t)$ for all $t \geq 0$. Thus, it follows that the achievement (3.2) and (3.1) along the trajectories of (2.23), is equivalent to force to zero, along the trajectories of (3.33), the following frequency error vector:

$$\hat{e}(t) = \big(\hat{e}_1(t), \quad \hat{e}_2(t), \quad \ldots, \hat{e}_N(t)\big)' \quad \text{with} \quad \hat{e}_i = \omega_i(t) - \omega_0 \tag{3.34}$$

subject to the achievement of the next additional consensus condition:

$$\lim_{t\to\infty} \hat{u}_i(t) = \lim_{t\to\infty} \hat{u}_j(t) \quad \forall\, i,j \in \mathcal{V}, \tag{3.35}$$

that is equivalent to force to zero the so-called average disagreement vector

$$\underbrace{\big(\varepsilon_1(t), \quad \varepsilon_2(t), \quad \ldots, \varepsilon_N(t)\big)'}_{\varepsilon(t)} = \underbrace{\left(I_{N\times N} - \frac{1_N 1_N'}{N}\right)}_{\Omega} \cdot \underbrace{\big(\hat{u}_1(t), \quad \hat{u}_2(t), \quad \ldots, \hat{u}_N(t)\big)'}_{\hat{u}(t)}, \tag{3.36}$$

where

$$\varepsilon_i(t) = \hat{u}_i(t) - \frac{1}{N}\sum_{k=1}^{N} \hat{u}_k(t) = 0 \quad \forall\, i \in \mathcal{V} \quad \Longleftrightarrow \quad \hat{u}_i(t) = \hat{u}_j(t) \quad \forall\, i,j \in \mathcal{V}.$$

Given that, let us now differentiate $e_i(t) = \omega_i(t) - \omega_0$, then by letting $\hat{A}_{i0}(t) = -\alpha_{i0}\hat{k}_{i0,1}(t)$, $\hat{A}_{ij}(t) = -\alpha_{ij}\hat{k}_{ij,1}(t)$, $\hat{\mathcal{A}}_{ij}(t) = -\alpha_{ij}\hat{k}_{ij,2}(t)$, after some algebraic manipulations, one derives:

$$\begin{aligned}\dot{\hat{e}}_i(t) = &-\alpha_{i0}\hat{k}_{i0,1}(t)\cdot\hat{e}_i(t-\tau_{i0}(t)) - \sum_{j=1}^{N}\alpha_{ij}\hat{k}_{ij,1}(t)\cdot\big[\hat{e}_i(t-\tau_{ij}(t)) - \hat{e}_j(t-\tau_{ij}(t))\big] \\ &-\sum_{j=1}^{N}\alpha_{ij}\hat{k}_{ij,2}(t)\cdot\big[\hat{u}_i(t-\tau_{ij}(t)) - \hat{u}_j(t-\tau_{ij}(t))\big] \\ =&\hat{A}_{i0}(t)\cdot\hat{e}_i(t-\tau_{i0}(t))) + \sum_{j=1}^{N}\hat{A}_{ij}(t)\cdot\big[\hat{e}_i(t-\tau_{ij}(t)) - \hat{e}_j(t-\tau_{ij}(t))\big] \\ &+\sum_{j=1}^{N}\hat{\mathcal{A}}_{ij}(t)\cdot\big[\hat{u}_i(t-\tau_{ij}(t)) - \hat{u}_j(t-\tau_{ij}(t)))\big].\end{aligned} \tag{3.37}$$

Now, in order to provide a compact state-space representation of the networked error dynamics associated with the vectors (3.34) and (3.36), and accordingly with the notation introduced for the delays in (3.13) and (3.14), where $q = \text{card}\{\mathcal{T}(t)\}$

and $m = \text{card}\{\mathcal{S}(t)\}$, it results

$$\dot{\hat{e}}(t) = \sum_{l=1}^{q} A_l(t)\hat{e}(t-\tau_l(t)) + \sum_{g=1}^{m} \hat{A}_g(t)\hat{e}(t-\sigma_g(t)) + \sum_{g=1}^{m} \hat{\mathcal{A}}_g(t)\varepsilon(t-\sigma_g(t)) \tag{3.38}$$

$$\dot{\varepsilon}(t) = \sum_{l=1}^{q} \Omega A_l(t)\hat{e}(t-\tau_l(t)) + \sum_{g=1}^{m} \Omega\hat{A}_g(t)\hat{e}(t-\sigma_g(t)) + \sum_{g=1}^{m} \Omega\hat{\mathcal{A}}_g(t)\varepsilon(t-\sigma_g(t)). \tag{3.39}$$

where the elements of the matrices $A_l(t)$, $\hat{A}_g$ and $\hat{\mathcal{A}}_g(t)$ are defined in (3.17), (3.18) and (3.19). Let us further note that, due the structure of $\hat{A}_g(t)$ and $\hat{\mathcal{A}}_g(t)$, it results that $\hat{A}_g 1_N = 0_N$, $\hat{\mathcal{A}}_g 1_N = 0_N$, thus it follows that in both (3.38) and (3.39), one has $\hat{\mathcal{A}}_g\varepsilon(t-\sigma_g) = \hat{\mathcal{A}}_g\Omega\hat{u}(t-\sigma_g) = \hat{\mathcal{A}}_g\hat{u}(t-\sigma_g)$.

For stability analysis purposes, and on the basis of the so-called Leibniz-Newton formula we introduce the following transformations:

$$\hat{e}(t-\tau(t)) = \hat{e}(t) - \int_{t-\tau(t)}^{t} \dot{\hat{e}}(s)ds \quad , \quad \varepsilon(t-\tau(t)) = \varepsilon(t) - \int_{t-\tau(t)}^{t} \dot{\varepsilon}(s)ds. \tag{3.40}$$

Hence, from (3.40), the networked closed-loop dynamics in (3.38)-(3.39) can be recast as:

$$\begin{aligned}\dot{\hat{e}}(t) =& \hat{\Phi}(t)\hat{e}(t) - \sum_{l=1}^{q} A_l(t)\int_{t-\tau_l(t)}^{t} \dot{\hat{e}}(s)ds - \sum_{g=1}^{m} \hat{A}_g(t)\int_{t-\sigma_g(t)}^{t} \dot{\hat{e}}(s)ds \\ &+ \sum_{g=1}^{m} \hat{\mathcal{A}}_g(t)\varepsilon(t) - \sum_{g=1}^{m} \hat{\mathcal{A}}_g(t)\int_{t-\sigma_g(t)}^{t} \dot{\varepsilon}(s)ds,\end{aligned} \tag{3.41}$$

$$\begin{aligned}\dot{\varepsilon}(t) =& \Omega\hat{\Phi}(t)\hat{e}(t) - \sum_{l=1}^{q} \Omega A_l(t)\int_{t-\tau_l(t)}^{t} \dot{\hat{e}}(s)ds - \sum_{g=1}^{m} \Omega\hat{A}_g(t)\int_{t-\sigma_g(t)}^{t} \dot{\hat{e}}(s)ds \\ &+ \Omega\sum_{g=1}^{m} \hat{\mathcal{A}}_g(t)\varepsilon(t) - \sum_{g=1}^{m} \Omega\hat{\mathcal{A}}_g(t)\int_{t-\sigma_g(t)}^{t} \dot{\varepsilon}(s)ds.\end{aligned} \tag{3.42}$$

where $\hat{\Phi}(t) = \sum_{l=1}^{q} A_l(t) + \sum_{g=1}^{m} \hat{A}_g(t)$, as in (3.28). Synchronization in the presence of multiple time-varying delays is proved here under the common Assumption 3.3.1, which requires that delays are bounded and slowly time varying signals [44, 94, 98, 99]. Inspired by [44], let us now construct the following Lyapunov-Krasovskii functional:

$$\begin{aligned}\overline{V}(t) =& \hat{e}(t)'\hat{P}\hat{e}(t) + \sum_{l=1}^{q}\int_{t-\tau_l(t)}^{t} \hat{e}(s)'\hat{Q}_l\hat{e}(s)ds + \sum_{g=1}^{m}\int_{t-\sigma_g(t)}^{t} \hat{e}(s)'\hat{Q}_g\hat{e}(s)ds \\ &+ \hat{\eta}\sum_{l=1}^{q}\int_{-\tau_l^\star}^{0}\int_{t+\theta}^{t} \dot{\hat{e}}(s)'\hat{W}_l\dot{\hat{e}}(s)dsd\theta + \hat{\eta}\sum_{g=1}^{m}\int_{-\sigma_g^\star}^{0}\int_{t+\theta}^{t} \dot{\hat{e}}(s)'\hat{W}_g\dot{\hat{e}}(s)dsd\theta \\ &+ \varepsilon(t)'\varepsilon(t) + \hat{\eta}\sum_{g=1}^{m}\int_{t-\sigma_g(t)}^{t} \varepsilon(s)'\hat{\mathcal{Q}}_g\varepsilon(s)ds + \hat{\eta}\sum_{g=1}^{m}\int_{-\sigma_g^\star}^{0}\int_{t+\theta}^{t} \dot{\varepsilon}(s)'\hat{\mathcal{W}}_g\dot{\varepsilon}(s)dsd\theta \\ &+ \sum_{i=1}^{N}\sum_{j=0}^{N}\frac{1}{2}\left(\hat{k}_{ij,1}^\star - \hat{k}_{ij,1}(t)\right)^2 + \sum_{i=1}^{N}\sum_{j=1}^{N}\frac{1}{2}\left(\hat{k}_{ij,2}^\star - \hat{k}_{ij,2}(t)\right)^2,\end{aligned} \tag{3.43}$$

where $\hat{P}$, $\hat{Q}_l$, $\hat{Q}_g$, $\hat{W}_l$, $\hat{W}_g$, $\hat{\mathcal{Q}}_g$, $\hat{\mathcal{W}}_g \in \mathbb{R}^{N\times B}$ are constant, symmetric, and positive definite matrices to be determined and $\hat{\eta}$ is a positive scalar. Following the requirements

of Theorem 2.2.1, let us note that the following relation is satisfied:

$$\hat{\alpha}(\hat{e}(t),\varepsilon(t)) \leq \overline{V}(t) \leq \hat{\beta}(\hat{e}(t-\hat{\tau}),\varepsilon(t-\hat{\tau})). \tag{3.44}$$

where $\hat{\alpha}(e(t),\varepsilon(t))$ and $\hat{\beta}(\hat{e}(t),\varepsilon(t))$ are continuous non-decreasing positive functions defined as follows:

$$\hat{\alpha}(e(t),\varepsilon(t)) = \hat{e}(t)'\hat{P}e(t) + \varepsilon(t)'\varepsilon(t). \tag{3.45}$$

$$\begin{aligned}\hat{\beta}(\hat{e}(t),\varepsilon(t)) =& \hat{e}(t)'\hat{P}\hat{e}(t) + \sum_{l=1}^{q}\int_{t-\hat{\tau}}^{t}\hat{e}(s)'\hat{Q}_l\hat{e}(s)ds + \sum_{g=1}^{m}\int_{t-\hat{\tau}}^{t}\hat{e}(s)'\hat{Q}_g e(s)ds \\ &+ \hat{\eta}\sum_{l=1}^{q}\int_{-\hat{\tau}}^{0}\int_{t+\theta}^{t}\dot{\hat{e}}(s)'\hat{W}_l\dot{\hat{e}}(s)ds d\theta + \hat{\eta}\sum_{g=1}^{m}\int_{-\hat{\tau}}^{0}\int_{t+\theta}^{t}\dot{\hat{e}}(s)'\hat{W}_g\dot{\hat{e}}(s)ds d\theta \\ &+ \varepsilon(t)'\varepsilon(t) + \hat{\eta}\sum_{g=1}^{m}\int_{t-\hat{\tau}}^{t}\varepsilon(s)'\hat{\mathcal{Q}}_g\varepsilon(s)ds + \hat{\eta}\sum_{g=1}^{m}\int_{-\hat{\tau}}^{0}\int_{t+\theta}^{t}\dot{\varepsilon}(s)'\hat{\mathcal{W}}_g\dot{\varepsilon}(s)ds d\theta \\ &+ \sum_{i=1}^{N}\sum_{j=0}^{N}\frac{1}{2}\left(\hat{k}^{\star}_{ij,1} - \hat{k}_{ij,1}(t)\right)^2 + \sum_{i=1}^{N}\sum_{j=1}^{N}\frac{1}{2}\left(\hat{k}^{\star}_{ij,2} - \hat{k}_{ij,2}(t)\right)^2,\end{aligned} \tag{3.46}$$

where $\hat{\tau} = \max_{l,g}\{\tau_l^{\star},\ \sigma_g^{\star}\}$. Now, differentiating (3.31) along the trajectories of (3.41) and (3.42), and because of $1_N'\varepsilon = 0$ which implies that $\varepsilon'\Omega = \varepsilon'$, it follows that:

$$\begin{aligned}\dot{\overline{V}}(t) =& \hat{e}(t)'\left(\hat{\Phi}(t)'\hat{P} + \hat{P}\hat{\Phi}(t)\right)\hat{e}(t) - 2\hat{e}(t)'\hat{P}\sum_{l=1}^{q}A_l(t)\int_{t-\tau_l(t)}^{t}\dot{\hat{e}}(s)ds \\ &- 2\hat{e}(t)'\hat{P}\sum_{g=1}^{m}\hat{A}_g(t)\int_{t-\sigma_g(t)}^{t}\dot{\hat{e}}(s)ds + 2\hat{e}(t)'\hat{P}\sum_{g=1}^{m}\hat{\mathcal{A}}_g(t)\varepsilon(t) - 2\hat{e}(t)'\hat{P}\sum_{g=1}^{m}\hat{\mathcal{A}}_g(t)\int_{t-\sigma_g(t)}^{t}\dot{\varepsilon}(s)ds \\ &+ \hat{e}(t)'\sum_{l=1}^{q}\hat{Q}_l\hat{e}(t) - \sum_{l=1}^{q}\hat{e}(t-\tau_l(t))'\hat{Q}_l\hat{e}(t-\tau_l(t))(1-\dot{\tau}_l(t)) \\ &+ \hat{e}(t)'\sum_{g=1}^{m}\hat{Q}_g\hat{e}(t) - \sum_{g=1}^{m}e(t-\sigma_g(t))'\hat{Q}_g\hat{e}(t-\sigma_g(t))(1-\dot{\sigma_g}(t)) \\ &+ \hat{\eta}\dot{\hat{e}}(t)'\sum_{l=1}^{q}\tau_l^{\star}\hat{W}_l\dot{\hat{e}}(t) - \hat{\eta}\sum_{l=1}^{q}\int_{t-\tau_l^{\star}}^{t}\dot{\hat{e}}(s)'\hat{W}_l\dot{\hat{e}}(s)ds \\ &+ \sum_{g=1}^{m}\sigma_g^{\star}\hat{W}_g\dot{\hat{e}}(t) - \hat{\eta}\sum_{g=1}^{m}\int_{t-\sigma_g^{\star}}^{t}\dot{\hat{e}}(s)'\hat{W}_g\dot{e}(s)ds \\ &+ 2\varepsilon(t)'\hat{\Phi}(t)\hat{e}(t) - 2\varepsilon(t)'\sum_{l=1}^{q}A_l(t)\int_{t-\tau_l(t)}^{t}\dot{\hat{e}}(s)ds - 2\varepsilon(t)'\sum_{g=1}^{m}\hat{A}_g(t)\int_{t-\sigma_g(t)}^{t}\dot{\hat{e}}(s)ds \\ &+ \varepsilon(t)'\left(\sum_{g=1}^{m}\hat{\mathcal{A}}_g(t)' + \sum_{g=1}^{m}\hat{\mathcal{A}}_g(t)\right)\varepsilon(t) - 2\varepsilon(t)'\sum_{g=1}^{m}\hat{\mathcal{A}}_g(t)\int_{t-\sigma_g(t)}^{t}\dot{\varepsilon}(s)ds \\ &+ \hat{\eta}\varepsilon(t)'\sum_{g=1}^{m}\hat{\mathcal{Q}}_g\varepsilon(t) - \hat{\eta}\sum_{g=1}^{m}\varepsilon(t-\sigma_g(t))'\hat{\mathcal{Q}}_g\varepsilon(t-\sigma_g(t))(1-\dot{\sigma_g}(t)) \\ &+ \hat{\eta}\dot{\varepsilon}(t)'\sum_{g=1}^{m}\sigma_g^{\star}\hat{\mathcal{W}}_g\dot{\varepsilon}(t) - \hat{\eta}\sum_{g=1}^{m}\int_{t-\sigma_g^{\star}}^{t}\dot{\varepsilon}(s)'\hat{\mathcal{W}}_g\dot{\varepsilon}(s)ds \\ &- \sum_{i=1}^{N}\sum_{j=1}^{N}\left(\hat{k}^{\star}_{ij,1} - \hat{k}_{ij,1}(t)\right)\dot{\hat{k}}_{ij,1}(t) - \sum_{i=1}^{N}\sum_{j=0}^{N}\left(\hat{k}^{\star}_{ij,2} - \hat{k}_{ij,2}(t)\right)\dot{\hat{k}}_{ij,2}(t)\end{aligned} \tag{3.47}$$

Now, by adding to the right-hand side of (3.47) the next two identically zero quantities:

$$\sum_{g=1}^{m}\sigma_g^\star\hat{e}(t)'\hat{R}_g\hat{e}(t)-\sum_{g=1}^{m}\sigma_g^\star\hat{e}(t)'\hat{R}_g\hat{e}(t)=0,$$
$$\eta\sum_{g=1}^{m}\sigma_g^\star\varepsilon(t)'\hat{\mathcal{R}}_g\varepsilon(t)-\eta\sum_{g=1}^{m}\sigma_g^\star\varepsilon(t)'\hat{\mathcal{R}}_g\varepsilon(t)=0,$$

where $\hat{R}_g\succ 0$ and $\hat{\mathcal{R}}_g\succ 0$, and by exploiting the delays' bounds provided by Assumption 3.3.1, namely, $\tau_l\in[0,\tau^\star)$, $\sigma_g\in[0,\sigma_g^\star)$, and $\dot{\tau}_l\leq d_l$, $\dot{\sigma}_g\leq d_g$, and because of, due to Lemma 3.3.1, it results that:

$$\varepsilon(t)'\left(\sum_{g=1}^{m}\hat{\mathcal{A}}_g(t)'+\sum_{g=1}^{m}\hat{\mathcal{A}}_g(t)\right)\varepsilon(t)\leq\lambda_2(t)\varepsilon'\varepsilon<0,$$

where $\lambda_2(t)<0$ is the greatest non-zero eigenvalue of the symmetric part of $\hat{\mathcal{A}}_g(t)\preceq 0$, then after some algebraic manipulation, (3.47) can be upper-estimated as follows:

$$\begin{aligned}
\dot{\bar{V}}(t)\leq&\hat{e}(t)'\left(\hat{\Phi}(t)'\hat{P}+\hat{P}\hat{\Phi}(t)+\sum_{l=1}^{q}\hat{Q}_l+\sum_{g=1}^{m}\hat{Q}_g+\sum_{g=1}^{m}\sigma_g^\star\hat{R}_g\right)\hat{e}(t)-2\hat{e}(t)'\hat{P}\sum_{l=1}^{q}A_l(t)\int_{t-\tau_l(t)}^{t}\dot{\hat{e}}(s)ds\\
&-2\hat{e}(t)'\hat{P}\sum_{g=1}^{m}\hat{A}_g(t)\int_{t-\sigma_g(t)}^{t}\dot{\hat{e}}(s)ds+2\hat{e}(t)'\hat{P}\sum_{g=1}^{m}\hat{\mathcal{A}}_g(t)\varepsilon(t)-2\hat{e}(t)'\hat{P}\sum_{g=1}^{m}\hat{\mathcal{A}}_g(t)\int_{t-\sigma_g(t)}^{t}\dot{\varepsilon}(s)ds\\
&-\sum_{l=1}^{q}\hat{e}(t-\tau_l(t))'\hat{Q}_l\hat{e}(t-\tau_l(t))(1-d_l)-\sum_{g=1}^{m}\hat{e}(t-\sigma_g(t))'\hat{Q}_g\hat{e}(t-\sigma_g(t))(1-d_g)\\
&+\hat{\eta}\dot{\hat{e}}(t)'\left(\sum_{l=1}^{q}\tau_l^\star\hat{W}_l+\sum_{g=1}^{m}\sigma_g^\star\hat{W}_g\right)\dot{\hat{e}}(t)-\hat{\eta}\sum_{l=1}^{q}\int_{t-\tau_l^\star}^{t}\dot{\hat{e}}(s)'\hat{W}_l\dot{\hat{e}}(s)ds-\hat{\eta}\sum_{g=1}^{m}\int_{t-\sigma_g^\star}^{t}\dot{\hat{e}}(s)'\hat{W}_g\dot{\hat{e}}(s)ds\\
&+2\varepsilon(t)'\hat{\Phi}(t)\hat{e}(t)-2\varepsilon(t)'\sum_{l=1}^{q}A_l(t)\int_{t-\tau_l(t)}^{t}\dot{\hat{e}}(s)ds-2\varepsilon(t)'\sum_{g=1}^{m}\hat{A}_g(t)\int_{t-\sigma_g(t)}^{t}\dot{\hat{e}}(s)ds\\
&+\varepsilon(t)'\left(\lambda_2(t)I_N+\hat{\eta}\sum_{g=1}^{m}\hat{\mathcal{Q}}_g+\eta\sum_{g=1}^{m}\sigma_g^\star\hat{\mathcal{R}}_g\right)\varepsilon(t)-2\varepsilon(t)'\sum_{g=1}^{m}\hat{\mathcal{A}}_g(t)\int_{t-\sigma_g(t)}^{t}\dot{\varepsilon}(s)ds\\
&-\hat{\eta}\sum_{g=1}^{m}\varepsilon(t-\sigma_g(t))'\hat{\mathcal{Q}}_g\varepsilon(t-\sigma_g(t))(1-d_g)+\eta\dot{\varepsilon}(t)'\sum_{g=1}^{m}\sigma_g^\star\hat{\mathcal{W}}_g\dot{\varepsilon}(t)\\
&-\hat{\eta}\sum_{g=1}^{m}\int_{t-\sigma_g^\star}^{t}\dot{\varepsilon}(s)'\hat{\mathcal{W}}_g\dot{\varepsilon}(s)ds-\sum_{g=1}^{m}\sigma_g^\star\hat{e}(t)'\hat{R}_g\hat{e}(t)-\hat{\eta}\sum_{g=1}^{m}\sigma_g^\star\varepsilon(t)'\hat{\mathcal{R}}_g\varepsilon(t)\\
&-\sum_{i=1}^{N}\sum_{j=1}^{N}\left(\hat{k}_{ij,1}^\star-\hat{k}_{ij,1}(t)\right)\dot{\hat{k}}_{ij,1}(t)-\sum_{i=1}^{N}\sum_{j=0}^{N}\left(\hat{k}_{ij,2}^\star-\hat{k}_{ij,2}(t)\right)\dot{\hat{k}}_{ij,2}(t)
\end{aligned}\tag{3.48}$$

Let us now introduce the following matrices:

$$\begin{aligned}
\hat{H}_1=\textstyle\sum_{g=1}^{m}\sigma_g^\star\hat{W}_g+\sum_{l=1}^{q}\tau_l^\star\hat{W}_l,\quad&\hat{H}_2(t)=\hat{\Phi}(t)'\hat{P}+\hat{P}\hat{\Phi}(t)+\textstyle\sum_{l=1}^{q}\hat{Q}_l+\sum_{g=l}^{m}\left(\hat{Q}_g+\sigma_g^\star\hat{R}_g\right),\\
\hat{M}_1=\textstyle\sum_{g=1}^{m}\sigma_g^\star\hat{\mathcal{W}}_g,\quad&\hat{M}_2(t)=\lambda_2(t)I_N+\hat{\eta}\textstyle\sum_{g=1}^{m}\left(\hat{\mathcal{Q}}_g+\sigma_g^\star\hat{\mathcal{R}}_g\right).
\end{aligned}\tag{3.49}$$

Then, according to [94, 75], by defining the following vector:

$$\hat{\rho}(t) = \left(\hat{e}(t)', \ \varepsilon(t)', \ \int_{t-\tau_l^\star}^{t} \dot{\hat{e}}(s)' ds, \ \int_{t-\sigma_g^\star}^{t} \dot{\hat{e}}(s)' ds, \ \int_{t-\sigma_g^\star}^{t} \dot{\varepsilon}(s)' ds \right)' \in \mathbb{R}^{5N}, \tag{3.50}$$

and by invoking the Jensen inequality (2.5) on the following integral terms:

$$\begin{aligned}
-\hat{\eta} \sum_{l=1}^{q} \int_{t-\tau_l^\star}^{t} \dot{\hat{e}}(s)' \hat{W}_l \dot{\hat{e}}(s) ds &\leq -\frac{\hat{\eta}}{\tau_l^\star} \left(\int_{t-\tau_l^\star}^{t} \dot{\hat{e}}(s) ds \right)' \hat{W}_l \left(\int_{t-\tau_l^\star}^{t} \dot{\hat{e}}(s) ds \right), \\
-\hat{\eta} \sum_{g=1}^{m} \int_{t-\sigma_g^\star}^{t} \dot{\hat{e}}(s)' \hat{W}_g \dot{\hat{e}}(s) ds &\leq -\frac{\hat{\eta}}{\sigma_g^\star} \left(\int_{t-\sigma_g^\star}^{t} \dot{\hat{e}}(s) ds \right)' \hat{W}_g \left(\int_{t-\sigma_g^\star}^{t} \dot{\hat{e}}(s) ds \right), \\
-\hat{\eta} \sum_{g=1}^{m} \int_{t-\sigma_g^\star}^{t} \dot{\varepsilon}(s)' \hat{\mathcal{W}}_g \dot{\varepsilon}(s) ds &\leq -\frac{\hat{\eta}}{\sigma_g^\star} \left(\int_{t-\sigma_g^\star}^{t} \dot{\varepsilon}(s) ds \right)' \hat{\mathcal{W}}_g \left(\int_{t-\sigma_g^\star}^{t} \dot{\varepsilon}(s) ds \right),
\end{aligned} \tag{3.51}$$

after substituting (3.49), and (3.51), the inequality (3.48) is further upper-estimated as follows:

$$\begin{aligned}
\dot{\bar{V}}(t) \leq & \rho(t)' \hat{\Sigma}(t) \hat{\rho}(t) + \hat{\eta} \dot{\hat{e}}(t)' \hat{H}_1 \dot{\hat{e}}(t) + \hat{\eta} \dot{\varepsilon}(t)' \hat{M}_1 \dot{\varepsilon}(t) - \sum_{l=1}^{q} \hat{e}(t-\tau_l(t))' \hat{Q}_l \hat{e}(t-\tau_l(t))(1-d_l) \\
& - \sum_{g=1}^{m} \hat{e}(t-\sigma_g(t))' \hat{Q}_g \hat{e}(t-\sigma_g(t))(1-d_g) - \hat{\eta} \sum_{g=1}^{m} \varepsilon(t-\sigma_g(t))' \hat{\mathcal{Q}}_g \varepsilon(t-\sigma_g(t))(1-d_g) \\
& - \sum_{g=1}^{m} \sigma_g^\star \hat{e}(t)' \hat{R}_g e(t) - \hat{\eta} \sum_{g=1}^{m} \sigma_g^\star \varepsilon(t)' \hat{\mathcal{R}}_g \varepsilon(t) \\
& - \sum_{i=1}^{N} \sum_{j=1}^{N} \left(\hat{k}_{ij,1}^\star - \hat{k}_{ij,1}(t) \right) \dot{\hat{k}}_{ij,1}(t) - \sum_{i=1}^{N} \sum_{j=0}^{N} \left(\hat{k}_{ij,2}^\star - \hat{k}_{ij,2}(t) \right) \dot{\hat{k}}_{ij,2}(t)
\end{aligned} \tag{3.52}$$

where

$$\hat{\Sigma}(t) = \begin{pmatrix}
\hat{H}_2(t) & 2\hat{P} \sum_{g=1}^{m} \hat{\mathcal{A}}_g(t) + 2\hat{\Phi}(t) & -2 \sum_{l=1}^{q} \hat{P} A_l(t) & -2 \sum_{g=1}^{m} \hat{P} \hat{A}_g(t) & -2 \sum_{g=1}^{m} \hat{P} \hat{\mathcal{A}}_g(t) \\
 & \hat{M}_2(t) & -2 \sum_{l=1}^{q} A_l(t) & -2 \sum_{g=1}^{m} \hat{A}_g(t) & -2 \sum_{g=1}^{m} \hat{\mathcal{A}}_g(t) \\
 & & -\frac{\hat{\eta}}{\tau_l^\star} \sum_{l=1}^{q} \hat{W}_l & 0_{N \times N} & 0_{N \times N} \\
 & 0 & & -\frac{\eta}{\sigma_g^\star} \sum_{g=1}^{m} \hat{W}_g & 0_{N \times N} \\
 & & & & -\frac{\hat{\eta}}{\sigma_g^\star} \sum_{g=1}^{m} \hat{\mathcal{W}}_g
\end{pmatrix}. \tag{3.53}$$

Define now the following augmented state vector:

$$\begin{aligned}
\hat{\xi}(t) = \big[& \hat{e}(t)', \ \varepsilon(t)', \ \hat{e}(t-\tau_1(t))', \ \ldots, \ \hat{e}(t-\tau_q(t))', \ \hat{e}(t-\sigma_1(t))', \ldots \\
& \ldots, \ \hat{e}(t-\sigma_m(t))', \varepsilon(t-\sigma_1(t))', \ \ldots, \ \varepsilon(t-\sigma_m(t))' \big]' \in \mathbb{R}^{2N+qN+2Nm},
\end{aligned} \tag{3.54}$$

then, by substituting (3.38) and (3.39) into the second and third term of (3.52), and after lengthy manipulations, (3.52) can finally be recast as next:

$$\begin{aligned}
\dot{\bar{V}}(t) \leq & \ \hat{\rho}(t)' \hat{\Sigma}(t) \hat{\rho}(t) + \hat{\eta} \hat{\xi}(t)' \hat{\Theta}(t) \hat{\xi}(t) \\
& - \sum_{i=1}^{N} \sum_{j=0}^{N} (\hat{k}_{ij,1}^\star - \hat{k}_{ij,1}(t))' \dot{\hat{k}}_{ij,1}(t) - \sum_{i=1}^{N} \sum_{j=1}^{N} (\hat{k}_{ij,2}^\star - \hat{k}_{ij,2}(t))' \dot{\hat{k}}_{ij,2}(t),
\end{aligned} \tag{3.55}$$

where $\hat{\Theta}(t)$ is an upper triangular block matrix in the from:

$$\hat{\Theta}(t) = \begin{pmatrix} -\frac{1}{\hat{\eta}}\sum_{g=1}^{m}\sigma_g^{\star}\hat{R}_g & 0_{N\times N} & \hat{\Theta}_{(1,2+i)} & \cdots \\ & -\frac{1}{\hat{\eta}}\sum_{g=1}^{m}\sigma_g^{\star}\hat{\mathcal{R}}_w & \vdots & \\ 0 & & \hat{\Theta}_{(2+i,2+i)} & \\ & & & \ddots \end{pmatrix}, \quad i = 1,2,\ldots,q+2m, \tag{3.56}$$

where $\hat{\Theta}_{(1,1)}$ and $\hat{\Theta}_{(2,2)} \prec 0$, whereas the other diagonal blocks take the following form:

$$\begin{aligned} \hat{\Theta}_{(2+l,2+l)} &= -\frac{(1-d_l)}{\hat{\eta}}\hat{Q}_l + \left(A_l(t)'\hat{H}_1A_l(t) + A_l(t)'\Omega'\hat{M}_1\Omega A_l(t)\right), \\ \hat{\Theta}_{(2+q+g,2+q+g)} &= -\frac{(1-d_g)}{\hat{\eta}}\hat{Q}_l + \left(\hat{A}_g(t)'\hat{H}_1\hat{A}_g(t) + \hat{A}_g(t)'\Omega'\hat{M}_1\Omega\hat{A}_g(t)\right), \\ \hat{\Theta}_{(2+q+m+g,2+q+m+g)} &= -\frac{(1-d_g)}{\hat{\eta}}\hat{\mathcal{Q}}_g + \left(\hat{\mathcal{A}}_g(t)'\hat{H}_1(t)\hat{A}_g(t) + \hat{\mathcal{A}}_g(t)'\hat{M}_1(t)\hat{\mathcal{A}}_g(t)\right). \end{aligned} \tag{3.57}$$

for $l = 1,2,\ldots,q$ and $g = 1,2,\ldots,m$. Now for the sake of compactness, let us rewrite (3.55) as:

$$\dot{V}(t) \leq \hat{\Lambda}_1(\hat{\rho}(t),\hat{k}_{ij,k}(t)) + \hat{\Lambda}_2(\xi(t),\hat{k}_{ij,k}(t)) + \hat{\Lambda}_3(\hat{k}_{ij,k}(t)) \tag{3.58}$$

being

$$\begin{aligned} &\hat{\Lambda}_1(\hat{\rho}(t),\hat{k}_{ij,k}(t)) = \hat{\rho}(t)'\hat{\Sigma}(t)\hat{\rho}(t) \quad , \quad \hat{\Lambda}_2(\hat{\xi}(t),\hat{k}_{ij,k}(t)) = \hat{\eta}\hat{\xi}(t)'\hat{\Theta}(t)\hat{\xi}(t) \\ &\hat{\Lambda}_3(\hat{k}_{ij,k}(t)) = -\sum_{i=1}^{N}\sum_{j=0}^{N}(\hat{k}_{ij,1}^{\star} - \hat{k}_{ij,1}(t))'\dot{\hat{k}}_{ij,1}(t) - \sum_{i=1}^{N}\sum_{j=1}^{N}(\hat{k}_{ij,2}^{\star} - \hat{k}_{ij,2}(t))'\dot{\hat{k}}_{ij,2}(t). \end{aligned} \tag{3.59}$$

Hence, if the LMIs (3.22)–(3.26) are satisfied, then the first two terms of (3.58), and thus the matrices $\hat{\Sigma}(t)$ in (3.53) and $\hat{\Theta}(t)$ in (3.56) are negative definite. Therefore, to have $\dot{V}(t) < 0$ we need to show that $\hat{\Lambda}_3(\hat{e}(t-\tau_{ij}),\varepsilon(t-\tau_{ij}),\hat{k}_{ij,k})$ is simply non positive. This fact will be proved by contradiction.

Indeed, given that by construction $\dot{\hat{k}}_{ij,k}(t) \geq 0$, obviously if each $\hat{k}_{ij,k}(t)$ is upper bounded, there will exist a constant $\hat{k}_{ij,k}^{\star}$ that guarantee the asymptotic stability of the closed-loop system. Otherwise, if we assumed that $\hat{k}_{ij,k}(t)$ were unbounded, we would get a contradiction. Indeed,both $\hat{\Lambda}_1(\hat{\rho}(t),\hat{k}_{ij,k}(t))$ and $\hat{\Lambda}_2(\xi(t),\hat{k}_{ij,k}(t))$ in (3.59) are quadratic functions of the error vectors $e(t)$ and $\varepsilon(t)$, while $\hat{\Lambda}_2(\xi(t),\hat{k}_{ij,k}(t))$ is a quadratic function also of the various $\hat{k}_{ij,k}(t)$, whereas $\hat{\Lambda}_3(\hat{k}_{ij,k})$ is simply a linear function of these various adaptive gains. Hence, if $\hat{k}_{ij,k}$ were unbounded, both $\hat{\Lambda}_2(\hat{\xi}(t),\hat{k}_{ij,k}(t))$ and $\hat{\Lambda}_3(\hat{k}_{ij,k})$ would diverge as well with $\hat{k}_{ij,k}(t)$, thus producing a contradiction. In fact, in that case, it would be possible to find a suitable value for $\hat{\eta}$ in (3.59) so that $|\hat{\Lambda}_2(\hat{\xi}(t),\hat{k}_{ij,k}(t))| \geq |\hat{\Lambda}_3(\hat{k}_{ij,k}(t))|$, $\forall\ \xi(t)$ and $\hat{k}_{ij,k}(t)$. However, since $\hat{\Lambda}_2(\hat{\xi}(t),\hat{k}_{ij,k}(t))$ is negative definite from the hypothesis, we have that $\dot{V}(t) < 0\ \forall$ $\hat{e}(t-\tau_{ij})$, $\varepsilon(t-\tau_{ij})$ and $\hat{k}_{ij,k}(t)$ against the assumption that $\hat{k}_{ij,k}$ diverged.
Finally, being $\hat{k}_{ij,k}(t)$ upper bounded and monotone increasing, then $\lim_{t\to\infty}\hat{k}_{ij,k}(t) =$

$c_{ij,k} < +\infty$. Thus, by choosing $\hat{k}^{\star}_{ij,k} = c_{ij,k}$, we have that $\dot{V}(t) < 0$ and thus also condition (2.2) of Theorem 2.2.1 is satisfied. Moreover, by choosing $\hat{\alpha}(s)$ as in (3.45), it follows that $\lim_{s\to\infty} \hat{\alpha}(s) = +\infty$, and hence the errors $\hat{e}(t)$ and $\varepsilon(t)$ globally uniformly converges to zero, and the frequency SC objectives result asymptotically achieved as well. This concludes the proof. ■

3.4 Voltage Secondary Controller Design

In the Chapter 2 (see Section 2.3), the model of an islanded MG was derived. In this section, based on this model and in order to solve the voltage SC problem (3.3) in the presence of communication delays among DGs we propose the following strategy:

$$\dot{v}_{n_i}(t) = \dot{\tilde{u}}_{n_i}(t) - \tilde{m}_i \cdot \text{sign}(\tilde{s}_i(t)), \tag{3.60}$$

$$\dot{\tilde{u}}_{n_i}(t) = -\sum_{j=0}^{N} \alpha_{ij} \tilde{k}_{ij}(t) \begin{bmatrix} v_i(t-\tau_{ij}(t)) - v_j(t-\tau_{ij}(t)) \\ \dot{v}_i(t-\tau_{ij}(t)) - \dot{v}_j(t-\tau_{ij}(t)) \end{bmatrix}, \tag{3.61}$$

where $\tilde{k}_{ij}(t) = [\tilde{k}_{ij,1}(t), \tilde{k}_{ij,2}(t)] \in \mathbb{R}^{1\times 2}$ is a vector of adaptive gains whose entries are updated according to:

$$\begin{array}{rcl} \dot{\tilde{k}}_{ij,1}(t) & = & \tilde{\zeta}_{ij,1} \cdot |v_i(t-\tau_{ij}(t)) - v_j(t-\tau_{ij}(t))|^2 \\ \dot{\tilde{k}}_{ij,2}(t) & = & \tilde{\zeta}_{ij,2} \cdot |\dot{v}_i(t-\tau_{ij}(t)) - \dot{v}_j(t-\tau_{ij}(t))|^2 \end{array} \tag{3.62}$$

with $\tilde{\zeta}_{ij,1}$ and $\tilde{\zeta}_{ij,2} \in \mathbb{R}_{>0}$ and $\tilde{k}_{ij,1}(0)$ and $\tilde{k}_{ij,2}(0) > 0$ and the switching function $\tilde{s}_i(t)$ in Equation (3.60) set as follows:

$$\tilde{s}_i = \dot{v}_i(t) + \tilde{z}_i(t) \tag{3.63}$$

$$\dot{\tilde{z}}_i(t) = \frac{\dot{v}_i(t)}{k_{v_i}} - \frac{1}{k_{v_i}} \dot{\tilde{u}}_{n_i}(t) \quad , \quad \tilde{z}_i(0) = -v_i(0) - \dot{v}_i(0) \tag{3.64}$$

Similar to previous subsection, the delays $\tau_{ij}(t)$ satisfy Assumption 3.3.1.

Remark 3.4.1 *Notice that the derivative of the DG's voltages $\dot{v}_i(t)$ in the voltage SC (3.61) are unknown and are not available from measurements. However, following [100], if the relative degree of the plant is known and constant, then robust exact differentiators with finite-time convergence properties can be employed to provide the full output-feedback control of any output variable of an uncertain dynamic system. Since the voltage dynamic (2.24) met this condition, and thanks to the finite-time convergence properties of standard high-order sliding mode differentiator [101, 102, 103, 104], in the remainder of the chapter we will refer to the quantities $\dot{v}_i$ as they were known, although they are estimated in practice by means of Levant differentiators. The Levant differentiation scheme is given below*

$$\begin{array}{rcl} \dot{\hat{v}}_i(t) & = & -c_1 \cdot |\hat{e}_{v,i}(t)|^{\frac{1}{2}} \cdot \text{sign}(\hat{e}_{v,i}(t)) + \bar{z}_i(t) \\ \dot{\bar{z}}_i(t) & = & -c_2 \cdot \text{sign}(\hat{e}_{v,i}(t)) \end{array} \tag{3.65}$$

where $\dot{\hat{v}}_i(t) \equiv \dot{v}_i(t)$, $\hat{e}_{v,i} = \hat{v}_i - v_i(t)$ is the sliding manifold of the differentiator and $c_1 > 1.5\bar{C}^{\frac{1}{2}}$, $c_2 > 1.1\bar{C}$, and $\bar{C}$ are the constant gains of the differentiator with $\bar{C}$ to be chosen large enough [103]. ■

Hereinafter the second main result of this chapter is outlined.

Theorem 3.4.1 *Consider the voltage dynamics Equation (2.24) under the voltage restoration SC Equations (3.60)-(3.64). Let Assumption 2.3.1 and Assumption 3.3.1 satisfied and let the communication topology $\mathcal{G}_N^c$ be described by a strongly connected graph $\mathcal{G}_N^c(\mathcal{V},\mathcal{E}^c)$, with weight α_{ij}, if $(i,j)\in\mathcal{E}^c$, 0 otherwise. Let node 0 be globally reachable on $\mathcal{G}_{N+1}^c$. Let $\tilde{A}_{i0}(t)=-\bar{B}_i\alpha_{i0}\tilde{k}_{i0}(t)$, $\tilde{A}_{ij}(t)=-\bar{B}_i\alpha_{ij}\tilde{k}_{ij}(t)\in\mathbb{R}^{2\times 2}$, and let*

$$A_0=[A_{0(r,y)}]\in\mathbb{R}^{2N\times 2N} \quad \text{with} \quad A_{0(r,y)}:\begin{cases}\bar{A}_i & \text{if } r=y=i\\ 0_{2\times 2} & \text{otherwise}\end{cases}, \tag{3.66}$$

$$\bar{\mathcal{A}}_l(t)=[A_{l(r,y)}(t)]\in\mathbb{R}^{2N\times 2N} \quad \text{with} \quad A_{l(r,r)}(t):\begin{cases}\tilde{A}_{i0}(t) & \text{if } \tau_l=\tau_{il},\ r=l=i\\ 0_{2\times 2} & \text{otherwise}\end{cases}, \tag{3.67}$$

$$\tilde{A}_g(t)=[\tilde{A}_{g(r,y)}(t)]\in\mathbb{R}^{2N\times 2N} \quad \text{with} \quad \tilde{A}_{g(r,y)}(t):\begin{cases}\tilde{A}_{ij}(t) & \text{if } \sigma_g=\tau_{ij},\ i\neq j,\ r=y=i\\ -\tilde{A}_{ij}(t) & \text{if } \sigma_g=\tau_{ij},\ i\neq j,\ r=i,\ y=j\\ 0_{2\times 2} & \text{otherwise}\end{cases} \tag{3.68}$$

with $r,y=1,2,\dots,N$, where by Lemma 3.3.1, results that

$$\tilde{\Phi}(t)=A_0+\sum_{l=1}^{q}\bar{\mathcal{A}}_l(t)+\sum_{g=1}^{m}\tilde{A}_g(t)\prec 0 \quad \forall \quad t\geq 0. \tag{3.69}$$

Let there exist $\tilde{m}_i>k_{v_i}\Gamma^Q=2k_{Q_i}\Pi_i^Q/\tau_{Q_i}$, and positive definite matrices $\tilde{P}$, $\tilde{Q}_l$, $\tilde{Q}_g$, $\tilde{R}_g$, $\tilde{W}_l$, $\tilde{W}_g\in\mathbb{R}^{N\times N}$ such that the following LMIs holds

$$\tilde{P}\tilde{\Phi}'(t)+\tilde{P}\tilde{\Phi}(t)\prec-\left(\sum_{l=1}^{q}\tilde{Q}_l+\sum_{g=1}^{m}\tilde{Q}_g+\sum_{g=1}^{m}\sigma_g^\star\tilde{R}_g\right) \tag{3.70}$$

$$-\sum_{g=1}^{m}\sigma_g^\star\tilde{R}_g\prec-\eta\left(A_0'\tilde{H}_1A_0\right) \tag{3.71}$$

$$-(1-d_l)\tilde{Q}_l\prec-\eta\left(\bar{\mathcal{A}}_l'(t)\tilde{H}_1\bar{\mathcal{A}}_l(t)\right) \tag{3.72}$$

$$-(1-d_g)\tilde{Q}_g\prec-\eta\left(\tilde{A}_g'(t)\tilde{H}_1\tilde{A}_g(t)\right) \tag{3.73}$$

where $\tilde{\eta}>0$, and

$$\tilde{H}_1=\sum_{g=1}^{m}\sigma_g^\star\tilde{W}_g+\sum_{l=1}^{q}\tau_l^\star\tilde{W}_l\succ 0 \quad , \quad \tilde{M}_1=\sum_{g=1}^{m}\sigma_g^\star\tilde{\mathcal{W}}_g\succ 0, \tag{3.74}$$

Then, condition (3.3) is verified, and the adaptive gains in (3.62) asymptotically converge to positive constants $\tilde{k}_{ij,1}^\star$ and $\tilde{k}_{ij,2}^\star$.

Lemma 3.4.1 *Let matrices A_0, $\bar{\mathcal{A}}_l(t)$, and $\tilde{A}_g(t)$ be defined as in (3.66), (3.67), (3.68). Assume $\mathcal{G}_N^c$ strongly connected, and node 0 in $\mathcal{G}_{N+1}^c$ globally reachable. Then $\tilde{\Phi}(t)=A_0+\sum_{l=1}^{q}\bar{\mathcal{A}}_l(t)+\sum_{g=1}^{m}\tilde{A}_g(t)$, as in (3.69), is Hurwitz, $\forall\ t\geq 0$.*

Proof of Lemma 3.4.1 *It is worth mentioning that $\tilde{\Phi}(t)$ in (3.69) is a strictly diagonally dominant block matrix, whose generic block element $\tilde{\Phi}_{(i,i)}\in\mathbb{R}^{2\times 2}$ on the main diagonal is defined as:*

$$\tilde{\Phi}_{(i,i)}(t)=\bar{A}_i+\tilde{A}_{i0}(t)+\sum_{j=1,i\neq j}^{N}\tilde{A}_{ij}(t) \tag{3.75}$$

To show that $\tilde{\Phi}(t)$ is negative definite, it suffices to prove that $\tilde{\Phi}_{(i,i)}(t)$, for $i = 1, \dots, N$, is a negative definite matrix. By construction $\dot{\tilde{k}}_{ij}(t) \geq 0$ and $\tilde{k}_{ij}(0) > 0$ (see Eq. (3.62)); then, according to the definition of $\tilde{A}_{ij}(t) = \bar{B}_i \alpha_{ij} \tilde{k}_{ij}(t)$, the term $\sum_{j=1}^{N} \tilde{A}_{ij}(t)$ is negative semi-definite. It follows that blocks $\tilde{\Phi}_{(i,i)}(t)$ in Eq. (3.75) are negative definite if the following matrices are negative definite:

$$\Psi_i(t) = A_i + \tilde{A}_{i0}(t) = \begin{bmatrix} 0 & 1 \\ -\frac{1}{k_{v_i}} \alpha_{ij} \tilde{k}_{i0,1}(t) & -\frac{1}{k_{v_i}} - \frac{1}{k_{v_i}} \alpha_{ij} \tilde{k}_{i0,2}(t) \end{bmatrix} \tag{3.76}$$

According to the construction $\tilde{k}_{i0}(t)$ in (3.62), it results that matrix $\Psi(t)$ is a negative definite. Consequently, it follows that the eigenvalues of $\tilde{\Phi}(t)$ have negative real part for all $t \geq 0$.

Proof of Theorem 3.4.1 ([105] and [106]) *By substituting (3.60)-(3.64) into (2.24), it yields:*

$$\begin{bmatrix} \dot{v}_i(t) \\ \ddot{v}_i(t) \end{bmatrix} = \bar{A}_i \begin{bmatrix} v_i(t) \\ \dot{v}_i(t) \end{bmatrix} + \begin{bmatrix} 0 \\ \frac{\dot{u}_i(t)}{k_{v_i}} \end{bmatrix} + \begin{bmatrix} 0 \\ \dot{\tilde{s}}_i(t) \end{bmatrix}, \tag{3.77}$$

$$\dot{\tilde{s}}_i = -\frac{\tilde{m}_i}{k_{v_i}} \text{sign}(\tilde{s}_i(t)) + \dot{\tilde{w}}_i(t). \tag{3.78}$$

For a differential equations with discontinuous right-hand side as (3.77) and (3.78), in the remainder, the resulting solutions $v_i(t)$, and $\tilde{s}_i(t)$ will be understood in the so-called Filippov sense. Namely, as the solution of an appropriate differential inclusion, the existence of which is guaranteed (owing on certain properties of the associated set-valued map) and for its absolute continuity is satisfied. The reader is referred to [73] for a comprehensive account of the necessary notions of non-smooth analysis.

Given that, and because of Assumption 2.3.1, and (2.28), $\|\dot{\tilde{w}}_i(t)\| \leq \Gamma_i^Q$, and $\tilde{m}_i > k_{v_i} \Gamma_i^Q$, and $\tilde{z}_i(0) = -v_i(0) - \dot{v}_i(0)$, by differentiating the following candidate Lyapunov functional:

$$\tilde{V}(t) = \frac{1}{2} \sum_{i=1}^{N} \tilde{s}_i(t)^2, \tag{3.79}$$

along the trajectories of (3.78), after straightforwards computations, it results that:

$$\dot{\tilde{V}}(t) = \sum_{i=1}^{N} \tilde{s}_i(t) \cdot \dot{\tilde{s}}_i(t) \leq \sum_{i=1}^{N} |\hat{s}_i(t) \cdot \dot{\tilde{w}}_i(t)| - \frac{\tilde{m}_i}{k_{v_i}} |\tilde{s}_i(t)| \leq -\sum_{i=1}^{N} \left(\frac{\tilde{m}_i}{k_{v_i}} - \Gamma_i^Q \right) \cdot |s_i(t)| < 0. \tag{3.80}$$

From this, one concludes that, except for points of Lebesgue measure zero (that can be disregarded in accordance with the Filippov Theory [73]), the condition $\hat{s}_i(t) = \dot{\hat{s}}_i(t) = 0$ is time-invariant for all $t \geq 0$. Now, by letting $\hat{s}_i = \dot{\hat{s}}_i = 0$ into (3.77), and by substituting (3.61), the following closed-loop dynamic takes place:

$$\begin{bmatrix} \dot{v}_i \\ \ddot{v}_i \end{bmatrix} = \bar{A}_i \cdot \begin{bmatrix} v_i \\ \dot{v}_i \end{bmatrix} - \bar{B}_i \sum_{j=0}^{N} \alpha_{ij} \tilde{k}_{ij} \begin{bmatrix} v_i(t - \tau_{ij}(t)) - v_j(t - \tau_{ij}(t)) \\ \dot{v}_i(t - \tau_{ij}(t)) - \dot{v}_j(t - \tau_{ij}(t)) \end{bmatrix}. \tag{3.81}$$

The point now is to find which conditions (3.81) have to met to asymptotically achieve the control objective (3.3). Now, given equation (3.81), defining the following voltage error

vector:

$$\tilde{e}(t) = \big(\tilde{e}_1(t), \quad \tilde{e}_2(t), \quad \ldots, \tilde{e}_N(t)\big)' \quad \text{with} \quad \tilde{e}_i(t) = \begin{bmatrix} v_i(t) - v_0 \\ \dot{v}_i(t) - \dot{v}_0 \end{bmatrix} \tag{3.82}$$

and by letting $\tilde{A}_{i0}(t) = -\bar{B}_i\alpha_{i0}\tilde{k}_{i0}(t)$, $\tilde{A}_{ij}(t) = -\tilde{B}_i\alpha_{ij}\tilde{k}_{ij}(t) \in \mathbb{R}^{2\times 2}$, *and by differentiating* $\tilde{e}_i(t)$ *and by considering* v_0 *is constant, after some algebraic manipulations, one derives:*

$$\dot{\tilde{e}}_i(t) = \bar{A}_i \cdot \tilde{e}(t) + \tilde{A}_{i0}(t) \cdot \tilde{e}_i(t - \tau_{i0}(t)) + \sum_{j=1}^{N} \tilde{A}_{ij}(t) \cdot \left[\tilde{e}_i(t - \tau_{ij}(t)) - \tilde{e}_j(t - \tau_{ij}(t))\right]. \tag{3.83}$$

Now, in order to provide a compact state-space representation of the networked error dynamics associated with the vectors (3.82), and accordingly with the notation introduced for the delays in (3.13) and (3.14), where $q = \text{card}\{\mathcal{T}(t)\}$ *and* $m = \text{card}\{\mathcal{S}(t)\}$, *it results:*

$$\dot{\tilde{e}}(t) = A_0 e(t) + \sum_{l=1}^{q} \bar{\mathcal{A}}_l(t)\tilde{e}(t - \tau_l(t)) + \sum_{g=1}^{m} \tilde{A}_g(t)\tilde{e}(t - \sigma_g(t)). \tag{3.84}$$

where, in accordance to (3.66)-(3.68), it results that:

$$A_0 = [A_{0(r,y)}] \in \mathbb{R}^{2N\times 2N} \quad \text{with} \quad A_{0(r,y)} : \begin{cases} \bar{A}_i & \text{if } r = y = i \\ 0_{2\times 2} & \text{otherwise} \end{cases},$$

$$\bar{\mathcal{A}}_l(t) = [\bar{\mathcal{A}}_{l(r,y)}(t)] \in \mathbb{R}^{2N\times 2N} \quad \text{with} \quad \bar{\mathcal{A}}_{l(r,r)}(t) : \begin{cases} \tilde{A}_{i0}(t) & \text{if } \tau_l = \tau_{il},\ r = l = i \\ 0_{2\times 2} & \text{otherwise} \end{cases},$$

$$\tilde{A}_g(t) = [\tilde{A}_{g(r,y)}(t)] \in \mathbb{R}^{2N\times 2N} \quad \text{with} \quad \tilde{A}_{g(r,y)}(t) : \begin{cases} \tilde{A}_{ij}(t) & \text{if } \sigma_g = \tau_{ij},\ i \neq j,\ r = y = i \\ -\tilde{A}_{ij}(t) & \text{if } \sigma_g = \tau_{ij},\ i \neq j,\ r = i,\ y = j \\ 0_{2\times 2} & \text{otherwise} \end{cases}$$

and $r, y = 1, 2, \ldots, N$. *For stability analysis purposes, and on the basis of the so-called Leibniz-Newton formula we introduce the following transformations:*

$$\tilde{e}(t - \tau(t)) = \tilde{e}(t) - \int_{t-\tau(t)}^{t} \dot{\tilde{e}}(s)ds. \tag{3.85}$$

Hence, from (3.85), the networked closed-loop dynamic in (3.84) can be recast as next:

$$\dot{\tilde{e}}(t) = \tilde{\Phi}(t)\tilde{e}(t) - \sum_{l=1}^{q} \bar{\mathcal{A}}_l(t) \int_{t-\tau_l(t)}^{t} \dot{\tilde{e}}(s)ds - \sum_{g=1}^{m} \tilde{A}_g(t) \int_{t-\sigma_g(t)}^{t} \dot{\tilde{e}}(s)ds, \tag{3.86}$$

where $\tilde{\Phi}(t) = A_0 + \sum_{l=1}^{q} \bar{\mathcal{A}}_l(t) + \sum_{g=1}^{m} \tilde{A}_g(t) \prec 0$ *by Lemma 3.4.1. Synchronization in the presence of multiple time-varying delays is proved here under the common Assumption 3.3.1,which requires that delays are bounded and slowly time varying signals [44, 94, 98,*

99]. Inspired by [44], let us now construct the following Lyapunov-Krasovskii functional:

$$\begin{aligned}\overline{V}(t) =&\tilde{e}(t)'\tilde{P}\tilde{e}(t) + \sum_{l=1}^{q}\int_{t-\tau_l(t)}^{t}\tilde{e}(s)'\tilde{Q}_l\tilde{e}(s)ds + \sum_{g=1}^{m}\int_{t-\sigma_g(t)}^{t}\tilde{e}(s)'\tilde{Q}_g\tilde{e}(s)ds\\ &+\tilde{\eta}\sum_{l=1}^{q}\int_{-\tau_l^\star}^{0}\int_{t+\theta}^{t}\dot{\tilde{e}}(s)'\tilde{W}_l\dot{\tilde{e}}(s)dsd\theta + \tilde{\eta}\sum_{g=1}^{m}\int_{-\sigma_g^\star}^{0}\int_{t+\theta}^{t}\dot{\tilde{e}}(s)'\tilde{W}_g\dot{\tilde{e}}(s)dsd\theta\\ &+\sum_{i=1}^{N}\sum_{j=1}^{N}\frac{1}{2}\left(\tilde{k}_{ij}^\star-\tilde{k}_{ij}(t)\right)'\left(\tilde{k}_{ij}^\star-\tilde{k}_{ij}(t)\right),\end{aligned} \tag{3.87}$$

where $\tilde{P}$, $\tilde{Q}_l$, $\tilde{Q}_g$, $\tilde{W}_l$, $\tilde{W}_g \in \mathbb{R}^{2N\times 2N}$ are constant, symmetric, and positive definite matrices to be determined and $\tilde{\eta}$ is a positive scalar. Following the requirements of Theorem 3.4.1, let us note that the following relation is satisfied:

$$\tilde{\alpha}(\tilde{e}(t)) \le \overline{V}(t) \le \tilde{\beta}(\tilde{e}(t-\hat{\tau})). \tag{3.88}$$

where $\tilde{\alpha}(\tilde{e}(t)$ and $\tilde{\beta}(\tilde{e}(t))$ are continuous non-decreasing positive functions defined as follows:

$$\tilde{\alpha}(\tilde{e}(t)) = \tilde{e}(t)'\tilde{P}\tilde{e}(t), \tag{3.89}$$

$$\begin{aligned}\tilde{\beta}(\tilde{e}(t)) =&e(t)'\tilde{P}\tilde{e}(t) + \sum_{l=1}^{q}\int_{t-\hat{\tau}}^{t}\tilde{e}(s)'\tilde{Q}_l\tilde{e}(s)ds + \sum_{g=1}^{m}\int_{t-\hat{\tau}}^{t}\tilde{e}(s)'\tilde{Q}_g e(s)ds\\ &+\tilde{\eta}\sum_{l=1}^{q}\int_{-\hat{\tau}}^{0}\int_{t+\theta}^{t}\dot{\tilde{e}}(s)'\tilde{W}_l\dot{\tilde{e}}(s)dsd\theta + \tilde{\eta}\sum_{g=1}^{m}\int_{-\hat{\tau}}^{0}\int_{t+\theta}^{t}\dot{\tilde{e}}(s)'\tilde{W}_g\dot{\tilde{e}}(s)dsd\theta\\ &+\sum_{i=1}^{N}\sum_{j=1}^{N}\frac{1}{2}\left(\tilde{k}_{ij}^\star-\tilde{k}_{ij}(t)\right)'\left(\tilde{k}_{ij}^\star-\tilde{k}_{ij}(t)\right),\end{aligned} \tag{3.90}$$

where $\hat{\tau} = \max_{l,g}\{\tau_l^\star,\ \ \sigma_g^\star\}$. Now, differentiating (3.79) along the trajectories of (3.86), it follows that:

$$\begin{aligned}\dot{\overline{V}}(t) =&\tilde{e}(t)'\left(\tilde{\Phi}(t)'\tilde{P}+\tilde{P}\tilde{\Phi}(t)\right)\tilde{e}(t) - 2\tilde{e}(t)'\tilde{P}\sum_{l=1}^{q}\bar{A}_l(t)\int_{t-\tau_l(t)}^{t}\dot{\tilde{e}}(s)ds\\ &-2\tilde{e}(t)'\tilde{P}\sum_{g=1}^{m}\tilde{A}_g(t)\int_{t-\sigma_g(t)}^{t}\dot{\tilde{e}}(s)ds - \sum_{l=1}^{q}\tilde{e}(t-\tau_l(t))'\tilde{Q}_l\tilde{e}(t-\tau_l(t))(1-\dot{\tau}_l(t))\\ &+\tilde{e}(t)'\sum_{l=1}^{q}\tilde{Q}_l\tilde{e}(t) + \tilde{e}(t)'\sum_{g=1}^{m}\tilde{Q}_g\tilde{e}(t) - \sum_{g=1}^{m}\tilde{e}(t-\sigma_g(t))'\tilde{Q}_g\tilde{e}(t-\sigma_g(t))(1-\dot{\sigma_g}(t))\\ &+\eta\dot{\tilde{e}}(t)'\sum_{l=1}^{q}\tau_l^\star\tilde{W}_l\dot{\tilde{e}}(t) - \tilde{\eta}\sum_{l=1}^{q}\int_{t-\tau_l^\star}^{t}\dot{\tilde{e}}(s)'\tilde{W}_l\dot{\tilde{e}}(s)ds\\ &+\tilde{\eta}\dot{\tilde{e}}(t)'\sum_{g=1}^{m}\sigma_g^\star\tilde{W}_g\dot{\tilde{e}}(t) - \tilde{\eta}\sum_{g=1}^{m}\int_{t-\sigma_g^\star}^{t}\dot{\tilde{e}}(s)'\tilde{W}_g\dot{\tilde{e}}(s)ds - \sum_{i=1}^{N}\sum_{j=0}^{N}\left(\tilde{k}_{ij}^\star-\tilde{k}_{ij}(t)\right)'\dot{\tilde{k}}_{ij}(t)\end{aligned} \tag{3.91}$$

Now, by exploiting Assumption 3.3.1, which requires that delays are bounded, namely $\tau_l \in [0,\tau^\star)$, $\sigma_g \in [0,\sigma_g^\star)$, and slowly time varying, i.e. $\dot{\tau}_l \le d_l < 1$, $\dot{\sigma}_g \le d_g < 1$ [44, 94, 99], and by adding to the right-hand side of (3.91) the next identically zero quadratic

function:

$$\sum_{g=1}^{m}\sigma_g^\star\tilde{e}(t)'\tilde{R}_g\tilde{e}(t)-\sum_{g=1}^{m}\sigma_g^\star\tilde{e}(t)'\tilde{R}_g\tilde{e}(t)=0,$$

where R_g is a positive definite matrix to be determined, after some algebraic manipulation, (3.91) can be upper-estimated as follows:

$$\begin{aligned}\dot{\bar{V}}(t)\leq&\tilde{e}(t)'\left(\tilde{\Phi}(t)'\tilde{P}+\tilde{P}\tilde{\Phi}(t)+\sum_{l=1}^{q}\tilde{Q}_l+\sum_{g=1}^{m}\tilde{Q}_g+\sum_{g=1}^{m}\sigma_g^\star\tilde{R}_g\right)\tilde{e}(t)-2\tilde{e}(t)'\tilde{P}\sum_{l=1}^{q}\tilde{\mathcal{A}}_l(t)\int_{t-\tau_l(t)}^{t}\dot{\tilde{e}}(s)ds\\&-2\tilde{e}(t)'\tilde{P}\sum_{g=1}^{m}\tilde{A}_g(t)\int_{t-\sigma_g(t)}^{t}\dot{\tilde{e}}(s)ds-\sum_{l=1}^{q}\tilde{e}(t-\tau_l(t))'\tilde{Q}_l\tilde{e}(t-\tau_l(t))(1-d_l)\\&-\sum_{g=1}^{m}\tilde{e}(t-\sigma_g(t))'\tilde{Q}_g\tilde{e}(t-\sigma_g(t))(1-d_g)+\tilde{\eta}\dot{\tilde{e}}(t)'\left(\sum_{l=1}^{q}\tau_l^\star\tilde{W}_l+\sum_{g=1}^{m}\sigma_g^\star\tilde{W}_g\right)\dot{\tilde{e}}(t)\\&-\tilde{\eta}\sum_{l=1}^{q}\int_{t-\tau_l^\star}^{t}\dot{\tilde{e}}(s)'\tilde{W}_l\dot{\tilde{e}}(s)ds-\tilde{\eta}\sum_{g=1}^{m}\int_{t-\sigma_g^\star}^{t}\dot{\tilde{e}}(s)'\tilde{W}_g\dot{\tilde{e}}(s)ds-\tilde{e}(t)'\sum_{g=1}^{m}\sigma_g^\star\tilde{R}_g\tilde{e}(t)\\&-\sum_{i=1}^{N}\sum_{j=0}^{N}\left(\tilde{k}_{ij}^\star-\tilde{k}_{ij}(t)\right)'\dot{\tilde{k}}_{ij}(t)\end{aligned}\tag{3.92}$$

Let us now introduce the following matrices:

$$\begin{aligned}\tilde{H}_1&=\sum_{g=1}^{m}\sigma_g^\star\tilde{W}_g+\sum_{l=1}^{q}\tau_l^\star\tilde{W}_l,\\\tilde{H}_2(t)&=\tilde{\Phi}(t)'\tilde{P}+\tilde{P}\tilde{\Phi}(t)+\sum_{l=1}^{q}\tilde{Q}_l+\sum_{g=1}^{m}\left(\tilde{Q}_g+\sigma_g^\star\tilde{R}_g\right).\end{aligned}\tag{3.93}$$

Then, according to [94, 75], by defining the following vector:

$$\tilde{\rho}(t)=\left(\tilde{e}(t)',\ \int_{t-\tau_l^\star}^{t}\dot{\tilde{e}}(s)'ds,\ \int_{t-\sigma_g^\star}^{t}\dot{\tilde{e}}(s)'ds\right)'\in\mathbb{R}^{6N},\tag{3.94}$$

and by invoking the Jensen inequality (2.5) on the following integral terms:

$$\begin{aligned}-\tilde{\eta}\sum_{l=1}^{q}\int_{t-\tau_l^\star}^{t}\dot{\tilde{e}}(s)'\tilde{W}_l\dot{\tilde{e}}(s)ds&\leq-\frac{\tilde{\eta}}{\tau_l^\star}\left(\int_{t-\tau_l^\star}^{t}\dot{\tilde{e}}(s)ds\right)'\sum_{l=1}^{q}\tilde{W}_l\left(\int_{t-\tau_l^\star}^{t}\dot{\tilde{e}}(s)ds\right),\\-\tilde{\eta}\sum_{g=1}^{m}\int_{t-\sigma_g^\star}^{t}\dot{\tilde{e}}(s)'\tilde{W}_g\dot{\tilde{e}}(s)ds&\leq-\frac{\tilde{\eta}}{\sigma_g^\star}\left(\int_{t-\sigma_g^\star}^{t}\dot{\tilde{e}}(s)ds\right)'\sum_{g=1}^{m}\tilde{W}_g\left(\int_{t-\sigma_g^\star}^{t}\dot{\tilde{e}}(s)ds\right),\end{aligned}\tag{3.95}$$

after substituting (3.93), *and* (3.95), *the inequality* (3.92) *is further upper-estimated as follows:*

$$\begin{aligned}\dot{\tilde{V}}(t) \leq & \tilde{\rho}(t)'\tilde{\Sigma}(t)\tilde{\rho}(t) + \eta\dot{\tilde{e}}(t)'\tilde{H}_1\dot{\tilde{e}}(t) - \sum_{l=1}^{q}\tilde{e}(t-\tau_l(t))'\tilde{Q}_l e(t-\tau_l(t))(1-d_l) \\ & - \tilde{e}(t)'\sum_{g=1}^{m}\sigma_g^\star\tilde{R}_g\tilde{e}(t) - \sum_{g=1}^{m}\tilde{e}(t-\sigma_g(t))'\tilde{Q}_g\tilde{e}(t-\sigma_g(t))(1-d_g) \\ & - \sum_{i=1}^{N}\sum_{j=0}^{N}\left(\tilde{k}_{ij}^\star - \tilde{k}_{ij}(t)\right)'\dot{\tilde{k}}_{ij}(t) \end{aligned} \tag{3.96}$$

where

$$\tilde{\Sigma}(t) = \begin{pmatrix} \tilde{H}_2(t) & -2\sum_{l=1}^{q}\tilde{P}\tilde{\mathcal{A}}_l(t) & -2\sum_{g=1}^{m}\tilde{P}\tilde{A}_g(t) \\ 0_{2N\times 2N} & -\frac{\tilde{\eta}}{\tau_l^\star}\sum_{l=1}^{q}\tilde{W}_l & 0_{2N\times 2N} \\ 0_{2N\times 2N} & 0_{2N\times 2N} & -\frac{\tilde{\eta}}{\sigma_g^\star}\sum_{g=1}^{m}\tilde{W}_g \end{pmatrix}. \tag{3.97}$$

Define now the following augmented state vector:

$$\begin{aligned}\tilde{\xi}(t) = & [\tilde{e}(t)',\ \tilde{e}(t-\tau_1(t))',\ \ldots,\ \tilde{e}(t-\tau_q(t))', \\ & \tilde{e}(t-\sigma_1(t))',\ldots,\ \tilde{e}(t-\sigma_m(t))']' \in \mathbb{R}^{2N(1+q+m)}, \end{aligned} \tag{3.98}$$

then, by substituting (3.84) *into the second term of* (3.96), *and after lengthy manipulations,* (3.96) *can finally be recast as next:*

$$\dot{\tilde{V}}(t) \leq \tilde{\rho}(t)'\tilde{\Sigma}(t)\tilde{\rho}(t) + \tilde{\eta}\tilde{\xi}(t)'\tilde{\Theta}(t)\tilde{\xi}(t) - \sum_{i=1}^{N}\sum_{j=0}^{N}\left(\tilde{k}_{ij}^\star - \tilde{k}_{ij}(t)\right)'\dot{\tilde{k}}_{ij}(t), \tag{3.99}$$

where $\tilde{\Theta}(t) \in \mathbb{R}^{2N(1+q+m)\times 2N(1+q+m)}$ *is an upper triangular block matrix in the from:*

$$\tilde{\Theta}(t) = \begin{pmatrix} \tilde{\Theta}_{1,1} & 2A_0'\tilde{H}_1A_1 & \ldots & \ldots & 2A_0'\tilde{H}_1A_q & 2A_0'\tilde{H}_1\tilde{A}_1 & \ldots & 2A_0'\tilde{H}_1\tilde{A}_m \\ 0_{2N\times 2N} & \tilde{\Theta}_{2,2} & 2A_1'\tilde{H}_1A_2 & \ldots & 2A_1'\tilde{H}_1A_q & 2A_1'\tilde{H}_1\tilde{A}_1 & \ldots & 2A_1'\tilde{H}_1\tilde{A}_m \\ \vdots & 0_{2N\times 2N} & \ddots & \ddots & \ldots & \ldots & \ldots & \vdots \\ \vdots & \vdots & \ddots & \ddots & 2A_q'\tilde{H}_1\tilde{A}_1 & \ldots & \ldots & \vdots \\ \vdots & \vdots & \vdots & \ddots & \tilde{\Theta}_{q+1,q+1} & 2\tilde{A}_1'\tilde{H}_1\tilde{A}_2 & \vdots & \vdots \\ \vdots & \vdots & \ldots & \ddots & 0_{2N\times 2N} & \tilde{\Theta}_{q+2,q+2} & \ddots & \vdots \\ \vdots & \vdots & \ldots & \ldots & \ldots & 0_{2N\times 2N} & \ddots & 2\tilde{A}_{m-1}'\tilde{H}_1\tilde{A}_m \\ 0_{2N\times 2N} & \ldots & \ldots & \ldots & \ldots & \ldots & 0_{2N\times 2N} & \tilde{\Theta}_{q+m+1,q+m+1} \end{pmatrix} \tag{3.100}$$

where the diagonal blocks take the following form:

$$\begin{aligned}\tilde{\Theta}_{(1,1)}(t) &= -\frac{1}{\tilde{\eta}}\sum_{g=1}^{m}\sigma_g^\star R_g + \left(A_0'\tilde{H}_1A_0\right), \\ \tilde{\Theta}_{(1+l,1+l)}(t) &= -\frac{(1-d_l)}{\tilde{\eta}}\tilde{Q}_l + \left(\tilde{\mathcal{A}}_l(t)'\tilde{H}_1\tilde{\mathcal{A}}_l(t)\right), \quad l = 1,2,\ldots,q, \\ \tilde{\Theta}_{(1+q+g,1+q+g)}(t) &= -\frac{(1-d_g)}{\tilde{\eta}}\tilde{Q}_g + \left(\tilde{A}_g(t)'\tilde{H}_1\tilde{A}_g(t)\right), \quad g = 1,2,\ldots,m. \end{aligned} \tag{3.101}$$

Now for the sake of compactness, let us rewrite (3.99) as:

$$\dot{\tilde{V}}(t) \leq \tilde{\Lambda}_1(\tilde{\rho}(t), \tilde{k}_{ij}(t)) + \tilde{\Lambda}_2(\tilde{\xi}(t), \tilde{k}_{ij}(t)) + \tilde{\Lambda}_3(\tilde{k}_{ij}(t)) \tag{3.102}$$

with

$$\tilde{\Lambda}_1(\tilde{\rho}(t), \tilde{k}_{ij}(t)) = \tilde{\rho}(t)'\tilde{\Sigma}(t)\tilde{\rho}(t) \quad , \quad \tilde{\Lambda}_2(\tilde{\xi}(t), \tilde{k}_{ij}(t)) = \tilde{\eta}\tilde{\xi}(t)'\tilde{\Theta}(t)\tilde{\xi}(t)$$
$$\tilde{\Lambda}_3(\tilde{k}_{ij}(t)) = -\sum_{i=1}^{N}\sum_{j=0}^{N}\left(\tilde{k}_{ij}^{\star} - \tilde{k}_{ij}(t)\right)'\dot{\tilde{k}}_{ij}(t). \tag{3.103}$$

Hence, if the LMIs (3.73)-(3.70) are satisfied, then according to the same explanations of Proof of Theorem 3.3.1 we have that $\dot{\tilde{V}}(t) < 0$ and thus also condition (2.2) of Theorem 2.2.1 is satisfied. Moreover, by choosing $\tilde{\alpha}(s)$ as in (3.89), it follows that $\lim_{s\to\infty}\bar{\alpha}(s) = +\infty$, and hence the errors $\tilde{e}(t)$ globally uniformly converges to zero, and the voltage SC objective result asymptotically achieved as well. Furthermore, it results that the adaptive gains of (3.61) also converge to constant quantities according to:

$$\lim_{t\to\infty}\tilde{k}_{ij}(t) = \tilde{k}_{ij}^{\star}. \tag{3.104}$$

This concludes the proof. ■

3.5 Results and Discussion

3.5.1 Test Rig Design

The proposed SCs are tested on a $220V_{RMS}$ (per phase rms), 50Hz, islanded MG of four DGs as the one depicted in Figure 3.1. The MG parameters are listed on Table 3.1. The electrical and communication network models are shown in Figure 3.1 with $\mathcal{E}_{N+1}^{c} = \{(0,1),(1,2),(2,1),(2,3),(3,2),(3,4),(4,3)\}$. The tuning parameters of the SCs systems Equations (3.6)-(3.12) and Equations (3.60)-(3.62) are set as

$$\begin{array}{c}\tilde{k}_{ij}(0) = [10,10],\ \hat{k}_{ij,1}(0) = 5,\ \hat{k}_{ij,2}(0) = 10,\\ \hat{\zeta}_{ij,1} = \tilde{\zeta}_{ij,1} = \hat{\zeta}_{ij,2} = \tilde{\zeta}_{ij,2} = 0.5,\ \hat{m}_i = 0.001,\ \tilde{m}_i = 0.1,\end{array} \quad \forall\ (i,j) \in \mathcal{E}_{N+1}^{c}. \tag{3.105}$$

We assume that only DG 1 can directly access the reference voltage v_0 and frequency ω_0. From Assumption 3.3.1, the time derivatives of the communication delays between agents, $\dot{\tau}_{ij} \in \mathbb{R}_{>0}$, were modeled as random variables with a uniform distribution in the range $|\dot{\tau}_{ij}| \leq d_l = d_g = 1$, and conditions $\tau_{ij} \in [0, 0.1]s$ are enforced by means of limiters [44, 94]. Moreover, according to the communication network model, $q = 1$ in (3.14) and $m = 6$ in (3.13). Hence, from (3.14)-(3.13), it results that $\mathcal{T}(t) = \{\tau_1(t)\}$ and $\mathcal{S}(t) = \{\sigma_1(t), \sigma_2(t), \ldots, \sigma_6(t)\}$ with $\tau_1(t) = \tau_{10}(t)$, $\sigma_1(t) = \tau_{12}(t)$, $\sigma_2(t) = \tau_{21}(t)$, $\sigma_3(t) = \tau_{23}(t)$, $\sigma_4(t) = \tau_{32}(t)$, $\sigma_5(t) = \tau_{34}(t)$ and $\sigma_6(t) = \tau_{43}(t)$. Finally, matrices $A_l(t) \in \mathbb{R}^{4\times4}$, $\bar{A}_l(t) \in \mathbb{R}^{8\times8}$, $\hat{A}_g(t) \in \mathbb{R}^{4\times4}$, $\hat{\mathcal{A}}_g(t) \in \mathbb{R}^{4\times4}$ and $\tilde{\mathcal{A}}_g(t) \in \mathbb{R}^{8\times8}$ have the following structures ($l = 1; g = 1, ..., 6$)

$$A_1(t) = \begin{pmatrix} \hat{A}_{10}(t) & 0 & 0 & 0 \\ 0 & 0 & 0 & 0 \\ 0 & 0 & 0 & 0 \\ 0 & 0 & 0 & 0 \end{pmatrix} \quad , \quad \hat{A}_1(t) = \begin{pmatrix} \hat{A}_{12}(t) & -\hat{A}_{12}(t) & 0 & 0 \\ 0 & 0 & 0 & 0 \\ 0 & 0 & 0 & 0 \\ 0 & 0 & 0 & 0 \end{pmatrix},$$

$$\hat{A}_2(t) = \begin{pmatrix} 0 & 0 & 0 & 0 \\ -\hat{A}_{21}(t) & \hat{A}_{21}(t) & 0 & 0 \\ 0 & 0 & 0 & 0 \\ 0 & 0 & 0 & 0 \end{pmatrix}, \quad \hat{A}_3(t) = \begin{pmatrix} 0 & 0 & 0 & 0 \\ 0 & \hat{A}_{23}(t) & -\hat{A}_{23}(t) & 0 \\ 0 & 0 & 0 & 0 \\ 0 & 0 & 0 & 0 \end{pmatrix},$$

$$\hat{A}_4(t) = \begin{pmatrix} 0 & 0 & 0 & 0 \\ 0 & 0 & 0 & 0 \\ 0 & -\hat{A}_{23}(t) & \hat{A}_{32}(t) & 0 \\ 0 & 0 & 0 & 0 \end{pmatrix}, \quad \hat{A}_5(t) = \begin{pmatrix} 0 & 0 & 0 & 0 \\ 0 & 0 & 0 & 0 \\ 0 & 0 & \hat{A}_{34}(t) & -\hat{A}_{34}(t) \\ 0 & 0 & 0 & 0 \end{pmatrix},$$

$$\hat{A}_6(t) = \begin{pmatrix} 0 & 0 & 0 & 0 \\ 0 & 0 & 0 & 0 \\ 0 & 0 & 0 & 0 \\ 0 & 0 & -\hat{A}_{43}(t) & \hat{A}_{43}(t) \end{pmatrix}, \quad \hat{\mathcal{A}}_1(t) = \begin{pmatrix} \hat{A}_{12}(t) & -\hat{A}_{12}(t) & 0 & 0 \\ 0 & 0 & 0 & 0 \\ 0 & 0 & 0 & 0 \\ 0 & 0 & 0 & 0 \end{pmatrix},$$

$$\hat{\mathcal{A}}_2(t) = \begin{pmatrix} 0 & 0 & 0 & 0 \\ -\hat{\mathcal{A}}_{21}(t) & \hat{\mathcal{A}}_{21}(t) & 0 & 0 \\ 0 & 0 & 0 & 0 \\ 0 & 0 & 0 & 0 \end{pmatrix}, \quad \hat{\mathcal{A}}_3(t) = \begin{pmatrix} 0 & 0 & 0 & 0 \\ 0 & \hat{\mathcal{A}}_{23}(t) & -\hat{\mathcal{A}}_{23}(t) & 0 \\ 0 & 0 & 0 & 0 \\ 0 & 0 & 0 & 0 \end{pmatrix},$$

$$\hat{\mathcal{A}}_4(t) = \begin{pmatrix} 0 & 0 & 0 & 0 \\ 0 & 0 & 0 & 0 \\ 0 & -\hat{\mathcal{A}}_{32}(t) & \hat{\mathcal{A}}_{32}(t) & 0 \\ 0 & 0 & 0 & 0 \end{pmatrix}, \quad \hat{\mathcal{A}}_5(t) = \begin{pmatrix} 0 & 0 & 0 & 0 \\ 0 & 0 & 0 & 0 \\ 0 & 0 & \hat{\mathcal{A}}_{34}(t) & -\hat{\mathcal{A}}_{34}(t) \\ 0 & 0 & 0 & 0 \end{pmatrix},$$

$$\hat{\mathcal{A}}_6(t) = \begin{pmatrix} 0 & 0 & 0 & 0 \\ 0 & 0 & 0 & 0 \\ 0 & 0 & 0 & 0 \\ 0 & 0 & -\hat{\mathcal{A}}_{43}(t) & \hat{\mathcal{A}}_{43}(t) \end{pmatrix}, \quad \bar{\mathcal{A}}_1(t) = \begin{pmatrix} \tilde{A}_{i0}(t) & 0_{2\times2} & 0_{2\times2} & 0_{2\times2} \\ 0_{2\times2} & 0_{2\times2} & 0_{2\times2} & 0_{2\times2} \\ 0_{2\times2} & 0_{2\times2} & 0_{2\times2} & 0_{2\times2} \\ 0_{2\times2} & 0_{2\times2} & 0_{2\times2} & 0_{2\times2} \end{pmatrix},$$

$$\tilde{A}_1(t) = \begin{pmatrix} \tilde{A}_{12}(t) & -\tilde{A}_{12}(t) & 0_{2\times2} & 0_{2\times2} \\ 0_{2\times2} & 0_{2\times2} & 0_{2\times2} & 0_{2\times2} \\ 0_{2\times2} & 0_{2\times2} & 0_{2\times2} & 0_{2\times2} \\ 0_{2\times2} & 0_{2\times2} & 0_{2\times2} & 0_{2\times2} \end{pmatrix}, \quad \tilde{A}_2(t) = \begin{pmatrix} 0_{2\times2} & 0_{2\times2} & 0_{2\times2} & 0_{2\times2} \\ -\tilde{A}_{21}(t) & \tilde{A}_{21}(t) & 0_{2\times2} & 0_{2\times2} \\ 0_{2\times2} & 0_{2\times2} & 0_{2\times2} & 0_{2\times2} \\ 0_{2\times2} & 0_{2\times2} & 0_{2\times2} & 0_{2\times2} \end{pmatrix},$$

$$\tilde{A}_3(t) = \begin{pmatrix} 0_{2\times2} & 0_{2\times2} & 0_{2\times2} & 0_{2\times2} \\ 0_{2\times2} & \tilde{A}_{23}(t) & -\tilde{A}_{23}(t) & 0_{2\times2} \\ 0_{2\times2} & 0_{2\times2} & 0_{2\times2} & 0_{2\times2} \\ 0_{2\times2} & 0_{2\times2} & 0_{2\times2} & 0_{2\times2} \end{pmatrix}, \quad \tilde{A}_4(t) = \begin{pmatrix} 0_{2\times2} & 0_{2\times2} & 0_{2\times2} & 0_{2\times2} \\ 0_{2\times2} & 0_{2\times2} & 0_{2\times2} & 0_{2\times2} \\ 0_{2\times2} & -\tilde{A}_{32}(t) & \tilde{A}_{32}(t) & 0_{2\times2} \\ 0_{2\times2} & 0_{2\times2} & 0_{2\times2} & 0_{2\times2} \end{pmatrix},$$

$$\tilde{A}_5(t) = \begin{pmatrix} 0_{2\times2} & 0_{2\times2} & 0_{2\times2} & 0_{2\times2} \\ 0_{2\times2} & 0_{2\times2} & 0_{2\times2} & 0_{2\times2} \\ 0_{2\times2} & 0_{2\times2} & \tilde{A}_{34}(t) & -\tilde{A}_{34}(t) \\ 0_{2\times2} & 0_{2\times2} & 0_{2\times2} & 0_{2\times2} \end{pmatrix}, \quad \tilde{A}_6(t) = \begin{pmatrix} 0_{2\times2} & 0_{2\times2} & 0_{2\times2} & 0_{2\times2} \\ 0_{2\times2} & 0_{2\times2} & 0_{2\times2} & 0_{2\times2} \\ 0_{2\times2} & 0_{2\times2} & 0_{2\times2} & 0_{2\times2} \\ 0_{2\times2} & 0_{2\times2} & -\tilde{A}_{43}(t) & \tilde{A}_{43}(t) \end{pmatrix}.$$

3.5.2 Case Study

The system is tested for 45 seconds. The list of events scheduled throughout the test is displayed as follows:

- Step 1 ($t = 0 - 5$sec): Only the PC is used with $\omega_{ni} = 2\pi 50$Hz, $v_{ni} = 220\text{V}_{\text{RMS}}$ (per phase rms);
- Step 2 ($t = 5$sec): The frequency SC Equations (3.6)-(3.12) is activated with $\omega_0 = 2\pi 50$Hz;
- Step 3 ($t = 10$sec): The voltage SC Equations (3.33)-(3.34) is activated with $v_0 = 220\text{V}_{\text{RMS}}$
- Step 4 ($t = 15 - 20$sec): The load (P_{L3}, Q_{L3}) is added;

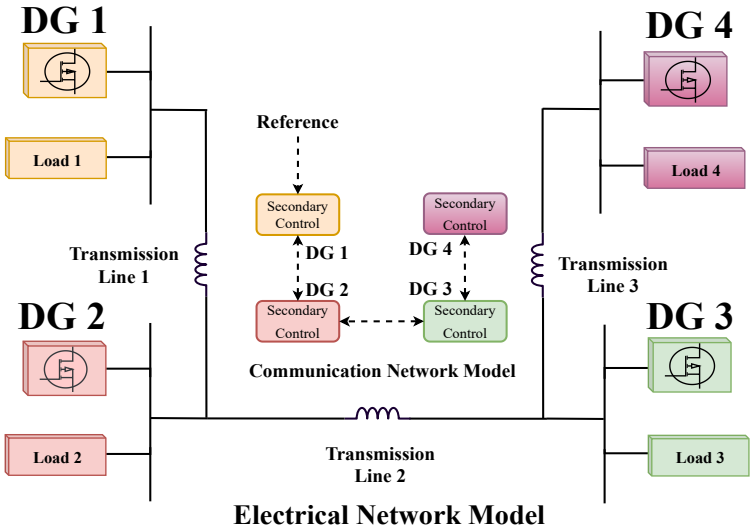

FIGURE 3.1: MG communication and electrical network models.

TABLE 3.1: Parameters of the Microgrid Test System

	DG1		DG2		DG3		DG4	
Model	τ_{P_1}	0.016	τ_{P_2}	0.016	τ_{P_3}	0.016	τ_{P_4}	0.016
	τ_{Q_1}	0.016	τ_{Q_2}	0.016	τ_{Q_3}	0.016	τ_{Q_4}	0.016
	k_{P_1}	$\times 10^{-5}$	k_{P_2}	3×10^{-5}	k_{P_3}	2×10^{-5}	k_{P_4}	1.5×10^{-5}
	k_{Q_1}	4.2×10^{-4}	k_{Q_2}	4.2×10^{-4}	k_{Q_3}	4.2×10^{-4}	k_{Q_4}	4.2×10^{-4}
	k_{v_1}	$1e^{-2}$	k_{v_2}	0.01	k_{v_3}	0.01	k_{v_4}	0.01
Load	P_{1_1}	0.01	P_{1_2}	0.01	P_{1_3}	0.01	P_{1_4}	0.01
	P_{2_1}	1	P_{2_2}	2	P_{2_3}	3	P_{2_4}	4
	P_{3_1}	1×10^4	P_{3_2}	1×10^4	P_{3_3}	1×10^4	P_{3_4}	1×10^4
	Q_{1_1}	0.01	Q_{1_2}	0.01	Q_{1_3}	0.01	Q_{1_4}	0.01
	Q_{2_1}	1	Q_{2_2}	2	Q_{2_3}	3	Q_{2_4}	4
	Q_{3_1}	1×10^4	Q_{3_2}	1×10^4	Q_{3_3}	1×10^4	Q_{3_4}	1×10^4
Line	$B_{12} = 10\Omega^{-1}$, $B_{23} = 10.67\Omega^{-1}$, $B_{34} = 9.82\Omega^{-1}$							

- Step 5 ($t = 25$sec): The reference value for the frequency SC is changed to $\omega_0 = 2\pi 50.1$Hz;
- Step 6 ($t = 35$sec): The set-point for the voltage SC is changed to $v_0 = 225 V_{RMS}$;

Let us now explain the obtained results shown from Figure 3.2-3.6. As can be observed from Figure 3.2 and Figure 3.3, in the first five seconds, when the PC is only switched on, all the corresponding voltages and frequencies are less than the reference values and the PC is not able to compensate for these deviations. At $t = 5$sec the frequency restoration control Equations (3.6)-(3.12) is activated with $\omega_0 = 2\pi 50$Hz and the DG's frequencies are restored to the expected value. At the same time, the power sharing constraints Equation (3.4) are achieved (see Figure 3.4). It is clear from Figure 3.3 that when the voltage SC is activated at $t = 10$sec, then also the output voltages are restored to 220V_{RMS}. We connect the sample load (P_{L3}, Q_{L3}) at $t = 15s$, and then disconnected it at $t = 20s$ by a three-phase breaker. The results show that the proposed SCs are robust against unexpected changes on demands. Moreover, we modify the frequency and voltage SC setpoints at $t = 25s$ and $t = 35$

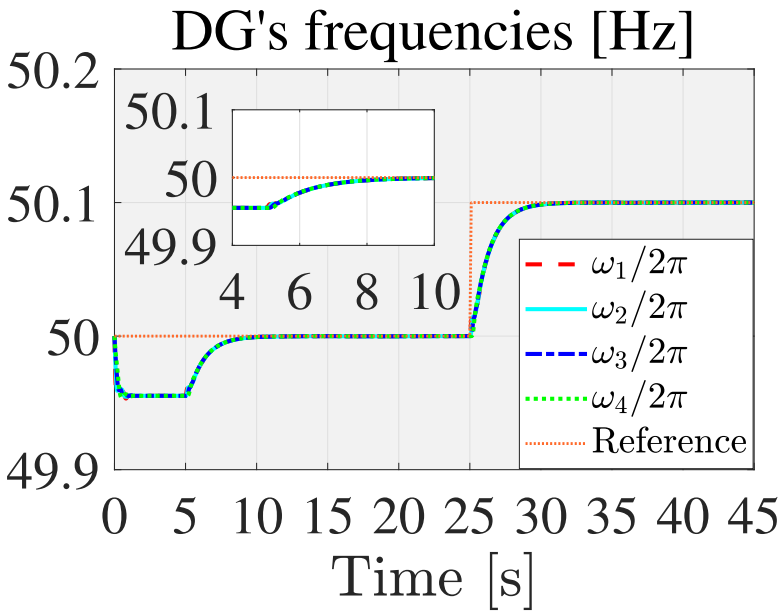

FIGURE 3.2: DG's frequency $\omega_i(t)$
under adaptive distributed SC, $i = 1, 2, 3, 4$.

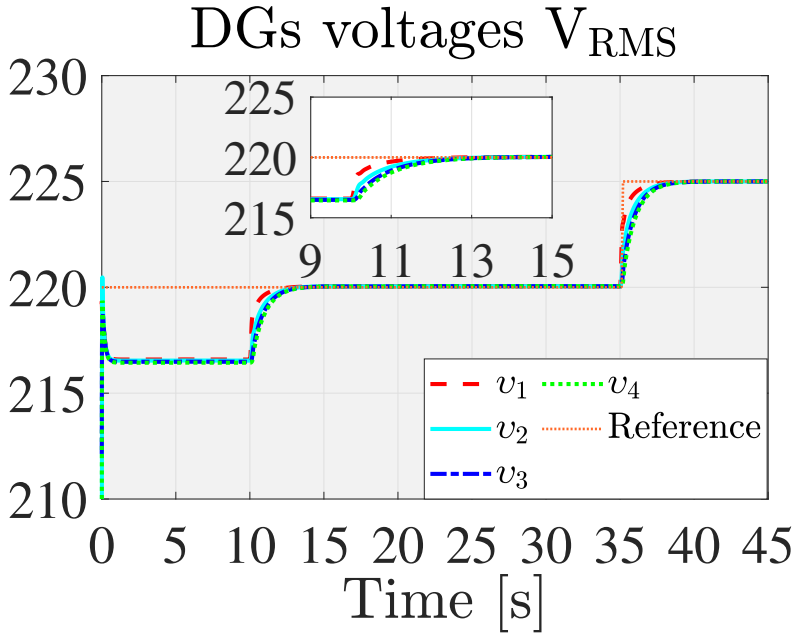

FIGURE 3.3: DG's voltage $v_i(t)$
under adaptive distributed SC, $i = 1, 2, 3, 4$.

to $\omega_0 = 2\pi 50.1Hz$ and $v_0 = 225V_{RMS}$ respectively. Consequently, all DG's frequencies and voltages converge to the setpoint values very quickly. Finally, the time evolutions of the proposed SCs are depicted in Figure 3.5 and Figure 3.6. The results verify that the frequency and voltage SCs show a satisfactory performance and a smooth control signals alleviating the chattering problem.

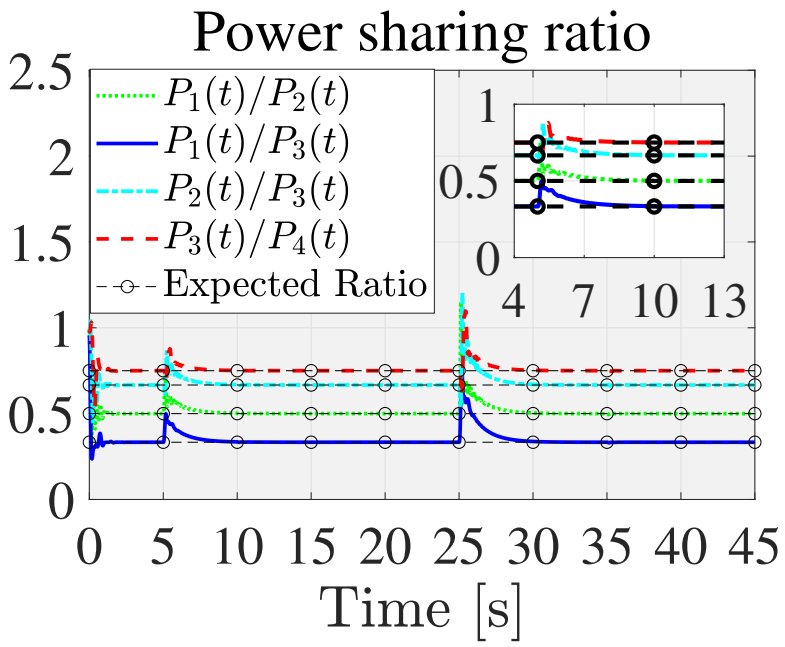

FIGURE 3.4: Comparison between the expected (i.e., k_{P_i}/k_{P_j}) and actual (i.e., P_i/P_j) power sharing ratio under adaptive distributed SC, $i = 1, 2, 3, 4$, $j \neq i$, $j > i$.

3.6 Conclusions

Here a novel robust distributed secondary restoration control protocol for inverter-based islanded microgrids is proposed. The method improves the current state of the art because it is fully distributed, model-free, and robust against delayed directed communications and parameters uncertainties. Moreover, since the control actions are continuous, they can be safely pulse width modulated by a fixed given frequency to not hurt the switching power artifacts.

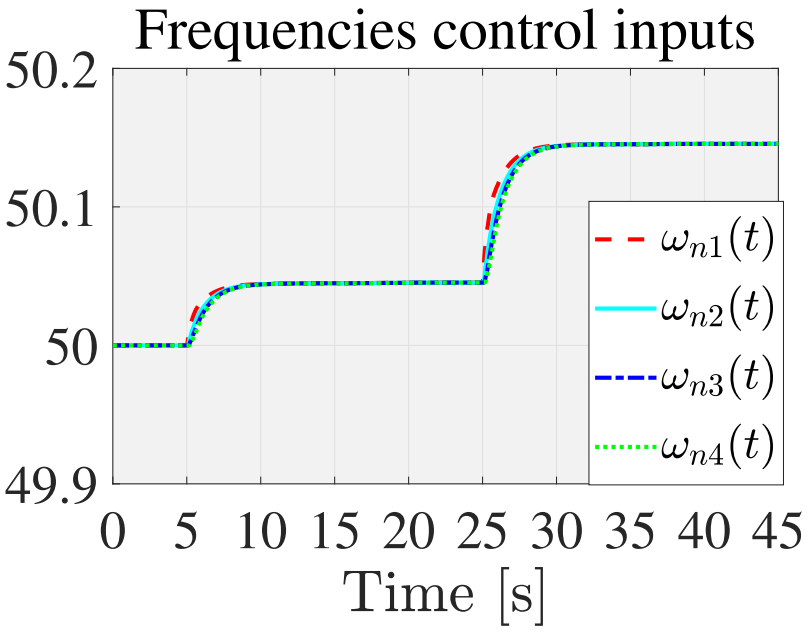

FIGURE 3.5: Frequency secondary control $\omega_{n_i}(t)$ under adaptive distributed SC, $i = 1, 2, 3, 4$.

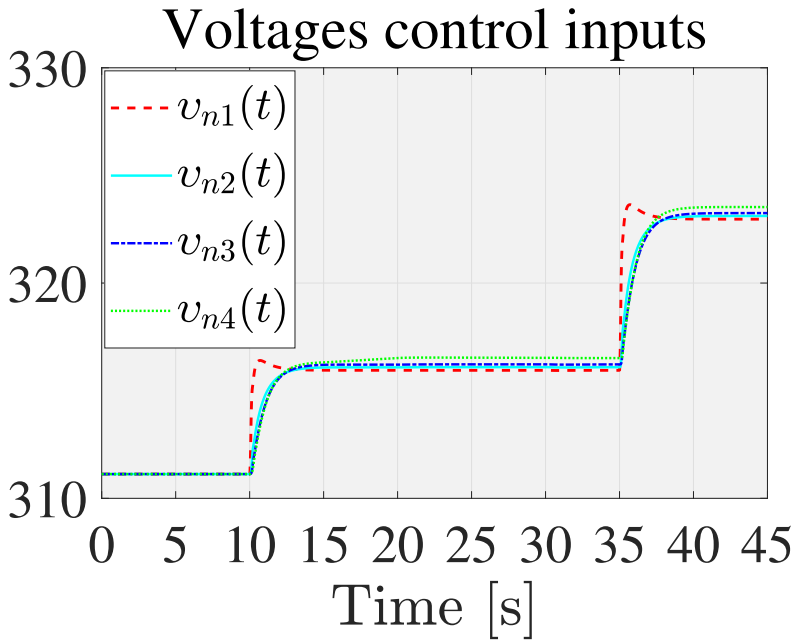

FIGURE 3.6: Voltage secondary control $v_{n_i}(t)$ under adaptive distributed SC, $t \geq 0$, $i = 1, 2, 3, 4$.

Chapter 4

Robust Distributed Optimal Voltage SC with Time-Varying Multiple Delays and Model Uncertainties

4.1 Introduction

This chapter aims to solve the problem of voltage restoration in droop-controlled inverter-based islanded microgrids under communication delays. To this aim, we propose a novel robust distributed voltage SC which is a combination between an integral sliding mode controller and a linear consensus scheme with constant weights. Lyapunov analysis and Linear Matrix Inequalities (LMI) are employed together to demonstrate the associated stability and convergence features. The allowable upper bound for communication delays is also estimated by linear matrix inequalities. Regulating the MG's voltages to the associated reference values additionally is taken into account by developing an optimization algorithm to find the optimal constant control gains.

This chapter is structured as follows. The contributions of this chapter and problem statement are presented in Section 4.2. Section 4.3 outlines the proposed optimal distributed voltage SC scheme under time-varying multiple delays. Moreover, the performance of proposed voltage SC analysed by using the Lyapunov-Krasovskii functional along with linear matrix inequalities. Section 4.4 is provided an optimization algorithm to find the optimal constant control gains and the allowable upper bound for communication delays. Finally, Section 4.5 and Section 4.6 are given the simulation results and conclusions respectively.

4.2 Main Contributions and Problem Statement

The contributions of this chapter are as follows. We herein introduce a novel optimal distributed voltage secondary control for an AC MG by involving an integral sliding mode controller and a linear consensus scheme with constant weights under communication delays between DGs and a class of parameter uncertainties and exogenous disturbances. In fact, the voltage SC presented in this chapter is a particular case of the one introduced in Chapter 3 with constant gains. Hence, it is worth mentioning that, since control gains here are constant, the LMIs which will be obtained later in the stability analysis, are based on constant control gains (not time-varying gains) which can be easily solved to find the stabilizing parameters of the voltage SC controller. Moreover, the most important idea of this chapter is that thanks to the

consideration of the gains as constant values, an optimization algorithm based on LMI is proposed to find the maximum delays and the best tuning for the gains.

Our objective in this chapter is, to design a novel distributed voltage SC to compensate for the unavoidable deviations of the DG's output voltages caused by the droop characteristics of the PCs from the expected set-points, ie.,

$$v_i(\infty) = v_0, \quad \forall i \in \mathcal{V}. \tag{4.1}$$

4.3 Voltage Secondary Controller Design

In order to solve the voltage SC problem (4.1) in the presence of communication delays among DGs we propose the following voltage restoration SC strategy for the voltage dynamic: (2.24)

$$\dot{v}_{n_i}(t) = -\sum_{j=0}^{N} \alpha_{ij}\tilde{k}_{ij} \begin{bmatrix} v_i(t-\tau_{ij}(t)) - v_j(t-\tau_{ij}(t)) \\ \dot{v}_i(t-\tau_{ij}(t)) - \dot{v}_j(t-\tau_{ij}(t)) \end{bmatrix} - \tilde{m}_i \cdot \text{sign}(\tilde{s}_i(t)) \tag{4.2}$$

where $v_{n_i}(t)$ is a distributed input control to achieve synchronization with respect to the DG's states. $\tilde{k}_{ij} = [\tilde{k}_{ij,1}, \tilde{k}_{ij,2}] \in \mathbb{R}^{1\times 2}$ and $\tilde{m}_i \in \mathbb{R}$ are the constant tuning parameter vectors and scalars, respectively. $\tau_{ij}(t)$ shows the time-varying delay between DGs communications and the switching function $\tilde{s}_i(t)$ in (4.2) set as follows

$$\tilde{s}_i(t) = \dot{v}_i(t) + z_i(t), \tag{4.3}$$

$$\dot{z}_i(t) = \frac{\dot{v}_i(t)}{k_{v_i}} - \frac{1}{k_{v_i}} \sum_{j=0}^{N} \alpha_{ij}\tilde{k}_{ij} \begin{bmatrix} v_i(t-\tau_{ij}(t)) - v_j(t-\tau_{ij}(t)) \\ \dot{v}_i(t-\tau_{ij}(t)) - \dot{v}_j(t-\tau_{ij}(t)) \end{bmatrix},$$

$$z_i(0) = -v_i(0) - \dot{v}_i(0). \tag{4.4}$$

Similar to Chapter 3, the delays $\tau_{ij}(t)$ satisfy Assumption 3.3.1. Hereinafter, the main result of this chapter is outlined. It is worth to remark that the DG's output voltage derivatives are not available from measurements. However, they can easily estimated and then used for output feedback purposes by means of differentiators implemented within each local controller, see Remark 3.4.1.

Theorem 4.3.1 *Consider the voltage dynamics Equation (2.24) under the voltage restoration SC Equations (4.2)-(4.4). Let Assumption 2.3.1 and Assumption 3.3.1 be satisfied and let there exist* $\tilde{m}_i > k_{v_i}\Gamma^Q = 2k_{Q_i}\Pi_i^Q/\tau_{Q_i}$. *Given an upper bound of time-delay function* $\tau^\star = max\left\{\tau_l^\star, \sigma_g^\star\right\} > 0$. *Moreover, if the local control gains* $\tilde{k}_{ij,1}$ *and* $\tilde{k}_{ij,2}$ *be greater than zero and if there exist symmetric positive definite matrices* $P, Q_l, \bar{Q}_g, R_l$ *and* $\bar{R}_g \in \mathbb{R}^{2N\times 2N}$, *such that the following LMIs:*

$$\begin{bmatrix} M_1 + 3\tau^\star A_0' H A_0 & \sum_{l=1}^{q} \tau^\star P\hat{A}_l & \sum_{g=1}^{m} \tau^\star P\tilde{A}_g \\ * & -\sum_{l=1}^{q} \tau^\star R_l & 0_{2N\times 2N} \\ * & * & -\sum_{g=1}^{m} \tau^\star \bar{R}_g \end{bmatrix} < 0 \tag{4.5a}$$

$$3\sum_{l=1}^{q} \tau^\star \hat{A}_l' H \sum_{l=1}^{q} \hat{A}_l + \bar{M}_1 < 0 \tag{4.5b}$$

$$3\sum_{g=1}^{m} \tau^\star \tilde{A}_g' H \sum_{g=1}^{m} \tilde{A}_g + \bar{M}_1 < 0 \tag{4.5c}$$

are feasible, where

$$H = \sum_{g=1}^{m} \bar{R}_g + \sum_{l=1}^{q} R_l, \quad M_1 = F'P + PF + \sum_{g=1}^{m} \bar{Q}_g + \sum_{l=1}^{q} Q_l \tag{4.6}$$

$$\bar{M}_1 = \sum_{l=1}^{q} -Q_l(1-d_l), \quad \tilde{M}_1 = \sum_{g=1}^{m} -\bar{Q}_g(1-d_g) \tag{4.7}$$

and

$$A_0 = [A_{0(r,y)}] \in \mathbb{R}^{2N\times 2N} \quad \text{with} \quad A_{0(r,y)} : \begin{cases} \bar{A}_i & \text{if } r = y = i \\ 0_{2\times 2} & \text{otherwise} \end{cases}, \tag{4.8}$$

$$\hat{A}_l = [\hat{A}_{l(r,y)}] \in \mathbb{R}^{2N\times 2N} \quad \text{with} \quad \hat{A}_{l(r,r)} : \begin{cases} A_{i0} & \text{if } \tau_l = \tau_{il},\ r = l = i \\ 0_{2\times 2} & \text{otherwise} \end{cases}, \tag{4.9}$$

$$\tilde{A}_g = [\tilde{A}_{g(r,y)}] \in \mathbb{R}^{2N\times 2N} \quad \text{with} \quad \tilde{A}_{g(r,y)} : \begin{cases} A_{ij} & \text{if } \sigma_g = \tau_{ij},\ i \neq j,\ r = y = i \\ -A_{ij} & \text{if } \sigma_g = \tau_{ij},\ i \neq j,\ r = i,\ y = j \\ 0_{2\times 2} & \text{otherwise} \end{cases} \tag{4.10}$$

being

$$A_{i0} = -\alpha_{i0} \cdot \bar{B}_i \cdot \tilde{k}_{i0} \in \mathbb{R}^{2\times 2} \tag{4.11}$$

$$A_{ij} = -\alpha_{ij} \bar{B}_i \cdot \tilde{k}_{ij} \in \mathbb{R}^{2\times 2} \tag{4.12}$$

and $r, y = \{1, 2, \ldots, N\}$, *and*

$$F = A_0 + \sum_{l=1}^{q} \hat{A}_l + \sum_{g=1}^{m} \tilde{A}_g \tag{4.13}$$

Then, condition (4.1) *is verified.*

Proof of Theorem 4.3.1 ([107]) *By substituting* (4.2)-(4.4) *into* (2.24), *it yields:*

$$\begin{bmatrix} \dot{v}_i(t) \\ \ddot{v}_i(t) \end{bmatrix} = \bar{A}_i \begin{bmatrix} v_i(t) \\ \dot{v}_i(t) \end{bmatrix} - \bar{B}_i \sum_{j=0}^{N} \alpha_{ij} \tilde{k}_{ij} \begin{bmatrix} v_i(t-\tau_{ij}(t)) - v_j(t-\tau_{ij}(t)) \\ \dot{v}_i(t-\tau_{ij}(t)) - \dot{v}_j(t-\tau_{ij}(t)) \end{bmatrix} + \begin{bmatrix} 0 \\ \dot{\tilde{s}}_i(t) \end{bmatrix} \tag{4.14}$$

and then, by computing the time derivative of (4.3) *along with the trajectories of* (4.4), *we reach to:*

$$\dot{\tilde{s}}_i(t) = -\frac{\tilde{m}_i}{k_{v_i}} \text{sign}(\tilde{s}_i) + \dot{\tilde{w}}_i(t) \tag{4.15}$$

Let us now select the following Lyapunov function:

$$\bar{V}(t) = \frac{1}{2} \sum_{i=1}^{N} \tilde{s}_i(t)^2 \tag{4.16}$$

so that the time derivative of $\bar{V}(t)$ *correspondingly takes the form:*

$$\dot{\bar{V}}(t) = \sum_{i=1}^{N} \tilde{s}_i(t) \cdot \dot{\tilde{s}}_i(t) = \sum_{i=1}^{N} \tilde{s}_i(t) \cdot \dot{\tilde{w}}_i(t) - \frac{\tilde{m}_i}{k_{v_i}} |\tilde{s}_i|). \tag{4.17}$$

Then by referring to Assumption 2.3.1, we manipulate (4.17) as:

$$\dot{\tilde{V}}(t) \leq -\sum_{i=1}^{N} \left(\frac{\tilde{m}_i}{k_{v_i}} - \Gamma_i^{Q}\right) \cdot |\tilde{s}_i(t)| < 0 \quad \forall \quad \tilde{m}_i > k_{v_i}\Gamma^{Q}. \tag{4.18}$$

so that by reaching to (4.18), $\tilde{V}(t) = 0 \; \forall \; t \geq 0$ is concluded. Consequently, the condition $\tilde{s}_i = \dot{\tilde{s}}_i = 0$ is invariant since the initial instant of time $t = 0$. Hence, by letting $\dot{\tilde{s}}_i = 0$, the following function is supported:

$$\text{sign}(\tilde{s}_i) \equiv \frac{k_{v_i}}{\tilde{m}_i}\dot{\tilde{w}}_i(t). \tag{4.19}$$

Therefore, by substituting (4.19) into equation (4.14), we get:

$$\begin{bmatrix} \dot{v}_i(t) \\ \ddot{v}_i(t) \end{bmatrix} = \bar{A}_i \begin{bmatrix} v_i(t) \\ \dot{v}_i(t) \end{bmatrix} - \tilde{B}_i \sum_{j=0}^{N} \alpha_{ij}\tilde{k}_{ij} \begin{bmatrix} v_i(t-\tau_{ij}(t)) - v_j(t-\tau_{ij}(t)) \\ \dot{v}_i(t-\tau_{ij}(t)) - \dot{v}_j(t-\tau_{ij}(t)) \end{bmatrix} \tag{4.20}$$

Let's define errors between the i-th DG and the voltage reference as:

$$e(t) = \begin{pmatrix} e_1(t), & e_2(t), & \ldots, e_N(t) \end{pmatrix}' \tag{4.21}$$

with

$$e_i(t) = \begin{bmatrix} v_i(t) - v_0 \\ \dot{v}_i(t) - \dot{v}_0 \end{bmatrix} \tag{4.22}$$

and by letting $A_{i0} = -\bar{B}_i\alpha_{i0}\tilde{k}_{i0}$, $A_{ij} = -\bar{B}_i\alpha_{ij}\tilde{k}_{ij} \in \mathbb{R}^{2\times 2}$, and by differentiating $e_i(t)$ and by considering v_0 is constant, after some algebraic manipulations, one derives:

$$\begin{aligned} \dot{e}_i(t) = \bar{A}_i e_i(t) &- \bar{B}_i\alpha_{i0} \cdot k_{i0} e_i(t-\tau_{i0}(t)) \\ &- \bar{B}_i \sum_{j=1}^{N} \alpha_{ij} \cdot \tilde{k}_{ij} \left[(e_i(t-\tau_{ij}(t)) - e_j(t-\tau_{ij}(t))\right] \end{aligned} \tag{4.23}$$

Then, by substituting (4.11) and (4.12), it results:

$$\dot{e}_i(t) = \bar{A}_i e_i(t) + A_{i0} e_i(t-\tau_{i0}(t)) + \textstyle\sum_{j=1}^{N} A_{ij} \left[e_i(t-\tau_{ij}(t)) - e_j(t-\tau_{ij}(t))\right] \tag{4.24}$$

Moreover, regarding (4.8)-(4.12), the multi-agent closed loop dynamics can be written as:

$$\dot{e}(t) = A_0 e(t) + \textstyle\sum_{l=1}^{N} \hat{A}_l e(t-\tau_l(t)) + \sum_{g=l}^{m} \tilde{A}_g e(t-\sigma_g(t)) \tag{4.25}$$

Then, according to equation (3.40) the multi-agent closed loop dynamics (4.25) can be recast according to as:

$$\dot{e}(t) = Fe(t) - \sum_{l=1}^{N} \hat{A}_l \int_{t-\tau_l(t)}^{t} \dot{e}(s)ds - \sum_{g=1}^{m} \tilde{A}_g \int_{t-\sigma_g(t)}^{t} \dot{e}(s)ds \tag{4.26}$$

It is worth mentioning that F in (4.13) is a strictly diagonally dominant block matrix, whose generic block element $F_{(i,i)} \in \mathbb{R}^{2\times 2}$ on the main diagonal is defined as:

$$F_{(i,i)} = \bar{A} + A_{i0} + \sum_{j=1, i\neq j}^{N} A_{ij} \tag{4.27}$$

To show that F is negative definite, it suffices to prove that $F_{(i,i)}$, for $i = 1, \ldots, N$, is a

negative. If local control gains $\tilde{k}_{ij,1}$ *and* $\tilde{k}_{ij,2}$ *for* $i,j = \{1,\dots,N\}$ *are greater than zero then, according to* (4.12)*, the term* $\sum_{j=1}^{N} A_{ij}$ *is negative semi-definite. Moreover, if local control gains* $\tilde{k}_{i0,1}$ *and* $\tilde{k}_{i0,2}$ *for* $i = \{1,\dots,N\}$ *are greater than zero then the term* $\bar{A} + A_{i0}$ *is negative semi-definite. Consequently, it follows that blocks* $F_{(i,i)}$ *in* (4.27) *are negative definite.*

Let us now construct the following Lyapunov Krasovskii functional:

$$V(e(t)) = \sum_{i=1}^{5} V_i(e(t)) \tag{4.28}$$

with

$$V_1(e(t)) = e(t)'Pe(t) \tag{4.29}$$

$$V_2(e(t)) = \sum_{l=1}^{q} \int_{t-\tau_l(t)}^{t} e(s)'Q_l e(s)ds \tag{4.30}$$

$$V_3(e(t)) = \sum_{g=1}^{m} \int_{t-\sigma_g(t)}^{t} e(s)'\bar{Q}_g e(s)ds \tag{4.31}$$

$$V_4(e(t)) = \sum_{l=1}^{q} \int_{-\tau_l(t)}^{0} \int_{t+\theta}^{t} \dot{e}(s)'R_l\dot{e}(s)dsd\theta \tag{4.32}$$

$$V_5(e(t)) = \sum_{g=1}^{m} \int_{-\sigma_g(t)}^{0} \int_{t+\theta}^{t} \dot{e}(s)'\bar{R}_g\dot{e}(s)dsd\theta \tag{4.33}$$

where, in accordance with the statement of Theorem 4.3.1, $P, Q_l, \bar{Q}_g, \bar{R}_g$ *and* $R_l \in \mathbb{R}^{2N\times 2N}$ *are symmetric positive definite matrices. Now, the time derivative of* $V_1(e(t))$ *in* (4.29) *along the trajectories of the system in* (4.26) *are given by:*

$$\begin{aligned}\dot{V}_1(e(t)) = e(t)'(F'P + PF)e(t) - 2e(t)'P\sum_{l=1}^{q}\hat{A}_l\int_{t-\tau_l(t)}^{t}\dot{e}(s)ds \\ - 2e(t)'P\sum_{g=1}^{m}\tilde{A}_g\int_{t-\sigma_g(t)}^{t}\dot{e}(s)ds.\end{aligned} \tag{4.34}$$

According to (2.4) *in Lemma 2.2.1,* (4.34) *can be rewritten as:*

$$\begin{aligned}\dot{V}_1(e(t)) \le e(t)'\left[F'P + PF\right]e(t) + e(t)'\left[\sum_{l=1}^{q}\tau^{\star}P\hat{A}_l R_l^{-1}\hat{A}_l'P\right]e(t) + \sum_{l=1}^{q}\int_{t-\tau_l(t)}^{t}\dot{e}(s)R_l\dot{e}(s)ds \\ + \sum_{l=1}^{q}\int_{t-\tau_l(t)}^{t}\dot{e}(s)R_l\dot{e}(s)ds + e(t)'\left[\sum_{g=1}^{m}\tau^{\star}P\tilde{A}_g\bar{R}_g^{-1}\tilde{A}_g'P\right]e(t).\end{aligned} \tag{4.35}$$

From (4.30) *and* (4.31)*, by differentiating* $V_2(e(t))$ *and* $V_3(e(t))$*, we get:*

$$\dot{V}_2(t) = e(t)'\sum_{l=1}^{q}Q_l e(t) - \sum_{l=1}^{q}e(t-\tau_l(t))'Q_l(1-\dot{\tau}_l(t))e(t-\tau_l(t)) \tag{4.36}$$

$$\dot{V}_3(t) = e(t)'\sum_{g=1}^{m}\bar{Q}_g e(t) - \sum_{g=1}^{m}e(t-\sigma_g(t))'\bar{Q}_g(1-\dot{\sigma}_g(t))e(t-\sigma_g(t)) \tag{4.37}$$

Then, by exploiting the bound on delays according to Assumption 3.3.1, (4.36) and (4.37) can be recast as follows:

$$\dot{V}_2(t) \leq e(t)' \sum_{l=1}^{q} Q_l e(t) - \sum_{l=1}^{q} e(t-\tau_l(t))' Q_l (1-d_l) e(t-\tau_l(t)) \tag{4.38}$$

$$\dot{V}_3(t) \leq e(t)' \sum_{g=1}^{m} \bar{Q}_g e(t) - \sum_{g=1}^{m} e(t-\sigma_g(t))' \bar{Q}_g (1-\bar{d}_g) e(t-\sigma_g(t)) \tag{4.39}$$

By taking the time derivative of the $V_4(e(t))$ and $V_5(e(t))$, it yields to:

$$\dot{V}_4(e(t)) = \sum_{l=1}^{q} \tau_l(t) \dot{e}(t)' R_l \dot{e}(t) - \sum_{l=1}^{q} \int_{t-\tau_l(t)}^{t} \dot{e}(s) R_l \dot{e}(s) ds \tag{4.40}$$

$$\dot{V}_5(e(t)) = \sum_{g=1}^{m} \sigma_g(t) \dot{e}(t)' \bar{R}_g \dot{e}(t) - \sum_{g=1}^{m} \int_{t-\sigma_g(t)}^{t} \dot{e}(s) \bar{R}_g \dot{e}(s) ds \tag{4.41}$$

Considering upper bound of time-delays $\tau^\star$, we can write:

$$\dot{V}_4(e(t)) \leq \sum_{l=1}^{q} \tau^\star \dot{e}(t)' R_l \dot{e}(t) - \sum_{l=1}^{q} \int_{t-\tau_l(t)}^{t} \dot{e}(s) R_l \dot{e}(s) ds \tag{4.42}$$

$$\dot{V}_5(e(t)) \leq \sum_{g=1}^{m} \tau^\star \dot{e}(t)' \bar{R}_g \dot{e}(t) - \sum_{g=1}^{m} \int_{t-\sigma_g(t)}^{t} \dot{e}(s) \bar{R}_g \dot{e}(s) ds \tag{4.43}$$

Now, by summing (4.34)-(4.43) and from (4.6)-(4.7), one derives:

$$\begin{aligned} \dot{V}(e(t)) \leq e(t)' \left[\sum_{l=1}^{q} \tau^\star P \hat{A}_l R_l^{-1} \hat{A}_l' P + \sum_{g=1}^{m} \tau^\star P \tilde{A}_g \bar{R}_g^{-1} \tilde{A}_g' P + M_1 \right] e(t) + \tau^\star \dot{e}(t)' H \dot{e}(t) \\ + e(t-\tau_l(t))' \bar{M}_1 e(t-\tau_l(t)) + e(t-\sigma_g(t))' \tilde{M}_1 e(t-\sigma_g(t)) \end{aligned} \tag{4.44}$$

Let us expand the term $\tau^\star \dot{e}(t)^T H \dot{e}(t)$ according to (4.25) as follows:

$$\begin{aligned} \tau^\star \dot{e}(t)' H \dot{e}(t) = \tau^\star e(t)' \left[A_0' H A_0 \right] e(t) + \tau^\star e(t-\tau_l(t))' \left[\sum_{l=1}^{q} \hat{A}_l' H \sum_{l=1}^{q} \hat{A}_l \right] e(t-\tau_l(t)) \\ + \tau^\star e(t-\sigma_g(t))' \left[\sum_{g=1}^{m} \tilde{A}_g' H \sum_{g=1}^{m} \tilde{A}_g \right] e(t-\sigma_g(t)) \\ + 2\tau^\star e(t)' \left[A_0 H \sum_{l=1}^{q} \hat{A}_l \right] e(t-\tau_l(t)) \\ + 2\tau^\star e(t-\tau_l(t))' \left[\sum_{l=1}^{q} \hat{A}_l' H \sum_{g=1}^{m} \tilde{A}_g \right] e(t-\sigma_g(t)) \\ + 2\tau^\star e(t)' \left[A_0 H \sum_{g=1}^{m} \tilde{A}_g \right] e(t-\sigma_g(t)) \end{aligned} \tag{4.45}$$

From (2.3) (see Lemma 2.2.1), and assuming

$$a(t) = A_0 e(t), \quad b(t) = H\sum_{l=1}^{q}\hat{A}_l e(t-\tau_l(t)), \quad \psi = H$$
$$\bar{a}(t) = A_0 e(t) \quad \bar{b}(t) = H\sum_{g=1}^{m}\tilde{A}_g e(t-\tau_p(t))$$
$$\hat{a}(t) = \sum_{l=1}^{q}\hat{A}_l e(t-\tau_l(t)), \quad \hat{b}(t) = H\sum_{g=1}^{m}\tilde{A}_g e(t-\tau_p(t)). \tag{4.46}$$

the following results can then be obtained:

$$2a(t)'b(t) \leq e(t)'A_0^T H A_0 e(t) + e(t-\tau_l(t))'\left[\sum_{l=1}^{q}\hat{A}_l' H \sum_{l=1}^{q}\hat{A}_l\right]e(t-\tau_l(t)) \tag{4.47}$$

$$2\bar{a}(t)'\bar{b}(t) \leq e(t)'A_0' H A_0 e(t) + e(t-\sigma_g(t))'\left[\sum_{g=1}^{m}\tilde{A}_g' H \sum_{g=1}^{m}\tilde{A}_g\right]e(t-\sigma_g(t)) \tag{4.48}$$

$$\begin{aligned}2\hat{a}(t)'\hat{b}(t) \leq\ & e(t-\tau_l(t))'\sum_{l=1}^{q}\hat{A}_l' H \sum_{l=1}^{q}A_l e(t-\tau_l(t)) \\ & + e(t-\sigma_g(t))'\left[\sum_{g=1}^{m}\tilde{A}_g' H \sum_{g=1}^{m}\tilde{A}_g\right]e(t-\sigma_g(t))\end{aligned} \tag{4.49}$$

Therefore, according to (4.47)-(4.49), (4.45) can be recast as:

$$\begin{aligned}\tau^\star \dot{e}(t)'H\dot{e}(t) \leq\ & \tau^\star e(t)'\left[3A_0' H A_0\right]e(t) + \tau^\star e(t-\tau_l(t))'\left[3\sum_{l=1}^{q}\hat{A}_l' H \sum_{l=1}^{q}\hat{A}_l\right]e(t-\tau_l(t)) \\ & + \tau^\star e(t-\sigma_g(t))'\left[3\sum_{g=1}^{m}\tilde{A}_g' H \sum_{g=1}^{m}\tilde{A}_g\right]e(t-\sigma_g(t))\end{aligned} \tag{4.50}$$

Now, by substituting (4.50) into (4.44), one derives:

$$\begin{aligned}\dot{V}(e(t)) \leq\ & e(t)'H_1 e(t) + e(t-\tau_l(t))'H_2 e(t-\tau_l(t)) \\ & + e(t-\tau_p(t))'H_3 e(t-\tau_p(t))\end{aligned} \tag{4.51}$$

being

$$H_1 = M_1 + \tau^\star M_2,\ H_2 = \bar{M}_1 + \tau^\star \bar{M}_2,\ H_3 = \hat{M}_1 + \tau^\star \hat{M}_2 \tag{4.52}$$

with

$$M_2 = 3A_0' H A_0 + \sum_{l=1}^{q} P\hat{A}_l R_l^{-1}\hat{A}_l' P + \sum_{g=1}^{m} P\tilde{A}_g \bar{R}_g^{-1}\tilde{A}_g' P$$

$$\bar{M}_2 = 3\sum_{l=1}^{q}\hat{A}_l' H \sum_{l=1}^{q}\hat{A}_l, \qquad \hat{M}_2 = 3\sum_{g=1}^{m}\tilde{A}_g' H \sum_{g=1}^{m}\tilde{A}_g.$$

Therefore, to have $\dot{V}(e(t)) \leq 0$, H_1, H_2 and H_3 in (4.51) should be negative definite. It should be noted that H_1 is a non-linear inequality due to the presence of terms R_l^{-1} and $\bar{R}_g^{-1}$. Hence, performing Schur complement on H_1 (see Lemma 2.2.3), (4.51) can be rewritten as in (4.5), which consists on LMI whose solutions can be easily found by using standard numerical solvers based on the the interior point method. Hence, if (4.5) are satisfied, then

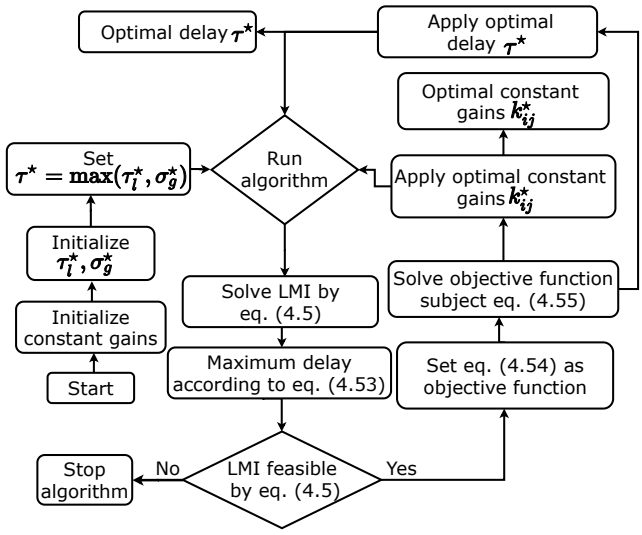

FIGURE 4.1: Process flow diagram of the developed optimization algorithm.

$\dot{V}(e(t)) \leq 0$ *in* (4.51) *and it results* $V(e(t))$ *converges to zero and thus condition* (3.3) *is in force. This concludes the proof.* ■

Remark 4.3.1 *In accordance with Theorem 4.3.1, it results that DG's voltages* (2.24) *under the control protocol* (4.2) *perform synchronization on the setpoint value in accordance with* (4.1). *From* (4.44)-(4.52) *and regarding to Theorem 3.3.1 it further results that an estimation of the maximum admissible delay tolerated by the voltage dynamics* (2.24) *can be lower estimated as follows:*

$$\tau^\star = \min\left\{\frac{\|M_1\|}{\|M_2\|}, \frac{\|\bar{M}_1\|}{\|\bar{M}_2\|}, \frac{\|\tilde{M}_1\|}{\|\tilde{M}_2\|}\right\} \tag{4.53}$$

4.4 Solving optimization over LMI

In this section, we explain how to solve the LMIs feasibility problem (4.5) so that we can find the robust values of the constant gains $\tilde{k}_{ij}$ that guarantee DG's voltages in (2.24) converge to the setpoint value. This problem can be converted into the following LMI optimization:

$$\max_{\tilde{k}_{ij,1}, \tilde{k}_{ij,2}} \min\left\{\frac{\|M_1\|}{\|M_2\|}, \frac{\|\bar{M}_1\|}{\|\bar{M}_2\|}, \frac{\|\tilde{M}_1\|}{\|\tilde{M}_2\|}\right\} \tag{4.54}$$

$$\text{Subject to } \begin{cases} \tilde{k}_{ij,1} > 0 \quad (i = 1, \ldots, N. \quad j = 0, \ldots, N) \\ \tilde{k}_{ij,2} > 0 \end{cases} \tag{4.55}$$

In the proposed optimization, we obtain the largest upper bound of the delay by solving (4.54)-(4.55) within the variables $\tilde{k}_{ij}$. The process of using the optimization algorithm to solve the LMI is shown in Figure 4.1 and summarizes in Algorithm 1.

According to this optimization algorithm, we find the maximum delay among DGs and the best tuning gains $\tilde{k}_{ij}$ such that DG's voltages (2.24) converge the setpoint value under the proposed protocol (4.2).

Algorithm 1: Optimization algorithm

- Initialize constant gains $\tilde{k}_{ij}$.
- Given upper bound of time delays as $\tau_l^\star$ and $\sigma_g^\star$.
- Consider $\tau^\star = max\left\{\tau_l^\star, \sigma_g^\star\right\}$.

repeat
- Solve the LMIs feasibility problem (4.5) with $\tau^\star$.
- Estimation of the maximum admissible delays according to (4.53).
- Check the LMIs feasibility problem (4.5) according to the obtained maximum delay.

if *LMIs problem* (4.5) *are not feasible* **then**
- Break.

else
- Solve objective function (4.54) subject to (4.55).
- Apply optimal constant gains $\tilde{k}_{ij}^\star$ and optimal delay $\tau^\star$ to LMI problems.

end
- Return optimal constant gains $\tilde{k}_{ij}^\star$.
- Return maximum delay $\tau^\star$.

until *LMIs problem* (4.5) *be feasible.*;

4.5 Verification of Results

In this section, to test the performance of the proposed secondary controller, the MATLAB®/Simulink® environment is used to build the simulation model of the 220V_{RMS} (per phase rms), $2\pi 50\text{rad/s}$, islanded MG of four DGs depicted in Figure. 2.1. The detailed parameters of the MG are presented in Table 3.1. The communication network model is considered to be the same topology as shown in Figure. 2.1. It is supposed that only DG 1 can directly access the reference voltage v_0 and frequency ω_0. The tuning gains of the protocol according to the optimization algorithm are obtained as $\tilde{k}_{10} = [0.01, 0.011]$, $\tilde{k}_{12} = [0.001, 0.822]$, $\tilde{k}_{23} = [0.01, 0.01]$, $\tilde{k}_{34} = [0.01, 0.01]$, $\tilde{m}_i = 5$. The time derivatives of the communication delays between DGs have been emulated as random variables with an uniform discrete distribution in the range $|\dot{\tau}_{ij}| \leq d_l = d_g = 1$ and conditions $\tau_{ij} \in [0, \tau^\star)$ are enforced. Notice that the delay margin $\tau^\star = 0.8\text{sec}$ was obtained from Algorithm 1. Algorithm 1 has been implemented in the MATLAB environment, and the LMI problem (4.5) built by means of the lmiedit symbolic interface and YALMIP toolbox. To make a more realistic scenario, the proposed frequency SC [40] is exploited as:

$$\omega_{n_i} = \hat{\omega}_i - \omega_i \tag{4.56}$$

$$\dot{\hat{\omega}}_i = \beta_i \cdot \sum_{j \in \mathcal{N}_i} (\omega_i - \omega_j) + g_i(\omega_i - \omega_0) + \gamma_i \cdot \sum_{j \in \mathcal{N}_i} (\hat{\omega}_i - \hat{\omega}_j) \tag{4.57}$$

where $\beta_i = \gamma_i = -20$, $\hat{\omega}_i(0) = 50$ for all $i = 1, 2, 3, 4$. Moreover, $g_1 = 1$ and $g_k = 0$, $k = 2, 3, 4$. Simulations were performed by using the Runge-Kutta fixed step solver with sampling time $T_s = 0.5 \times 10^{-3}\text{sec}$. The simulation model of the MG is tested for 35 seconds.The list of events scheduled during the test is summed up as follows:

- At the startup ($t = 0\text{sec}$): Only the PC is operated with $\omega_{ni} = 2\pi 50\text{rad/s}$, $v_{ni} = 220\text{V}_{\text{RMS}}$ (per phase rms);

- At $t = 5$sec: The frequency SC (4.57) is activated with $\omega_0 = 2\pi 50\text{rad/s}$;
- At $t = 10$sec: The voltage SC (4.2) is switched on with $v_0 = 220\text{V}_{\text{RMS}}$;
- At $t = 15$sec: The load (P_{L3}, Q_{L3}) is added to the MG;
- At $t = 20$sec: The setpoint for the frequency SC is changed to $\omega_0 = 2\pi 50.1\text{rad/s}$.
- At $t = 25$sec: The setpoint for the voltage SC is changed to $v_0 = 225\text{V}_{\text{RMS}}$.
- At $t = 30$sec: The load (P_{L3}, Q_{L3}) is disconnected.

It is clear from Figures 4.2 and 4.3, during the first 5 seconds, when both SCs are switched off, all the corresponding voltages and frequencies deviate from their desired values and need to be adjusted. To restore the microgrid's voltage and frequency to the desired values the proposed frequency (4.57) and the proposed voltage SC (4.2) are enabled at $t = 5$sec and 10sec respectively with $\omega_0 = 2\pi 50\text{rad/s}$ and $v_0 = 220\text{V}_{\text{RMS}}$.

As can be observed from Figure 4.3, the voltage SC protocol (4.2) guarantees the achievement of the SC aims under communication delays between DGs. Furthermore, Figure 4.4 and Figure 4.5 demonstrate that the proposed voltage SC protocol is robust against unexpected changes on demands. Moreover, we change the frequency and voltage SC setpoints at $t = 20$sec and $t = 25$sec to $\omega_0 = 2\pi 50.1\text{rad/s}$ and $v_0 = 225\text{V}_{\text{RMS}}$ respectively. Consequently, all DG's frequencies and voltages converge to the setpoint values. It can be seen from Figure 4.5 that the voltage SC shows a satisfactory performance and a smooth control signal alleviating the chattering problem.

4.6 Conclusion

In this chapter, a novel optimal distributed secondary voltage restoration control for MG systems by involving an integral sliding mode controller and a linear consensus scheme with constant wights under multiple time-variant delays is proposed. The performance of the proposed scheme is thoroughly analyzed by combining both the Lyapunov-Krasovskii theorem and the linear matrix inequality. A linear matrix inequality criterion is also employed to estimate the maximum delay for communications. Furthermore, an optimization algorithm is proposed to find the optimal constant control gains. Further work will investigate the design of distributed secondary frequency controller within communication delays.

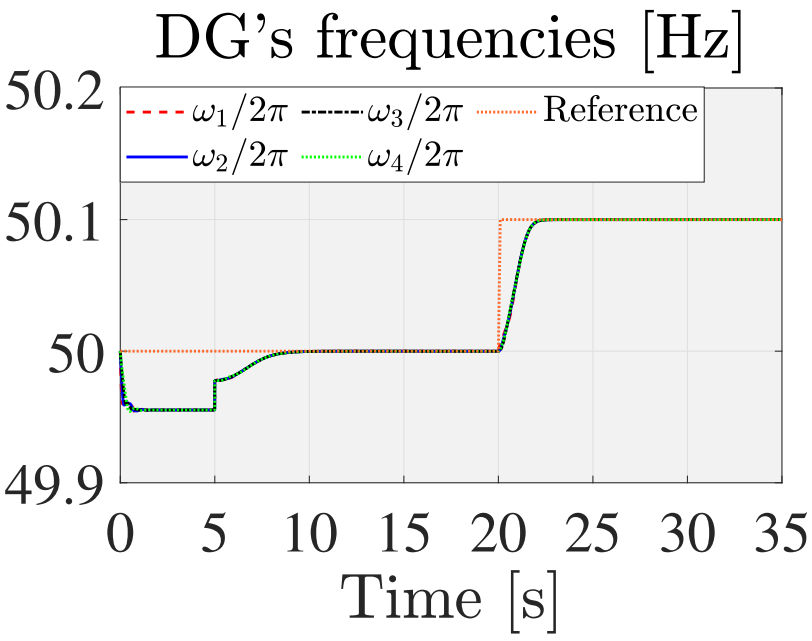

FIGURE 4.2: DG's frequency $\omega_i(t)$ under the proposed frequency SC [40], $i = 1, 2, 3, 4$.

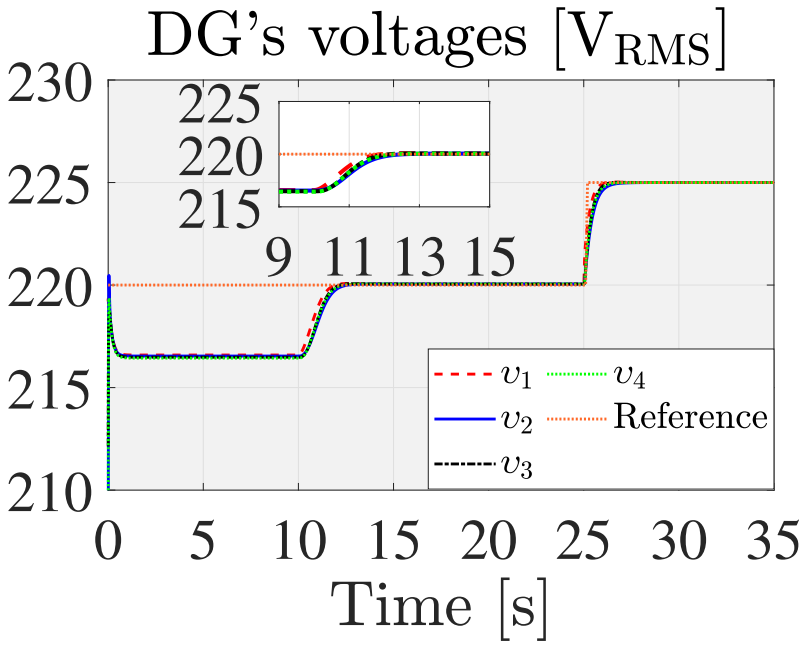

FIGURE 4.3: DG's voltage $v_i(t)$ under distributed optimal voltage SC, $i = 1, 2, 3, 4$.

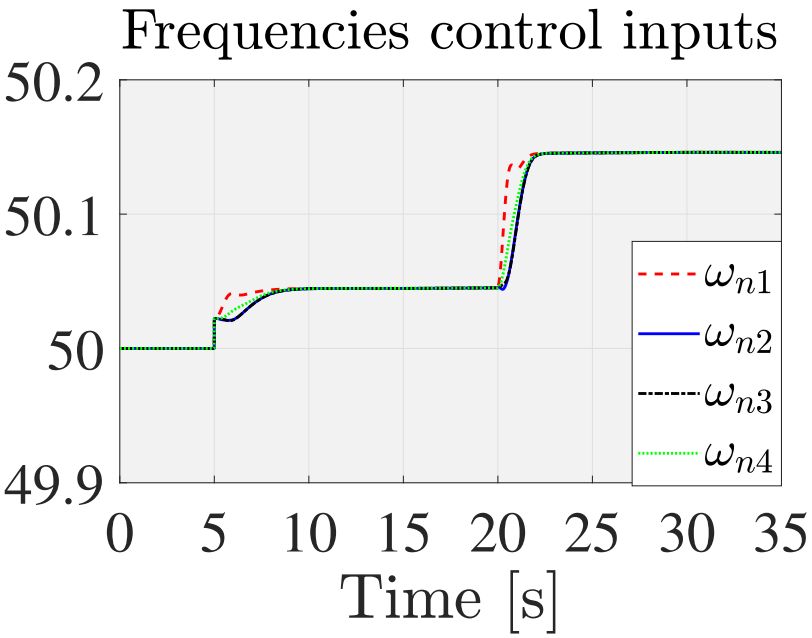

FIGURE 4.4: Frequency secondary control $\omega_{n_i}(t)$ under the proposed frequency SC [40], $i = 1, 2, 3, 4$.

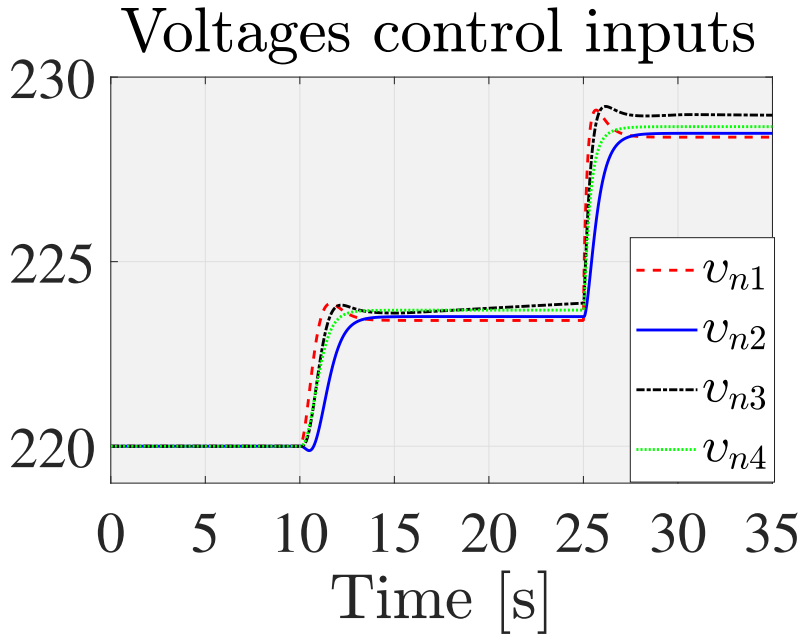

FIGURE 4.5: Voltage secondary control $v_{n_i}(t)$ under distributed optimal voltage SC, $i = 1, 2, 3, 4$.

Chapter 5

Distributed Finite-Time SC by Coupled Sliding-Mode Technique

5.1 Introduction

In the Chapter 2, the model of an inverter-based microgrid has been presented. This chapter presents a novel distributed SC protocol based on the coupled sliding-mode approach, which not only guarantees the exact finite-time restoration among voltages and frequencies of the inverter-based islanded microgrid, but also preserves the active power sharing among DGs. For each distributed generator with no direct access to reference values, a finite-time distributed estimator is locally designed and implemented in each DG unit to provide the reference value of frequency and voltage in a finite time.

This chapter is structured as follows. In Section 5.2, we present the main contributions of this chapter as well as the problem statement. Section 5.3, outlines the proposed distributed SCs scheme. Moreover, the stability and convergence features of the resulting closed-loop system are investigated using the Lyapunov tools. In Section 5.4, the performance and effectiveness of the proposed SCs are verified by simulating it on a nonlinear inverter-based MG. Finally, Section 5.5 provides a summary and concluding remarks.

5.2 Statement of Contributions and Problem Formulation

Aiming at improving the current state of the art of SCs in microgrids, this chapter proposes a robust SC control to restore the system frequency and terminal voltage to the nominal values and guarantee the accurate active power sharing. In comparison with the existing works, the main contributions of this paper can be summarized as follows

1) A novel distributed SC based on SMC is proposed which is able to restore the DG's voltages to the desired value in a finite time under parameters uncertainties and unexpected load variations.

2) A finite-time frequency strategy is designed which guarantees the frequency regulation within a finite time under uncertainties.

3) A finite-time frequency and active power control strategy is designed which guarantees the frequency regulation and active power sharing accuracy within a finite time.

4) For DGs with no direct access to their reference values, a finite-time distributed sliding mode estimator is implemented for both secondary frequency and voltage schemes. The estimator determines local estimates of the global reference values of the voltage and frequency for DGs in a finite time, and provides this information for the distributed SC schemes.

5) The proposed SC schemes only use the local and neighbors information, so they need cost-effective dispersed communication structures in a full distributed fashion.

6) Lyapunov functions are employed to analyze the performance of the proposed controllers and guarantee the accuracy of the finite-time frequency/voltage restoration and active power sharing.

As mentioned in Chapter 1, the primary control causes the frequency and voltage amplitudes of MGs to deviate from the reference values. Therefore, Secondary control can be employed to compensate these deviations. Hence, our objective in this chapter is, to design distributed SCs for:

1. Restoring the frequency of each DG to the reference value in a finite time, that is:
$$\omega_{i,ss} = \omega_0 \quad \forall\, i \in \mathcal{V}. \tag{5.1}$$

2. Preserving the real power sharing accuracy, as:
$$\frac{P_j^m}{P_i^m} = \frac{k_{P_i}}{k_{P_j}} \quad \forall\, i,\ j \in \mathcal{V}. \tag{5.2}$$

3. Restoring the DG's voltages v_i of the MG to the expected setpoint v_0 in a finite time as:
$$v_{i,ss} = v_0 \quad \forall\, i \in \mathcal{V}. \tag{5.3}$$

In the following, we design the robust finite-time secondary frequency and voltage restoration controller. The design is based on a distributed implementation of the terminal sliding mode control paradigm [108]. First, since in general $k_{v_i} \ll \tau_{Q_i}$, it is assumed $k_{v_i} = 0$ in (2.15) (see [109]), which it yields:
$$v_i(t) = v_{n_i}(t) - k_{Q_i} \cdot Q_i^m(t). \tag{5.4}$$

Let us define $\tilde{w}_i(t) = -k_{Q_i} \cdot Q_i^m(t)$. Taking the time derivative of $\tilde{w}_i(t)$ yields:
$$\dot{\tilde{w}}_i(t) = -k_{Q_i} \cdot \dot{Q}_i^m(t) \tag{5.5}$$

Regarding Assumption 2.3.1, $\dot{\tilde{w}}_i(t)$ meets the following restrictions:
$$|\dot{\tilde{w}}_i(t)| \leq \Gamma_i^Q \tag{5.6}$$

where Γ_i^Q are positive known constants.

Then, taking the time derivative on both sides of equations (2.14) and (5.4) one can conclude:
$$\dot{\omega}_{ni}(t) = \dot{\omega}_i(t) + k_{P_i}\dot{P}_i^m(t) = \hat{u}_i(t) + k_{P_i}\bar{u}_i(t), \tag{5.7}$$

$$\dot{v}_{ni}(t) = \dot{v}_i(t) - \dot{\tilde{w}}_i(t) = \tilde{u}_i(t), \tag{5.8}$$

where $\hat{u}_i(t) = \dot{\omega}_i(t)$, $\bar{u}_i(t) = \dot{P}_i^m(t)$ and $\tilde{u}_i(t) = \dot{v}_i(t) - \dot{\tilde{w}}_i(t)$ represent the frequency, active power and voltage inputs respectively. Therefore, the set points can be expressed as:

$$\omega_{ni}(t) = \int (\hat{u}_i(t) + k_{P_i}\bar{u}_i(t))dt, \tag{5.9}$$

$$v_{ni}(t) = \int \tilde{u}_i(t)dt. \tag{5.10}$$

Remark 5.2.1 *Note that to realize the accurate frequency regulation and the accurate active power sharing among DGs simultaneously, it is assumed that the active power is measurable. Whereas, if restoring frequency of DGs is only important, the active power is considered as the uncertain term, namely,*

$$\dot{\tilde{w}}_i(t) = -k_{P_i} \cdot \dot{P}_i^m(t), \tag{5.11}$$

and following Assumption 2.3.1, $\dot{\tilde{w}}_i(t)$ meets the following restriction:

$$|\dot{\tilde{w}}_i(t)| \leq \Gamma_i^P \tag{5.12}$$

where Γ_i^P are positive known constants. ■

5.3 Finite Time Frequency Regulation and Active Power Sharing

The control law for the finite-time frequency restoration and the active power sharing is proposed as follows in which the active power of each DG unit is known:

• Frequency controller

$$\hat{u}_i(t) = u_{\omega_i}^{eq}(t) + u_{\omega_i}^{sw}(t), \tag{5.13a}$$

$$u_{\omega_i}^{eq}(t) = \dot{\hat{\omega}}_i(t) + k_i^{\omega}\left(\dot{\xi}_i^{\omega}(t) - s_i^{\omega}(t) + \sum_{j\in\mathcal{N}_i^c} \dot{e}_j^{\omega}(t)\right), \tag{5.13b}$$

$$\dot{u}_{\omega_i}^{sw}(t) = -T^{\omega}u_{\omega_i}^{sw} - M^{\omega}\text{sign}\big(s_i^{\omega}(t)\big). \tag{5.13c}$$

• Active power controller

$$\bar{u}_i(t) = u_{P_i}^{eq}(t) + u_{P_i}^{sw}(t), \tag{5.14a}$$

$$u_{P_i}^{eq}(t) = k_i^P\left(\dot{e}_i^P(t) - s_i^P(t) + \sum_{j\in\mathcal{N}_i^c} k_{P_j}\dot{P}_j(t)\right), \tag{5.14b}$$

$$\dot{u}_{P_i}^{sw}(t) = -T^P u_{P_i}^{sw}(t) - M^P\text{sign}\big(s_i^P(t)\big). \tag{5.14c}$$

where $k_i^{\omega} = \frac{1}{|\mathcal{N}_i^c|+\alpha_{i0}}$, $k_i^P = \frac{1}{|\mathcal{N}_i^c|}$, M^{ω} and $M^P \in \mathbb{R}_{\geq 0}$ are constant gains. The terms $e_i^{\omega}(t)$ and $e_i^P(t)$ respectively represent the frequency and active power errors for i-th DG, which can be expressed as:

$$e_i^{\omega}(t) = \omega_i(t) - \widehat{\omega}_i(t), \tag{5.15}$$

$$e_i^P(t) = \sum_{j\in\mathcal{N}_i^c}\big(k_{P_i}\cdot P_i^m(t) - k_{P_j}\cdot P_j^m(t)\big). \tag{5.16}$$

where $\widehat{\omega}_i(t)$, represents the DG$_i$'s estimate of ω_0 which can be computed by:

$$\dot{\widehat{\omega}}_i(t) = -\gamma^{\omega} \sum_{j=0}^{N} a_{ij}[\widehat{\omega}_i(t) - \widehat{\omega}_j(t)] - \beta^{\omega} \text{sign}\Big(\sum_{j=0}^{N} a_{ij}[\widehat{\omega}_i(t) - \widehat{\omega}_j(t)]\Big). \tag{5.17}$$

where γ^{ω} and β^{ω} are non-negative and positive constants respectively. The corresponding adjacent weight for the leader is a_{i0}. Note that $\widehat{\omega}_0 \triangleq \omega_0$ and if $a_{i0} \neq 0$, then $\widehat{\omega}_i(t) = \omega_0$.

Furthermore, $\xi_i^{\omega}(t)$ is defined as the coupled form of frequency error, which can be calculated as:

$$\xi_i^{\omega} = \frac{1}{k_i^{\omega}} e_i^{\omega}(t) - \sum_{j \in \mathcal{N}_i^c} e_j^{\omega}(t). \tag{5.18}$$

Let us consider M^{ω} in (5.13) and M^P in (5.14) as $M^{\omega} = K_T^{\omega} + \eta^{\omega}$ and $M^P = K_T^P + \eta^P$, respectively, so that these terms are chosen to satisfy the following conditions:

$$K_T^{\omega} \geq T^{\omega} \cdot M^{\omega}, \tag{5.19}$$
$$K_T^P \geq T^P \cdot M^P, \tag{5.20}$$

with T^{ω} and $T^P \in \mathbb{R}_{\geq 0}$. Furthermore, the sliding variables $s_i^{\omega}(t)$ and $s_i^P(t)$ are calculated as:

$$s_i^{\omega}(t) = \dot{\xi}_i^{\omega}(t) + c^{\omega} \text{sign}(\xi_i^{\omega}(t)) |\xi_i^{\omega}(t)|^{\alpha^{\omega}}, \tag{5.21}$$
$$s_i^P(t) = \dot{e}_i^P(t) + c^P \text{sign}(e_i^P(t)) |e_i^P(t)|^{\alpha^P}. \tag{5.22}$$

where $\alpha^P, \alpha^{\omega} \in (0,1)$ and $c^P, c^{\omega} > 0$. It is worth mentioning that the use of these nonlinear sliding variables not only keeps the advantages of rapid convergence but also reduces the chattering phenomenon through the low-pass filters (5.13c) and (5.14c).

Once the sliding-mode variables $s_i^{\omega}(t) = 0$ and $s_i^P(t) = 0$ are established, (5.21) and (5.22) can be recast as:

$$\dot{\xi}_i^{\omega}(t) = -c^{\omega} \text{sign}(\xi_i^{\omega}(t)) |\xi_i^{\omega}(t)|^{\alpha^{\omega}}, \tag{5.23}$$
$$\dot{e}_i^P(t) = -c^P \text{sign}(\mathrm{e_i^P(t)}) |e_i^P(t)|^{\alpha^P}. \tag{5.24}$$

We are now in a position to state the first main result of this chapter.

Theorem 5.3.1 *Considering the distributed sliding-mode estimator in (5.17), we assume that at least one path from the virtual leader to each DG exists at every instant. If the tuning parameters satisfy $\beta^{\omega} > 0$, then $\widehat{\omega}_i(t)$ is equal to ω_0 in a finite time T_f^{ω} by:*

$$T_f^{\omega} = \max_{\mathrm{i}} \{|\widehat{\omega}_i(0) - \omega_0|\} / \beta^{\omega}.$$

■

Proof of Theorem 5.3.1 *We refer to Theorem 3.1 in [110] for details.* ■

Theorem 5.3.2 *Consider the frequency dynamics (2.23) under the frequency restoration SC (5.13) and the active power controller (5.14). Let inequalities (5.19) and (5.20) be in force. If the local control gains satisfy $\eta^{\omega} > 0$ and $\eta^P > 0$, sliding variables $s_i^{\omega}(t)$ in (5.21) and $s_i^P(t)$ in (5.22) converge to zero in the finite time $T_i^{\star} = max(T_i^{\omega}, T_i^P)$ with $T_i^{\omega} \leq \frac{k_i^{\omega} \cdot s_i^{\omega}(0)}{\eta^{\omega}}$*

and $T_i^P \leq \frac{k_i^P \cdot s_i^P(0)}{\eta^P}$ *respectively. Consequently, the errors of frequency and active power converge to zero and the frequency restoration condition* (5.1) *and the active power-sharing* (5.2) *can be obtained in the following finite time:*

$$\bar{T}_i^\star = \max(\bar{T}_i^\omega, \bar{T}_i^P)$$

subject to

$$\begin{cases} \bar{T}_i^\omega \leq T_i^\star + (\bar{V}_i^\omega(T_i^\star))^{(1-\alpha^\omega)/2}/c^\omega(1-\alpha^\omega)2^{(\alpha^\omega-1)/2}, \\ \bar{T}_i^P \leq T_i^\star + (\bar{V}_i^P(T_i^\star))^{(1-\alpha^P)/2}/c^P(1-\alpha^P)2^{(\alpha^P-1)/2}. \end{cases} \tag{5.25}$$

with

$$V_i^\omega(t) = \frac{k_i^\omega \cdot (s_i^\omega(t))^2}{2}, \quad V_i^P(t) = \frac{k_i^P \cdot (s_i^P(t))^2}{2} \tag{5.26}$$

■

Proof of Theorem 5.3.2 ([111],[112]) *According to the time derivative of* (5.15) *and* (5.18)*, the sliding-mode manifold* (5.21) *can be rewritten as follows:*

$$\dot{s}_i^\omega(t) = \frac{1}{k_i^\omega}\left(\dot{\omega}_i(t) - \dot{\hat{\omega}}_i(t)\right) + c^\omega \text{sign}(\xi_i^\omega(t))|\xi_i^\omega(t)|^{\alpha^\omega} - \sum_{j\in\mathcal{N}_i^c} \dot{e}_j^\omega(t) \tag{5.27}$$

and from (5.7), (5.27) *can be expressed as:*

$$\dot{s}_i^\omega(t) = \frac{1}{k_i^\omega}\left(\hat{u}_i(t) - \dot{\hat{\omega}}_i(t)\right) + c^\omega \text{sign}(\xi_i^\omega(t))|\xi_i^\omega|^{\alpha^\omega} - \sum_{j\in\mathcal{N}_i^c} \dot{e}_j^\omega(t) \tag{5.28}$$

Substituting the local control (5.13a) *into* (5.28) *yields:*

$$\dot{s}_i^\omega(t) = \frac{1}{k_i^\omega}\left(u_{\omega_i}^{eq}(t) + u_{\omega_i}^{sw}(t) - \dot{\hat{\omega}}_i(t)\right) + c^\omega \text{sign}(\xi_i^\omega(t))|\xi_i^\omega(t)|^{\alpha^\omega} - \sum_{j\in\mathcal{N}_i^c} \dot{e}_j^\omega(t) \tag{5.29}$$

Additionally, substituting (5.13b) *into* (5.29) *yields:*

$$\dot{s}_i^\omega(t) = \frac{u_{\omega_i}^{sw}(t)}{k_i^\omega} \tag{5.30}$$

From (5.19)*, the following constraint under the condition* $u_{\omega_i}^{sw}(t_0) = 0$ *can be held:*

$$K_T^\omega \geq T^\omega M^\omega \geq T^\omega |u_{\omega_i}^{sw}(t)|_{\max} \geq T^\omega |u_{\omega_i}^{sw}(t)| \tag{5.31}$$

Thus, the following inequality is always met:

$$T^\omega |u_{\omega_i}^{sw}(t)| \leq K_T^\omega. \tag{5.32}$$

Applying the same analysis on the sliding-mode manifold (5.22) *yields:*

$$\dot{s}_i^P(t) = \frac{u_{P_i}^{sw}(t)}{k_i^P} \tag{5.33}$$

Regarding (5.20) *and* (5.14c)*, the following inequality under the condition of* $u_{P_i}^{sw}(t_0) = 0$ *can be obtained:*

$$T^P |u_{P_i}^{sw}(t)| \leq K_T^P. \tag{5.34}$$

The Lyapunov function candidate of each DG can be defined as:

$$E_i(t) = V_i^{\omega}(t) + V_i^{P}(t) \tag{5.35}$$

where

$$V_i^{\omega}(t) = \frac{k_i^{\omega} \cdot (s_i^{\omega}(t))^2}{2}, \quad V_i^{P}(t) = \frac{k_i^{P} \cdot (s_i^{P}(t))^2}{2} \tag{5.36}$$

By Taking the time-derivative of $V_i^{\omega}(t)$ and using (5.30), we get that:

$$\dot{V}_i^{\omega}(t) = k_i^{\omega} s_i^{\omega}(t) \dot{s}_i^{\omega}(t) = s_i^{\omega}(t) \dot{u}_{\omega_i}^{sw}(t) \tag{5.37}$$

Moreover, from (5.13c) we can write:

$$\begin{aligned} \dot{V}_i^{\omega}(t) &= s_i^{\omega}(t)\Big(- M^{\omega} \text{sign}(s_i^{\omega}(t)) - T^{\omega} u_{\omega_i}^{sw}(t)\Big) \\ &= -\big(K_T^{\omega} + \eta^{\omega}\big)|s_i^{\omega}(t)| - T^{\omega} u_{\omega_i}^{sw}(t) s_i^{\omega}(t) \\ &= \Big(- T^{\omega} u_{\omega_i}^{sw}(t) s_i^{\omega} - K_T^{\omega}|s_i^{\omega}|(t)\Big) - \eta^{\omega}|s_i^{\omega}(t)| \end{aligned} \tag{5.38}$$

According to (5.19) and (5.32), (5.38) can be finally recast as:

$$\begin{aligned} \dot{V}_i^{\omega}(t) &\leq \Big(K_T^{\omega}|s_i^{\omega}(t)| - K_T^{\omega}|s_i^{\omega}(t)|\Big) - \eta^{\omega}|s_i^{\omega}(t)| \\ &= -\eta^{\omega}|s_i^{\omega}(t)| = -\eta^{\omega}\sqrt{\frac{2}{k_i^{\omega}}}(V_i^{\omega}(t))^{0.5} < 0 \end{aligned} \tag{5.39}$$

Taking the time-derivative of $V_i^{P}(t)$ and using the similar analysis as above, it results that:

$$\dot{V}_i^{P}(t) \leq -\eta^{P}\sqrt{\frac{2}{k_i^{P}}}(V_i^{P}(t))^{0.5} < 0 \quad \forall\, \eta^{P} > 0. \tag{5.40}$$

Thus, by combining (5.39) and (5.40), one derives that:

$$\dot{E}_i(t) = \dot{V}_i^{\omega}(t) + \dot{V}_i^{P}(t) < 0 \quad \forall\, \eta^{P} > 0,\ \eta^{\omega} > 0$$

The case of $E_i(t) = 0$ yields in $s_i^{\omega}(t) = \dot{s}_i^{\omega}(t) = 0$ and $s_i^{P}(t) = \dot{s}_i^{P}(t) = 0$ in the finite time $T_i^{\star}$, which according to the Lemma 2.2.4 can be rewritten as:

$$T_i^{\star} = \max(T_i^{\omega}, T_i^{P})$$

subject to:

$$\begin{cases} T_i^{\omega} \leq \sqrt{2k_i^{\omega} V_i^{\omega}(0)/(\eta^{\omega})^2} \\ T_i^{P} \leq \sqrt{2k_i^{P} V_i^{P}(0)/(\eta^{P})^2} \end{cases}$$

It can be proved that when the sliding variables $s_i^{\omega}(t)$ and $s_i^{P}(t)$ converge to zero, the errors of the frequency and the active power goes to zero in the $\bar{T}_i^{\star}$.

Now, we select the Lyapunov function as $\bar{E}_i = \bar{V}_i^{\omega} + \bar{V}_i^{P}$ with:

$$\bar{V}_i^{P}(t) = (e_i^{P}(t))^2/2 \tag{5.41}$$

$$\bar{V}_i^{\omega}(t) = (\xi_i^{\omega}(t))^2/2 \tag{5.42}$$

Such that the time derivative of the time derivative of $\bar{V}_i^P(t)$ and $\bar{V}_i^\omega(t)$ can be derived as:

$$\begin{aligned}\dot{\bar{V}}_i^P(t) &= e_i^P(t)\dot{e}_i^P(t) = -e_i^P(t)c^P\text{sign}(\text{e}_\text{i}^\text{P}(\text{t}))|e_i^P(t)|^{\alpha^P} = -c^P|e_i^P(t)|^{1+\alpha^P} \\ &= -c^P 2^{(1+\alpha^P)/2}(\bar{V}_i^P(t))^{(1+\alpha^P)/2} < 0 \qquad (5.43)\\ \dot{\bar{V}}_i^\omega(t) &= \xi_i^\omega(t)\dot{\xi}_i^\omega(t) = -\xi_i^\omega(t)c^\omega\text{sign}(\xi_i^\omega(t))|\xi_i^\omega(t)|^{\alpha^\omega} = -c^P|\xi_i^\omega(t)|^{1+\alpha^\omega} \\ &= -c^\omega 2^{(1+\alpha^\omega)/2}(\bar{V}_i^\omega(t))^{(1+\alpha^\omega)/2} < 0 \qquad (5.44)\end{aligned}$$

Hence, combining (5.43) and (5.44), concludes:

$$\bar{E}_i(t) = \bar{V}_i^P(t) + \bar{V}_i^\omega(t) < 0$$

Considering $\bar{E}_i(t) = 0$, the errors of the frequency and the active power converge to zero while the conditions (5.1)and (5.2) are preserved in the finite time $\bar{T}_i^\star = \max(\bar{T}_i^\omega, \bar{T}_i^P)$. Consequently, the theorem is proved. ■

Remark 5.3.1 *Note that if only achieving the accurate frequency restoration is considered, we can only use eq. (5.13) and assume that the active power is not measurable and is considered as an uncertain term. In this condition, we have*

$$\omega_{ni}(t) = \int \hat{u}_i(t)dt, \qquad (5.45)$$

5.3.1 Finite-time Voltage Regulation

In this subsection, we intend to propose a new voltage restoration SC strategy with the purpose of voltage regulation. To this aim, we consider:

$$\tilde{u}_i(t) = u_{v_i}^{eq}(t) + u_{v_i}^{sw}(t), \qquad (5.46a)$$

$$u_{v_i}^{eq}(t) = -\dot{\tilde{w}}_i(t) + \dot{\hat{v}}_i(t) + k_i^v\left(\dot{\xi}_i^v(t) - s_i^v(t) + \sum_{j\in\mathcal{N}_i^c}\dot{e}_j^v(t)\right), \qquad (5.46b)$$

$$\dot{u}_{v_i}^{sw}(t) = -T^v u_{v_i}^{sw}(t) - M^v\text{sign}\big(s_i^v(t)\big). \qquad (5.46c)$$

where $k_i^v = \frac{1}{|\mathcal{N}_i^c|+\alpha_{i0}}$, $T^v \geq 0$ and $M^v \in \mathbb{R}_{\geq 0}$ are constant gains, while the terms $e_i^v(t)$ and $\xi_i^v(t)$ respectively denote the error and the coupled form of error for the i-th DG, calculated as follows:

$$e_i^v(t) = v_i(t) - \hat{v}_i(t), \qquad (5.47)$$

$$\xi_i^v(t) = \frac{1}{k_i^v}e_i^v(t) - \sum_{j\in\mathcal{N}_i^c} e_j^v(t). \qquad (5.48)$$

where $\hat{v}_i(t)$ gives an estimate of v_0 for i-th DG as follows:

$$\dot{\hat{v}}_i(t) = -\gamma^v\sum_{j=0}^{N} a_{ij}[\hat{v}_i(t) - \hat{v}_j(t)] - \beta^v\text{sign}\left(\sum_{j=0}^{N} a_{ij}[\hat{v}_i(t) - \hat{v}_j(t)]\right). \qquad (5.49)$$

where the constants γ^v and β^v are non-negative and positive respectively, and a_{i0} is the corresponding adjacent weights for the leader. We define $\hat{v}_0 \triangleq v_0$ so that $a_{i0} \neq 0$ gives $\hat{v}_i = v_0$. Note that the constant M^v in (5.46) is chosen as $M^v = \Gamma_i^Q + K_T^v + \eta^v$ to

satisfy the following inequality:

$$K_T^v \geq T^v \cdot M^v \tag{5.50}$$

The sliding variable of the voltage controller can be defined in the same way as the frequency controller, as:

$$s_i^v(t) = \dot{\xi}_i^v(t) + c^v \text{sign}(\xi_i^v(t))|\xi_i^v(t)|^{\alpha^v} \tag{5.51}$$

where $\alpha^v \in (0,1)$ and $c^v > 0$.

Theorem 5.3.3 *Considering the distributed sliding-mode estimator in (5.49), we assume that at least one path from the virtual leader to each DG exists at every instant. Let the tuning parameters satisfy $\beta^v > 0$. Then, $\widehat{v}_i$ is equal to $\widehat{v}_0$ in a finite time*

$$T_f^v = \max_i\{|\widehat{v}_i(0) - v_0|\}/\beta^v, \quad t \geq T_f^v.$$

■

Proof of Theorem 5.3.3 *We refer to [110] for details.* ■

Theorem 5.3.4 *Consider the voltage dynamics (5.4) under the voltage restoration SC (5.46). Let Assumption 2.3.1 and (5.50) be satisfied. If the local control gains satisfy $\eta^v > 0$, sliding variable $s_i^v(t)$ in (5.51) converges to zero in the finite time $T_i^v \leq \frac{k_i^v s_i^v(0)}{\eta^v}$. Hence, the errors converge to zero, and accordingly, the voltage restoration condition (5.3) can be achieved in the following finite time:*

$$\bar{T}_i^v \leq T_i^v + \left(\bar{V}_i^v(T_i^v)\right)^{(1-\alpha^v)/2}/c^v(1-\alpha^v)2^{(\alpha^v-1)/2}. \tag{5.52}$$

where

$$V_i^v(t) = \frac{k_i^v \cdot (s_i^v(t))^2}{2} \tag{5.53}$$

Proof of Theorem 5.3.4 *The proof is similar to analyse the stability of the frequency restoration and is omitted here.* ■

5.4 Simulation Studies

In this section, to evaluate the performance of the proposed SC scheme, we use the MATLAB®/Simulink® environment to build the simulation model of a $220V_{RMS}$ (per phase rms), 50Hz (314rad/s) islanded MG (see Figure. 2.1). The considered sample microgrid consists of four DGs, four local loads and four transmission lines. The detailed parameters of the microgird are summarized in Table 3.1. We consider that the SC communication network $\mathcal{G}_{\mathcal{N}^c}$ has the same topology as the power network shown in Figure. 2.1. We assume that only DG 1 can directly access the reference voltage v_0 and frequency ω_0. As η^ω and T^ω should be greater than zero, and in order to satisfy (5.19), we choose $\eta^\omega = 0.5$, $T^\omega = 0.1$ and $k_T^\omega = 0.5$. Likewise, we choose $\eta^P = 0.5$, $T^P = 0.1$ and $K_T^P = 0.5$ to hold (5.20). Similarly, to satisfy (5.50), we set $K_T^v = \eta^v = 5$ and $T^v = 0.1$.

Moreover, in accordance with Theorems 5.3.1 and 5.3.3, the tuning parameters of the distributed estimators are selected as $\gamma^\omega = \gamma^v = 10$, $\beta^\omega = \beta^v = 18$. The system is tested for 35 seconds. The list of events scheduled throughout the test is summarized as follows:

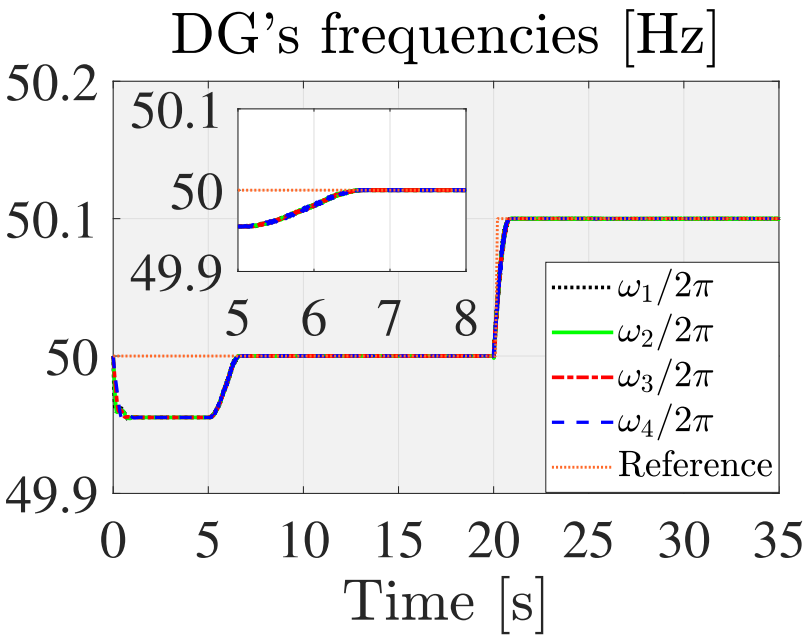

FIGURE 5.1: DG's frequency $\omega_i(t)$ under distributed finite-time SC, $i = 1, 2, 3, 4$.

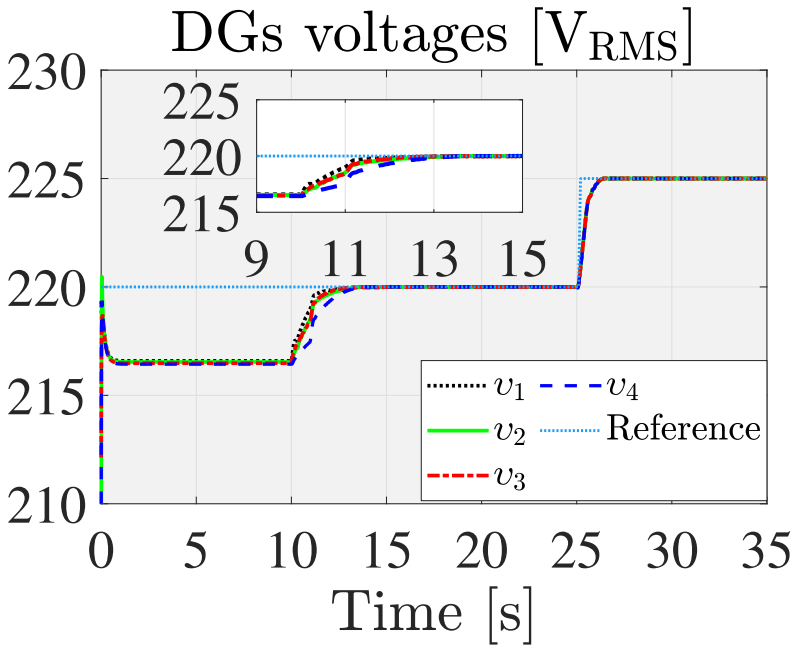

FIGURE 5.2: DG's voltage $v_i(t)$ under distributed finite-time SC, $i = 1, 2, 3, 4$.

- Step 1 ($t = 0 - 5$s): Only the PC is used with $\omega_{ni} = 2\pi 50$rad/s, $v_{ni} = 220\text{V}_{\text{RMS}}$ (per phase rms).
- Step 2 ($t = 5$s): The frequency SC (5.13) and the real power control (5.14) are activated with $\omega_0 = 2\pi 50$rad/s.
- Step 3 ($t = 10$s): The voltage SC (5.46) is activated with $v_0 = 220\text{V}_{\text{RMS}}$.
- Step 4 ($t = 15 - 20$s): The load (P_{L3}, Q_{L3}) is added/removed by using a three-phase breaker.

- Step 5 ($t = 20$s): The frequency SC's setpoint is changed to $\omega_0 = 2\pi 50.1$rad/s.
- Step 6 ($t = 25$s): The setpoint for the voltage SC is changed to $v_0 = 225 V_{RMS}$.

As can be observed from Figures. 5.1 and 5.2, during Step 1, when both SCs are switched off, all the corresponding voltages and frequencies are less than the reference values and the PC cannot prevent their deviations from the setpoints. To adjust the microgrid's voltage and frequency to the desired values and achieve an accurate real power sharing, the proposed frequency and the real power control are activated at $t = 5s$ with $\omega_0 = 2\pi 50$rad/s. Furthermore, the proposed voltage SC is enabled at $t = 10s$ with $v_0 = 220 V_{RMS}$.

Figures. 5.1 and 5.2 also demonstrate that the proposed distributed SC robustly restores the DG's frequencies and voltages to the expected values in the finite time. It is clear from Figure. 5.3 that the proposed SC preserves the active power sharing.

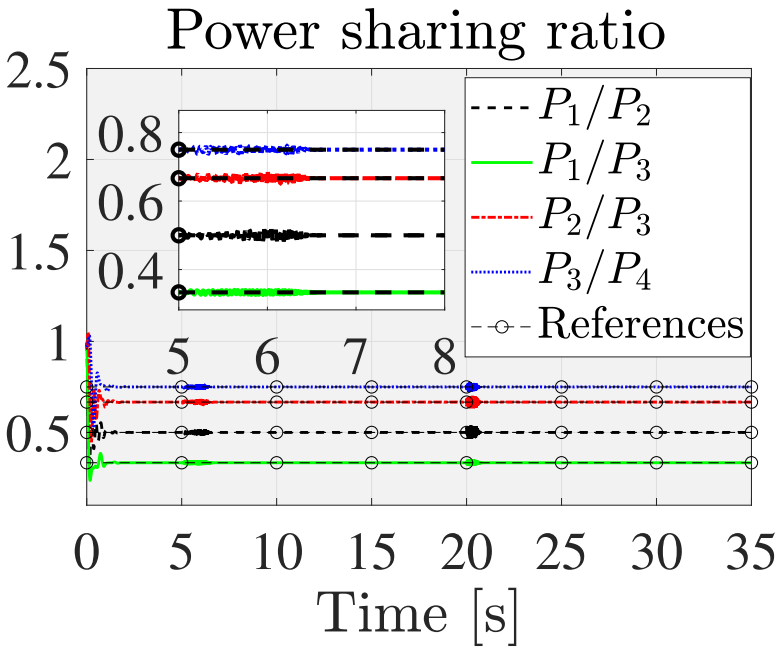

FIGURE 5.3: Comparison between the expected (i.e., k_{P_i}/k_{P_j}) and actual (i.e., P_i/P_j) power sharing ratio under distributed finite-time SC, $i = 1, 2, 3, 4$, $j \neq i$, $j > i$.

We add the sample load (P_{L3}, Q_{L3}) at $t = 15s$, and then remove it at $t = 20s$ by a three-phase breaker. The results show that the proposed SCs are robust against unexpected changes on demands.

Moreover, we modify the frequency and voltage SC setpoints at $t = 20s$ and $t = 25$ to $\omega_0 = 2\pi 50.1Hz$ and $v_0 = 225 V_{RMS}$ respectively. Consequently, all DG's frequencies and voltages converge to the setpoint values very quickly. The time evolutions of the proposed SCs are depicted in Figures. 5.4 and 5.5. The results verify that the frequency and voltage SCs show a satisfactory performance and a smooth control signals reducing the chattering problem.

5.5 Conclusion

In this chapter, the distributed SC protocols including the finite-time frequency restoration, voltage restoration and active power sharing accuracy are proposed. For each

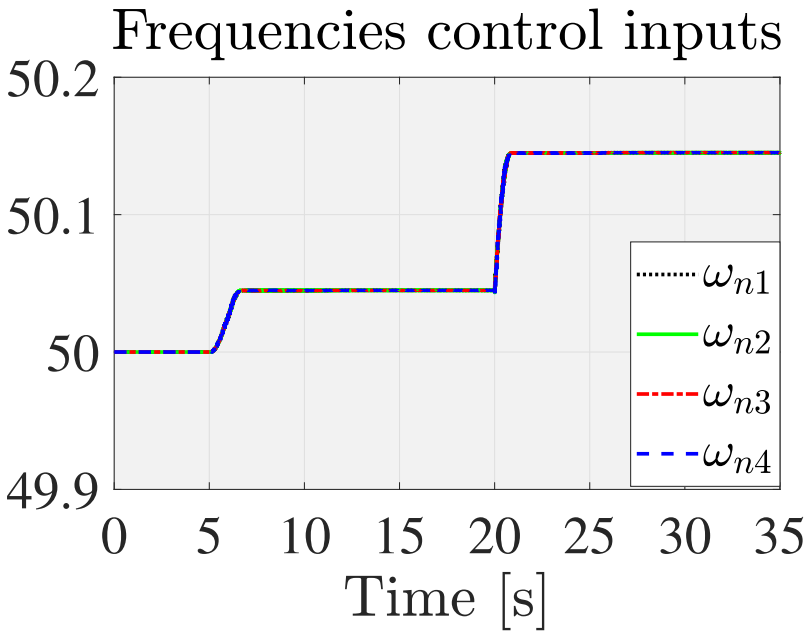

FIGURE 5.4: Frequency secondary control $\omega_{n_i}(t)$ under distributed finite-time SC, $i = 1, 2, 3, 4$.

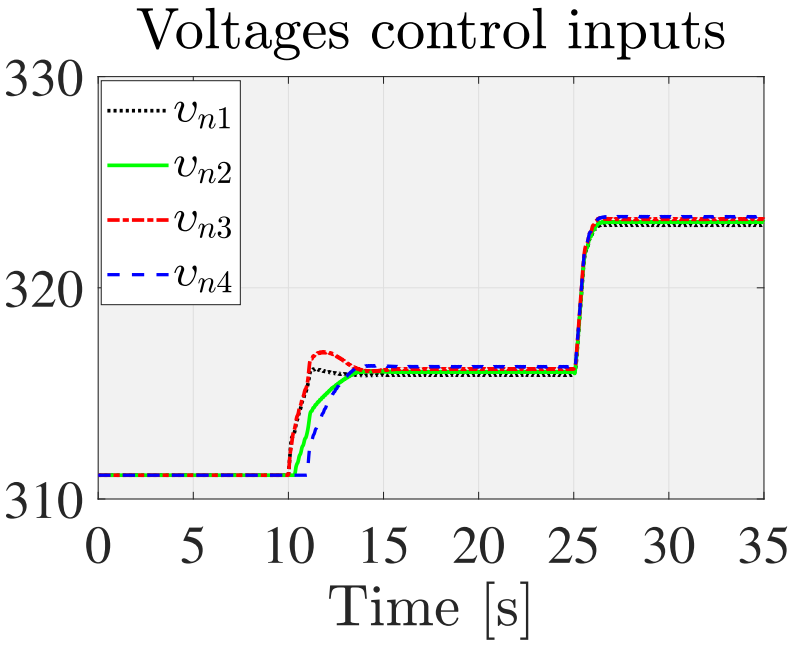

FIGURE 5.5: Voltage secondary control $v_{n_i}(t)$ under distributed finite-time SC, $i = 1, 2, 3, 4$.

DG with no access to the information about the SC's setpoints, the finite-time distributed estimators are employed to provide an estimate of the SC's setpoints. The proposed distributed SCs use this provided information to regulate all the voltage and frequency terms to their reference values in a finite time while preserving the real active power sharing.

Chapter 6

Certainty Equivalence Model Predictive Operation Control

In this chapter, a novel certainty equivalence MPC approach is formulated for the operation of the mentioned islanded MG in Section 2.4, where the uncertain input is assumed to be given by the nominal forecast values. The formulation is based on the model from Section 2.4 and therefore intended for the control of islanded MGs with high share of RES. This chapter is structured as follows. In Section 6.1, we describe the concept of MPC. The main contributions of this chapter are provided in Section 6.2. After that, a control-oriented MG model is derived in Section 6.3. In Section 6.4 we quantify the operating costs of the MG. In Section 6.5, we illustrate the properties of the resulting MPC in a numerical case study. Lastly, we provide a summary and concluding remarks in Section 6.6.

6.1 Concept of Model Predictive Control

Model predictive control is an optimal control based approach that has been used in many process industries [113, 114, 115, 116]. The purpose of MPC is to compute a control input at an instant time by minimizing a cost function of a finite horizon control problem [117, 118, 119, 120]. More specifically, MPC intends to achieve an optimal input trajectory that minimizes a cost function J over a prediction horizon N. Hence, the states and internal variables of the system are forecasted in the future. Unfortunately, the states and internal variables are affected not only by the control input but also by an uncertain input (see Figure 6.1). Note that because the uncertain input is usually unknown, its forecast is often used in the optimal control problem.

6.2 Main Contributions

In this chapter, we will propose a certainty equivalence MPC approach for the operation of islanded MG. This approach assumes that the uncertain input follows the nominal forecast of load and available renewable infeed. The closed-loop setup of the proposed certainty equivalence MPC scheme for operation of islanded MG is shown in Figure 6.1.

The main contributions of this chapter are as:

i) We derive the model of an islanded MG with uncertain renewable generation and loads with very high share of RES. This model, motivated by [121, 122, 72], considers a possible limitation of renewable infeed while limitations on

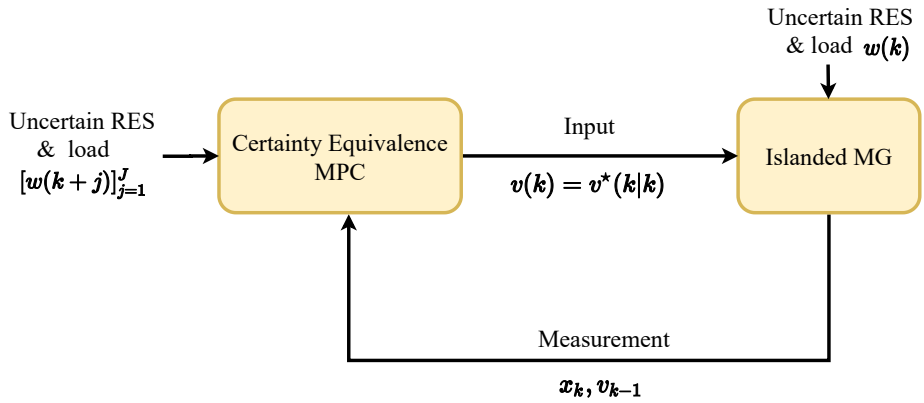

FIGURE 6.1: Certainty equivalence MPC scheme for operation of islanded MG at time instant k and $\forall j = 0, ..., J-1$.

transmission lines are approximately accounted for using DC power flow approximations.

ii) We model storage devices as grid-forming units and consider the conversion losses of storage units in the model by quadratic functions to reduce the error in storage units state of charge prediction.

iii) we propose a certainty MPC problem for the optimal operation of an MG with very high share of renewable energy sources.

In what follows, we will derive a control-oriented MG model of the form (2.29). We start by posing some assumptions.

Assumption 6.2.1 (Lower control layers) *The lower control layers, i.e., primary and secondary control are considered to compensate the frequency and voltage deviations by providing setpoints to the units as well as establishing the power sharing (see, e.g., [123, 124]) among the grid-forming units. Notice that the MG can run autonomously in these layers for several minutes.*

Assumption 6.2.2 (Conventional units) *In terms of time, conventional units have a shorter start-up and shutdown times than the sampling time of (MPC), meaning that switching actions are supposed to be instantaneous. Changes in power are instantaneous, i.e., no climb rates need to be considered.*

Assumption 6.2.3 (Storage units) *The state of charge can be estimated sufficiently accurately and is accessible to the operation control. The error introduced by neglecting self discharge and conversion losses of storage units is small compared to the uncertainty introduced by renewable infeed and loads.*

Assumption 6.2.4 (RES units and loads) *Assuming that the disturbance of the load and the renewable power output are known in advance.*

Assumption 6.2.5 (Transmission lines) *It is assumed that the resistance of the electrical coupling among units and loads of MG as well as reactive power flow is negligible. Since the voltage amplitudes in the network are constant and the phase angle differences small, the DC power flow approximations [48] can be employed.*

6.3 Certainty Model Predictive Control

6.3.1 Plant model interface

The power setpoints of the units $u(k) = [u_t(k)' \; u_s(k)' \; u_r(k)']' \in \mathbb{R}^U$, called the real-valued manipulated variables containing $u_t(k)' \in \mathbb{R}^T_{\geq 0}$ as setpoints of the T conventional units, $u_s(k)' \in \mathbb{R}^S$ the setpoints of the S storage units and $u_r(k) \in \mathbb{R}^R_{\geq 0}$ the setpoints of the R (RES). To show that conventional units are enabled or disabled, we will consider a Boolean input for each conventional units and we collect all Boolean inputs in a vector $\delta_t(k) \in \{0,1\}^T$. Moreover, the stored energies of the storage units are gathered in the state vector $x(k) \in \mathbb{R}^S_{\geq 0}$. The uncertain external inputs of the model is expressed by $w(k) = [w_r(k)' \; w_d(k)']'$, where $w_r(k) \in \mathbb{R}^R_{\geq 0}$ shows the maximum available power of the renewable units under given weather conditions and $w_d(k) \in \mathbb{R}^D_{\geq 0}$ the load.

6.3.2 Power of units

We consider $p(k) = [p_t(k)' \; p_s(k)' \; p_r(k)']'$ as the vector of power values, which consists of the power of conventional units, $p_t(k) \in \mathbb{R}^T_{\geq 0}$, storage units, $p_s \in \mathbb{R}^S$, and RES, $p_r(k) \in \mathbb{R}^R_{\geq 0}$. It is worth noting that in islanded mode, since production, consumption and storage power must be balanced in presence of uncertain load and renewable infeed, the power of the units $p(k) \in \mathbb{R}^U$ is not necessarily equal to the setpoints $u(k)$.

Active power at RES units

Let the active power of renewable units, $p_{\mathrm{r}}(k)$, as well as the corresponding setpoints, $u_{\mathrm{r}}(k)$, be bounded by:

$$p_{\mathrm{r}}^{\min} \leq p_r(k) \leq p_{\mathrm{r}}^{\max}, \tag{6.1a}$$
$$p_{\mathrm{r}}^{\min} \leq u_r(k) \leq p_{\mathrm{r}}^{\max}. \tag{6.1b}$$

Furthermore, we consider that the power infeed $p_{\mathrm{r},i}(k) \in \mathbb{R}_{\geq 0}$ of any renewable unit $i \in \mathcal{N}_{[1,R]}$ can be constrained by the power setpoint $u_{\mathrm{r},i}(k) \in \mathbb{R}_{\geq 0}$. Notice that the power tracks the setpoint when the maximum possible infeed under current weather conditions $w_{\mathrm{r},i}(k) \in \mathbb{R}_{\geq 0}$ be greater than or equal $u_{\mathrm{r},i}(k)$. This can be characterized by using the element-wise min operator as follows:

$$p_r(k) = \min(u_r(k), w_r(k)). \tag{6.2}$$

To solve the optimization problem, the authors in [125] reformulated (6.2) to a set of linear inequalities including integer variables as following:

$$p_{\mathrm{r}}(k) \leq u_{\mathrm{r}}(k), \tag{6.3a}$$
$$p_{\mathrm{r}}(k) \geq u_{\mathrm{r}}(k) + (\mathrm{diag}\,(w_{\mathrm{r}}(k)) - \mathrm{M_r} I_R)\delta_{\mathrm{r}}(k), \tag{6.3b}$$
$$p_{\mathrm{r}}(k) \leq w_{\mathrm{r}}(k), \tag{6.3c}$$
$$p_{\mathrm{r}}(k) \geq w_{\mathrm{r}}(k) - (\mathrm{diag}\,(w_{\mathrm{r}}(k)) - \mathrm{m_r} I_R)(1_R - \delta_{\mathrm{r}}(k)). \tag{6.3d}$$

where $\delta_{\mathrm{r}}(k) \in \{0,1\}^R$ represents the free variable and $\mathrm{m_r} \in \mathbb{R}$, $\mathrm{m_r} < \min(p_{\mathrm{r}}^{\min})$ and $\mathrm{M_r} \in \mathbb{R}_{\geq 0}$, $\mathrm{M_r} > \max(p_{\mathrm{r}}^{\max})$ are the constant coefficients which are computed offline.

TABLE 6.1: Model-specific variables

Symbol	Explanation	Unit	Size
x	Energy of storage units (state)	pu h	S
u_t	Setpoint inputs of conventional units	pu	T
u_s	Setpoint inputs of storage units	pu	S
u_r	Setpoint inputs of renewable units	pu	R
u	Setpoint inputs of all units	pu	U
δ_t	Boolean inputs of conventional units	—	T
v	Vector of all control inputs	—	Q
w_r	Uncertain available renewable power	pu	R
w_d	Uncertain load	pu	D
w	Vector of all uncertain inputs	pu	W
p_t	Active power of conventional units	pu	T
p_s	Active power of storage units	pu	S
p_r	Active power of renewable units	pu	R
p	Active power of all units	pu	U
p_e	Power over transmission lines	pu	E
δ_r	Boolean auxiliary variables	—	R
ρ	Real-valued auxiliary variable	—	1
$\bar{q}$	Vector of all auxiliary variables	—	Q

Active power at conventional units

We consider if the conventional unit $i \in \mathcal{N}_{[1,T]}$ is enabled, i.e., if $\delta_{\mathrm{t},i}(k) = 1$, then its active power is bounded by $p_{\mathrm{t},i}^{\min} \in \mathbb{R}_{\geq 0}$ and $p_{\mathrm{t},i}^{\max} \in \mathbb{R}_{\geq 0}$. If the unit is disabled, i.e., $\delta_{\mathrm{t},i}(k) = 0$, then naturally $p_{\mathrm{t},i}(k) = 0$. The active power of conventional units with $p_\mathrm{t}^{\min} \in \mathbb{R}_{\geq 0}^{T}$, $p_\mathrm{t}^{\max} \in \mathbb{R}_{\geq 0}^{T}$ can be written in vector form as:

$$\operatorname{diag}\left(p_\mathrm{t}^{\min}\right) \delta_\mathrm{t}(k) \leq p_\mathrm{t}(k) \leq \operatorname{diag}\left(p_\mathrm{t}^{\max}\right) \delta_\mathrm{t}(k), \tag{6.4a}$$

The same holds for the active power setpoints, i.e.,

$$\operatorname{diag}\left(p_\mathrm{t}^{\min}\right) \delta_\mathrm{t}(k) \leq u_\mathrm{t}(k) \leq \operatorname{diag}\left(p_\mathrm{t}^{\max}\right) \delta_\mathrm{t}(k). \tag{6.4b}$$

Active power at storage units

Since we assume all storage units are always enabled, all their active power setpoints, active power values are bounded as:

$$p_\mathrm{s}^{\min} \leq p_\mathrm{s}(k) \leq p_\mathrm{s}^{\max}, \tag{6.5a}$$
$$p_\mathrm{s}^{\min} \leq u_\mathrm{s}(k) \leq p_\mathrm{s}^{\max}. \tag{6.5b}$$

where $p_\mathrm{s}^{\min} \in \mathbb{R}_{\leq 0}^{S}$ and $p_\mathrm{s}^{\max} \in \mathbb{R}_{\geq 0}^{S}$ represent the known lower and upper power limits.

6.3.3 Power sharing of grid-forming units

Note that the power of all unites does not necessarily equal to the power setpoints that are assigned to the system due to variations of load and renewable infeed. We

assumed that all storage and conventional units are controlled by the lower control layers so that they share the changes in load and renewable infeed in a desired proportional manner. This so called proportional power sharing (see, e.g., [123, 124]) depends on the design parameter $\chi_i \in \mathbb{R}_{>0}$ for all grid-forming units. A practical choice for χ_i is, e.g., proportional to the nominal power of the corresponding units.

Power sharing can be formalised as follows. Two units $i \in \mathcal{N}_{[1,T+S]}$ and $j \in \mathcal{N}_{[1,T+S]}$, $i \neq j$ are said to share their active power proportionally according to $\chi_i \in \mathbb{R}_{>0}$ and $\chi_j \in \mathbb{R}_{>0}$, if the next relation holds:

$$\frac{p_i(k) - u_i(k)}{\chi_i} = \frac{p_j(k) - u_j(k)}{\chi_j} \tag{6.6}$$

By defining a new auxiliary free variable $\rho(k) \in \mathbb{R}$ and considering that only enabled units, namely units i with $\delta_{\mathrm{t},i}(k) = 1$, can participate in power sharing, (6.6) can be recast for all grid-forming units with $K_\mathrm{t} = \operatorname{diag}\left([\frac{1}{\chi_1} \cdots \frac{1}{\chi_T}]'\right)$ and $K_\mathrm{s} = \operatorname{diag}\left([\frac{1}{\chi_{(T+1)}} \cdots \frac{1}{\chi_{(T+S)}}]'\right)$ as [125]

$$K_\mathrm{t}(p_\mathrm{t}(k) - u_\mathrm{t}(k)) = \rho(k)\delta_\mathrm{t}(k) \text{ and} \tag{6.7a}$$
$$K_\mathrm{s}(p_\mathrm{s}(k) - u_\mathrm{s}(k)) = \rho(k)1_S. \tag{6.7b}$$

For the formulation of the optimisation problem, [125] by using a similar strategy as described in [126] transform (6.7a) into the following set of linear inequalities with integer variables:

$$K_\mathrm{t}(p_\mathrm{t}(k) - u_\mathrm{t}(k)) \leq \mathrm{M}_\mathrm{t}\delta_\mathrm{t}(k), \tag{6.8a}$$
$$K_\mathrm{t}(p_\mathrm{t}(k) - u_\mathrm{t}(k)) \geq \mathrm{m}_\mathrm{t}\delta_\mathrm{t}(k), \tag{6.8b}$$
$$K_\mathrm{t}(p_\mathrm{t}(k) - u_\mathrm{t}(k)) \leq 1_T\rho(k) - \mathrm{m}_\mathrm{t}(1_T - \delta_\mathrm{t}(k)), \tag{6.8c}$$
$$K_\mathrm{t}(p_\mathrm{t}(k) - u_\mathrm{t}(k)) \geq 1_T\rho(k) - \mathrm{M}_\mathrm{t}(1_T - \delta_\mathrm{t}(k)). \tag{6.8d}$$

where $\mathrm{M}_\mathrm{t} \in \mathbb{R}$ can be calculated offline and its value should be greater than the biggest possible value of $\rho(k)$. Hence, with the biggest possible value for the storage units, $\rho_\mathrm{s}^{\max} = \max(K_\mathrm{s}(p_\mathrm{s}^{\max} - p_\mathrm{s}^{\min}))$, and for the conventional units, $\rho_\mathrm{t}^{\max} = \max(K_\mathrm{t}(p_\mathrm{t}^{\max} - p_\mathrm{t}^{\min}))$, M_t has to be chosen such that $\max\left(\rho_\mathrm{s}^{\max}, \rho_\mathrm{t}^{\max}\right) < \mathrm{M}_\mathrm{t}$. Moreover, $\mathrm{m}_\mathrm{t} = -\mathrm{M}_\mathrm{t}$.

6.3.4 Dynamics of storage units

The dynamics of all storage units can be formulated as:

$$x(k+1) = x(k) - \mathrm{T}_\mathrm{s}p_\mathrm{s}(k) - \mathrm{T}_\mathrm{s}\mathbb{F}\left(p_\mathrm{s}(k)\right), \tag{6.9}$$

Let $\mathrm{T}_\mathrm{s} \in \mathbb{R}_{>0}$ be the sampling time. The stored energy is denoted by $x(k)$ with initial state $x(0) = x_0$. The constraint of the stored energy is given by:

$$x^{\min} \leq x(k+1) \leq x^{\max}, \tag{6.10}$$

with $x^{\min} = 0_S$ and $x^{\max} \in \mathbb{R}^S_{\geq 0}$. In particular, $\mathbb{F}\left(p_\mathrm{s}(k)\right) = [f_1\left(p_{\mathrm{s},1}(k)\right), \ldots, f_S\left(p_{\mathrm{s},S}(k)\right)]'$ is a vector of $S \in \mathbb{N}$ where each of its element represents a model of conversion losses of storage units, considered to be a convex quadratic function as follows:

$$f_i\left(p_{\mathrm{s},i}(k)\right) = a p_{\mathrm{s},i}(k)^2 + b p_{\mathrm{s},i}(k) + c, \quad a, b, c \in \mathbb{R} \tag{6.11}$$

where $p_{s,i}(k)$ is assumed to be limited as:

$$p_{s,i}(k) \in \mathcal{D}_i = \{p_{s,i}(k) | p_{s,i}^{\min} \leq p_{s,i}(k) \leq p_{s,i}^{\max}\} \tag{6.12}$$

To solve the optimization problem, it is useful to reformulate the function $f(p_{s,i}(k))$ as piecewise affine functions, i.e, (see, e.g., [126]):

$$f_i(p_{s,i}(k)) = \begin{cases} A_{1,i}p_{s,i}(k) + B_{1,i}, & p_{s,i}(k) \in \mathcal{D}_{1,i}, \\ A_{2,i}p_{s,i}(k) + B_{2,i}, & p_{s,i}(k) \in \mathcal{D}_{2,i}, \\ \quad \vdots & \\ A_{r,i}p_{s,i}(k) + B_{r,i}, & p_{s,i}(k) \in \mathcal{D}_{r,i}. \end{cases} \tag{6.13}$$

in which $A_{y,i}$, $B_{y,i} \in \mathbb{R}$ and the following holds:

$$\bigcup_{1 \leq y \leq r} \mathcal{D}_{y,i} = \mathcal{D}_i \tag{6.14a}$$

$$\bigcap_{1 \leq y \leq r} \mathcal{D}_{y,i} = 0 \tag{6.14b}$$

and on the borders of sequential $\mathcal{D}_y$, the linear segments are connected, which means that $f_i(p_{s,i}(k))$ is continuous.

The condition $p_{s,i}(k)$ at each partition $\mathcal{D}_{y,i}$ can be associated to a binary variable $\delta_{y,i}(k) \in \{0, 1\}$, $\forall y = 1, 2, \ldots, r$, satisfying the exclusive-or condition:

$$\bigoplus_{y=1}^{r} [\delta_{y,i}(k) = 1]. \tag{6.15}$$

such that:

$$[\delta_{y,i}(k) = 1] \longleftrightarrow p_{s,i}(k) \in \mathcal{D}_{y,i} \tag{6.16}$$

From (6.15) there exists some $\delta_{y,i}(k) = 1$, which implies $p_{s,i}(k) \in \mathcal{D}_{y,i}$, a contradiction by (6.14b). (6.14)-(6.16) are therefore equivalent to:

$$\mathbb{J}_{y,i}^T p_{s,i}(k) - \mathbb{H}_{y,i}^T \leq \mathbb{M}_i^\star [1 - \delta_{y,i}(k)] \tag{6.17a}$$

$$\sum_{y=1}^{r} \delta_{y,i}(k) = 1 \tag{6.17b}$$

with $\mathbb{J}_{y,i} = \begin{bmatrix} 1 & -1 \end{bmatrix}$ for $y = \{1, \ldots, r\}$ and $i = \{1, \ldots, S\}$ and $\mathbb{H}_{y,i}$ represents a vector of 2, where the first row of $\mathbb{H}_{y,i}$ is equal to the lower bound of the $D_{y,i}$ with a minus sign while its second row is the upper bound. $\mathbb{M}_i^\star$ in (6.17a) can be computed as:

$$\mathbb{M}_i^\star \cong \max_{p_{s,i}(k) \in \mathcal{D}_i} \mathbb{J}_{y,i}^T p_{s,i}(k) - \mathbb{H}_{y,i}^T \tag{6.18}$$

By using this binary variable, we can recast (6.13) as follows:

$$f_i(p_{s,i}(k)) = \begin{cases} A_{1,i}p_{s,i}(k) + B_{1,i}, & \text{if } \delta_{1,i}(k) = 1, \\ A_{2,i}p_{s,i}(k) + B_{2,i}, & \text{if } \delta_{2,i}(k) = 1, \\ \quad \vdots & \\ A_{r,i}p_{s,i}(k) + B_{r,i}, & \text{if } \delta_{r,i}(k) = 1. \end{cases} \tag{6.19}$$

Therefore, (6.19) can be rewritten as:

$$f_i\big(p_{\mathrm{s,i}}(k)\big) = \sum_{y=1}^{r} [A_{y,i} p_{\mathrm{s,i}}(k) + B_{y,i}]\delta_{y,i}(k). \tag{6.20}$$

Unfortunately, (6.20) is nonlinear, since it involves products between logical variables and inputs. Therefore, we transform it into equivalent mixed-integer linear inequalities. This can be done using a similar strategy as proposed in [126]. To this aim, we set:

$$f_i\big(p_{\mathrm{s,i}}(k)\big) = \sum_{y=1}^{r} z_{y,i}(k) \tag{6.21a}$$

$$z_{y,i}(k) \cong [A_{y,i} p_{s,i}(k) + B_{y,i}]\delta_{y,i}(k). \tag{6.21b}$$

Then, (6.21b) is equivalent to:

$$\begin{aligned}
&z_{y,i}(k) \leq \widetilde{M}_i \delta_{y,i}(k),\\
&z_{y,i}(k) \geq \widetilde{m}_i \delta_{y,i}(k),\\
&z_{y,i}(k) \leq A_{y,i} p_{s,i}(k) + B_{y,i} - \widetilde{m}_i(1-\delta_{y,i}(k)), &(6.22)\\
&z_{y,i}(k) \geq A_{y,i} p_{s,i}(k) + B_{y,i} - \widetilde{M}_i(1-\delta_{y,i}(k)). &(6.23)
\end{aligned}$$

being

$$\widetilde{M}_i \cong \max_{y=1,\ldots,r} \Big\{ \max_{p_{s,i}(k)\in\mathcal{D}_i} A_{i,y} p_{s,i}(k) + B_{i,y} \Big\}. \tag{6.24a}$$

$$\widetilde{m}_i \cong \min_{y=1,\ldots,r} \Big\{ \max_{p_{s,i}(k)\in\mathcal{D}_i} A_{i,y} p_{s,i}(k) + B_{i,y} \Big\}. \tag{6.24b}$$

Remark 6.3.1 *Notice that in [125], the dynamics of all storage units are considered without piecewise affine losses model, namely,*

$$x(k+1) = x(k) - \mathrm{T_s} p_{\mathrm{s}}(k), \tag{6.25}$$

with

$$x^{\min} \leq x(k+1) \leq x^{\max}, \tag{6.26}$$

6.3.5 Transmission network

Following [71, 127], the DC power flow approximations can be employed to extract the power of transmission lines, $p_e(k) = [p_{e,1}(k) \quad \ldots \quad p_{e,E}(k)]'$. Hence, the power on lines can be formulated from the power of units and load using the following linear equation:

$$p_e(k) = F \cdot [p(k)' \quad w_d(k)']', \tag{6.27a}$$

where $F \in \mathbb{R}^{E\times(U+D)}$ represents a matrix that links the power flowing over the lines with the power produced or consumed by the units and loads. More details about the derivation of F described in [71, 128]. It is assumed that $p_e(k)$ be bounded by:

$$p_e^{\min} \leq p_e(k) \leq p_e^{\max} \tag{6.27b}$$

with $p_e^{\min} \in \mathbb{R}^E_{\leq 0}$ and $p_e^{\max} \in \mathbb{R}^E_{\geq 0}$. This assumption is reasonable due to the physical limitation in transmission capability of the lines. Moreover, the produced power

must be equal to the consumed power at all times, e.g.

$$1_T' p_t(k) + 1_S' p_s(k) + 1_R' p_r(k) = 1_D' w_d(k). \tag{6.27c}$$

6.3.6 Overall model

In accordance with equations considered for the different parts of an islanded MG, the overall model can be formulated as follows. The constraints on power and set-point originate from (6.4), (6.1) and (6.5), namely,

$$\begin{bmatrix} \mathrm{diag}\left(p_{\mathrm{t}}^{\max}\right)\delta_{\mathrm{t}}(k) \\ p_{\mathrm{s}}^{\max} \\ p_{\mathrm{r}}^{\max} \end{bmatrix} \leq u(k) \leq \begin{bmatrix} \mathrm{diag}\left(p_{\mathrm{t}}^{\min}\right)\delta_{\mathrm{t}}(k) \\ p_{\mathrm{s}}^{\min} \\ p_{\mathrm{r}}^{\min} \end{bmatrix} \tag{6.28a}$$

and

$$\begin{bmatrix} \mathrm{diag}\left(p_{\mathrm{t}}^{\max}\right)\delta_{\mathrm{t}}(k) \\ p_{\mathrm{s}}^{\max} \\ p_{\mathrm{r}}^{\max} \end{bmatrix} \leq p(k) \leq \begin{bmatrix} \mathrm{diag}\left(p_{\mathrm{t}}^{\min}\right)\delta_{\mathrm{t}}(k) \\ p_{\mathrm{s}}^{\min} \\ p_{\mathrm{r}}^{\min} \end{bmatrix} \tag{6.28b}$$

By referring to (6.9), the dynamics of the storage unit are described by

$$x(k+1) = x(k) - \mathrm{T_s} p_{\mathrm{s}}(k) - \mathrm{T_s}[f_1(p_{\mathrm{s},1}(k)), \ldots, f_S(p_{\mathrm{s,S}}(k))]', \tag{6.28c}$$

with constraint functions

$$x^{\min} \leq x(k+1) \leq x^{\max}, \tag{6.28d}$$

$$f_i(p_{\mathrm{s,i}}(k)) = \sum_{y=1}^{r} z_{y,i}(k) \tag{6.28e}$$

$$\begin{aligned} &z_{y,i}(k) \leq \widetilde{M}_i \delta_{y,i}(k), \\ &z_{y,i}(k) \geq \widetilde{m}_i \delta_{y,i}(k), \\ &z_{y,i}(k) \leq A_{y,i} p_{s,i}(k) + B_{y,i} - \widetilde{m}_i(1 - \delta_{y,i}(k)), \\ &z_{y,i}(k) \geq A_{y,i} p_{s,i}(k) + B_{y,i} - \widetilde{M}_i(1 - \delta_{y,i}(k)). \end{aligned} \tag{6.28f}$$

The renewable infeed which is a function of the setpoint and the available power under weather conditions is given by (6.3) as

$$p_{\mathrm{r}}(k) \leq u_{\mathrm{r}}(k), \tag{6.28g}$$

$$p_{\mathrm{r}}(k) \geq u_{\mathrm{r}}(k) + (\mathrm{diag}\,(w_{\mathrm{r}}(k)) - \mathrm{M_r} I_R)\delta_{\mathrm{r}}(k), \tag{6.28h}$$

$$p_{\mathrm{r}}(k) \leq w_{\mathrm{r}}(k), \tag{6.28i}$$

$$p_{\mathrm{r}}(k) \geq w_{\mathrm{r}}(k) - (\mathrm{diag}\,(w_{\mathrm{r}}(k)) - \mathrm{m_r} I_R)(1_R - \delta_{\mathrm{r}}(k)). \tag{6.28j}$$

Power sharing of the grid-forming units is described by (6.7) which, using (6.8), can be recast into

$$K_t(p_t(k) - u_t(k)) \leq M_t\delta_t(k), \tag{6.28k}$$
$$K_t(p_t(k) - u_t(k)) \geq m_t\delta_t(k), \tag{6.28l}$$
$$K_t(p_t(k) - u_t(k)) \leq 1_T\rho(k) - m_t(1_T - \delta_t(k)), \tag{6.28m}$$
$$K_t(p_t(k) - u_t(k)) \geq 1_T\rho(k) - M_t(1_T - \delta_t(k)). \tag{6.28n}$$

Lastly, the power limit of the transmission lines is introduced by (6.27), i.e.,

$$p_e^{\min} \leq F \cdot [p_t(k)' \quad 'p_s(k)' \quad 'p_r(k)' \quad w_d(k)']' \leq p_e^{\max} \tag{6.28o}$$
$$1_T'p_t(k) + 1_S'p_s(k) + 1_R'p_r(k) = 1_D'w_d(k). \tag{6.28p}$$

Now, let us compute a compact form of (6.28). From (6.28c) and by denoting $\bar{q}(k) = [p(k)'\ \delta_r(k)'\ \rho(k)']'$ and $B = [0_{S\times T} \quad -T_s(I_S + \mathbb{F}) \quad 0_{S\times 2R+1}]$, we can obtain Eq. (2.29a), namely,

$$x(k) + B\bar{q}(k) - x(k+1) = 0, \tag{6.29a}$$

By following (6.28d), we have

$$H_1 \cdot x(k+1) \leq h_1, \tag{6.29b}$$

with $H_1 = \text{diag}([1_S' \ -1_S']')$ and $h_1 = [(x^{\max})'\ (-x^{\min})']'$.

Finally, according to (6.28a)-(6.28b) and (6.28n)-(6.28p), the next equations can be yield as

$$H_2 \cdot \begin{bmatrix} v(k)' & \bar{q}(k)' & w(k)' \end{bmatrix}' \leq h_2, \tag{6.29c}$$
$$G \cdot \begin{bmatrix} v(k)' & \bar{q}(k)' & w(k)' \end{bmatrix}' = g, \tag{6.29d}$$

where H_2 and h_2 in (2.29c) are formed such that they reflect (6.1), (6.3)–(6.5), (6.8) and (6.27b). Additionally, G and g in (2.29d) are formed such that they reflect (6.7b), (6.27a) and (6.27).

6.4 Operating Costs

In this section, an operating cost function for an MG is extracted which reflects the main objectives: (i) economic operation, (ii) low number of switching actions, (iii) high use of RES and (iv) desired state of storage units. Let us employ cost functions that are motivated by [129].

The cost function at each node $i \in \mathcal{V}$ consists of two parts. The first part is specified by $\ell_o(v(k-1), v(k), \bar{q}(k+1)) \in \mathbb{R}_{\geq 0}$ that reflects items (i)–(iii) and the second part is denoted by $\ell_s(\bar{q}(k)) \in \mathbb{R}_{\geq 0}$ that corresponds to (iv).

The economically motivated cost comprises (i) operating costs of conventional units, $\ell_t^{\text{rt}}(v(k), \bar{q}(k+1)) \in \mathbb{R}_{\geq 0}$, (ii) costs caused by switching conventional units on or off, $\ell_t^{\text{sw}}(v(k-1), v(k)) \in \mathbb{R}_{\geq 0}$, and (iii) costs incurred by low utilisation of

renewable sources, $\ell_{\mathrm{r}}(\bar{q}(k+1)) \in \mathbb{R}_{\geq 0}$, i.e.,

$$\ell_{\mathrm{o}}(v(k-1), v(k), \bar{q}(k+1)) = \ell_{\mathrm{t}}^{\mathrm{rt}}(v(k), \bar{q}(k+1)) + \ell_{\mathrm{t}}^{\mathrm{sw}}(v(k-1), v(k)) + \ell_{\mathrm{r}}(\bar{q}(k+1)). \tag{6.30}$$

By following [130], the operating cost of the conventional units can be formulated as:

$$\ell_{\mathrm{t}}^{\mathrm{rt}}(v(k), \bar{q}(k+1) = c_{\mathrm{t}}'\delta_{\mathrm{t}}(k) + \tilde{c}_{\mathrm{t}}'p_t(k) + p_t(k)' \operatorname{diag}(\hat{c}_{\mathrm{t}})\, p_t(k), \tag{6.31}$$

with weights $c_{\mathrm{t}} \in \mathbb{R}_{>0}^{T}$, $\tilde{c}_{\mathrm{t}} \in \mathbb{R}_{>0}^{T}$ and $\hat{c}_{\mathrm{t}} \in \mathbb{R}_{>0}^{T}$.

The switching cost of a conventional generator can be modeled by considering that it was disabled at time instant $k-1$ and is enabled at time instant k, or was enabled at time instant $k-1$ and is disabled at time instant k, i.e,

$$\ell_{\mathrm{t}}^{\mathrm{sw}}(v(k), v(k-1)) = (\delta_{\mathrm{t}}(k-1) - \delta_{\mathrm{t}}(k))' \operatorname{diag}(c_{\mathrm{t}}^{\mathrm{sw}})\, (\delta_{\mathrm{t}}(k-1) - \delta_{\mathrm{t}}(k)) \tag{6.32}$$

with weight $c_{\mathrm{t}}^{\mathrm{sw}} \in \mathbb{R}_{>0}^{T}$.

The renewable unit costs can be adjusted by considering a penalty for using less than the maximal power $p_r^{\max}$, i.e.,

$$\ell_{\mathrm{r}}(v(k), \bar{q}(k+1)) = (p_r^{\max} - p_{\mathrm{r}}(k+1))' \operatorname{diag}(\hat{c}_{\mathrm{r}})\, (p_r^{\max} - p_{\mathrm{r}}(k+1)) + \tilde{c}_{\mathrm{r}}' u_{\mathrm{r}}(k) \tag{6.33}$$

with weight $\tilde{c}_{\mathrm{r}} \in \mathbb{R}_{>0}^{R}$, $\hat{c}_{\mathrm{r}} \in \mathbb{R}_{>0}^{R}$. Note that $u_{\mathrm{r}}(k)$ is added to ensure that the setpoint does not exceed the maximum available power $w_{\mathrm{r}}(k+1)$.

Finally, storing energy usually causes conversion losses. To represent the costs associated with these losses, the term

$$\ell_{\mathrm{s}}(\bar{q}(k)) = \bar{c}_{\mathrm{s}} + p_s(k)' \operatorname{diag}(\tilde{c}_{\mathrm{s}})\, p_s(k) \tag{6.34}$$

with weight $\tilde{c}_{\mathrm{s}} \in \mathbb{R}_{>0}^{S}$, $\hat{c}_{\mathrm{s}} \in \mathbb{R}_{>0}^{S}$ are included in the cost function.

6.5 Case study

In this section, we intend to verify the properties of the certainty equivalence model predictive control strategy proposed in Section 6.3. The microgrid structure depicted in Figure 2.3 is used for the simulations. It consists of a storage, a conventional and a renewable unit. The detailed parameters of the microgird are summarized in Table 6.2.

TABLE 6.2: Parameters of the Microgrid Test System

Parameter	Value	Weight	Value
$[p_t^{\min}, p_r^{\min}, p_s^{\min}]$	$[0.4, 0, -1]$ pu	c_{t}	0.1178
$[p_t^{\max}, p_r^{\max}, p_s^{\max}]$	$[1, 2, 1]$ pu	$\hat{c}_{\mathrm{t}}$	0.0048 1/pu
$[x^{\min}, x^{\max}]$	$[0, 7]$ pu h	$\tilde{c}_{\mathrm{t}}$	0.751 1/pu
$[\tilde{x}^{\min}, \tilde{x}^{\max}]$	$[0.5, 6.5]$ pu h	$\tilde{c}_{\mathrm{r}}$	0.0001
x^0	3 pu h	$\hat{c}_{\mathrm{r}}$	1 1/pu
$[K_t, K_s]$	$[1, 1]$	$\tilde{c}_{\mathrm{s}}$	0.09
$\widetilde{M}_i$	0.1	$\hat{c}_{\mathrm{s}}$	0.01
$\widetilde{m}_i$	-0.17	$c_{\mathrm{t}}^{\mathrm{sw}}$	0.1

We considered the susceptance and conductance of the transmission lines between units and load equal to $b_{ij} = -20pu$ and $g_{ij} = 0pu$, respectively. Thus, according to equation (6.27a), the relation between the power of the units and the load and the power of the transmission is obtained as follows:

$$\begin{bmatrix} p_{e,1}(k) \\ p_{e,2}(k) \\ p_{e,3}(k) \\ p_{e,4}(k) \end{bmatrix} = \begin{bmatrix} 1 & 0 & 0 & 0 \\ 0 & -1/3 & 1/3 & 0 \\ 0 & 2/3 & 1/3 & 0 \\ 0 & 1/3 & 2/3 & 0 \end{bmatrix} \begin{bmatrix} p_{t,1}(k) \\ p_{s,1}(k) \\ p_{r,1}(k) \\ w_{d,1}(k) \end{bmatrix} \tag{6.35}$$

It is assumed that the transmission power of each line is between -1.3pu and 1.3pu. Simulations were performed by using MATLAB 2018b with a sampling time of $T_s =$ 30 min and a simulation horizon of 7 d, i.e., 336 data points. For MPC, a prediction horizon of $N = 12$, a sampling time of $T_s = 30$ min were selected. Note that the storage unit has a relatively high capacity compared to the rated power which shows in $x^{\max} = 7$pu. Also the model of conversion losses of storage unit is modeled by a quadratic function as $f_1\big(p_{s,1}(k)\big) = 0.09p_{s,1}(k)^2 + 0.01$. Moreover, we reformulate the function $f_1\big(p_{s,1}(k)\big)$ as the following linear cases:

$$f_1\big(p_{s,1}(k)\big) = \begin{cases} -0.135p_{s,1}(k) - 0.035, & -1 \le p_{s,1}(k) \le -0.5, \\ -0.045p_{s,1}(k) + 0.01, & -0.5 \le p_{s,1}(k) \le 0, \\ 0.045p_{s,1}(k) + 0.01, & 0 \le p_{s,1}(k) \le 0.5, \\ 0.135p_{s,1}(k) - 0.035, & 0.5 \le p_{s,1}(k) \le 1. \end{cases} \tag{6.36}$$

In accordance with equations (6.24a), (6.24b) and (6.36), we chosen $\widetilde{M}_i = 0.1$ and $\widetilde{m}_i = -0.17$. We formulate the MPC problems in MATLAB using the YALMIP toolbox and solve numerically with Gurobi. Here, we first compare the prediction error of the state of charge in the cases with considering the dynamic storage with piecewise affine loss model (6.9)-(6.24) and the dynamic storage without piecewise affine loss model (6.25)-(6.28d) in the MPC problem. We formulated this error as $e(k) = x(k) - \tilde{x}(k)$, wherein $x(k)$ is the actual state of charge of the nonlinear loss model given the same power values whereas $\tilde{x}(k)$ is the forecast of the state of charge. To show the results of this comparison, for both cases an analysis was carried out. In the analysis, closed-loop simulations were performed over 366 simulation steps. For each simulation step, the state of charge prediction of the controllers (over 12 prediction steps) were compared to a prediction performed with the nonlinear plant model for the same storage power values. Then, at each prediction step, the probability distribution of the prediction errors was visualised in the form of box plots(see Figure 6.2). The circle of each box marks the median value of prediction errors of 336 data points in each prediction step. The box around the median values contains all data from the 25th to the 75th percentile. The down dash of each box represents the lowest occurring value of prediction errors in each step whereas the up dash marks the highest occurring value.

It can be seen in Figure 6.2 that including the conversion losses in the proposed model predictive controller, the prediction error is reduced. For example, at $N =$ 1, when the conversion loss model is not employed in the controller, the median value is 5×10^{-3}. By adding the conversion loss model in the controller, this value is decreased 3 times to 1.5×10^{-3}. It is worth noting that this ratio increases as the prediction horizon raises. As can be observed from the last step of Figure 6.2, the median value of the error equal to 9×10^{-2} when the conversion loss model is not included in the controller whereas this value is reduced to 2×10^{-2} when the conversion loss model is added to MPC problem formulation.

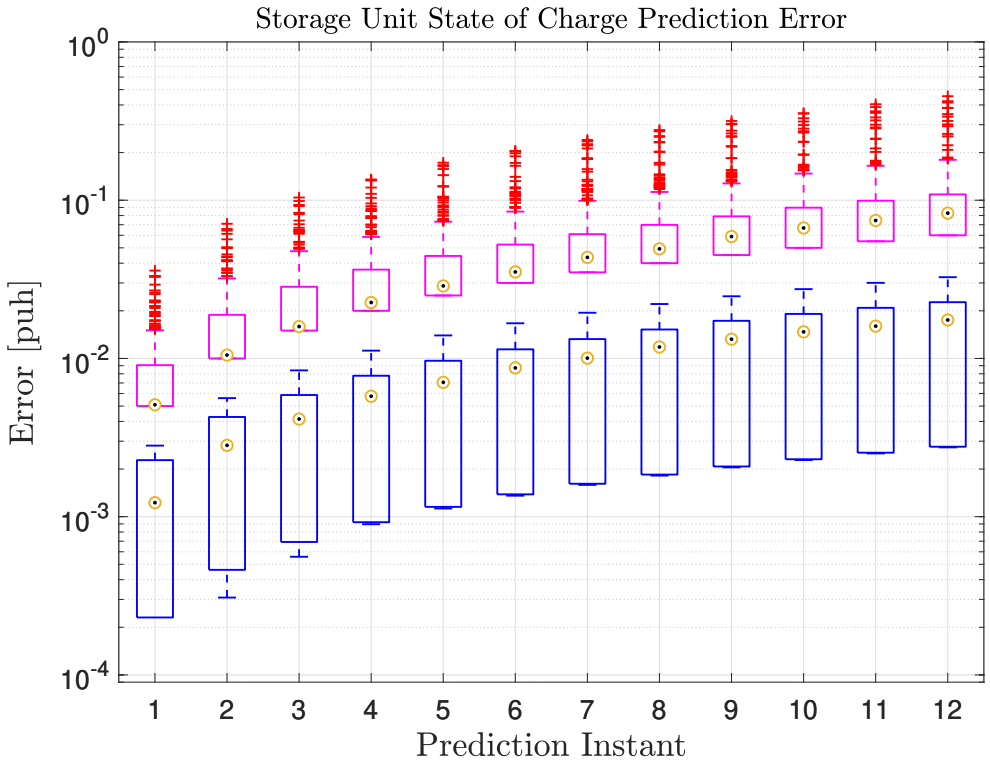

FIGURE 6.2: The prediction error of the state of charge (Up) With the dynamic storage without piecewise affine loss model (6.25)-(6.28d) in the controller; (Down) With the dynamic storage with piecewise affine loss model (6.9)-(6.24) in the controller.

The closed-loop simulation results of power of units and load as well as stored energy and line power of the MG are depicted in Figure 6.3. It can be noted that at the beginning of period, since the available power of renewable is low, the storage unit is discharging. When the battery is empty, the conventional generator is enabled to provide power to the load. As soon as the available power of the renewable unit is sufficient to provide power to the load, the conventional unit is disabled and the storage unit is begin charged. When the stored energy reaches the upper end of the desired state of charge, the setpoint of the wind turbine is set such that the wind power only covers the load. Thus, the stored energy approximately remains at $x^{\max} = 6.5$ pu h. At some point, the available renewable unit power cannot entirely cover the load and the storage is discharged. When the renewable unit reaches the minimum value $x^{\min} = 0.5$ pu h. and the storage unit is totally discharged, the conventional unit is activated again to provide power to the load. In the end of the simulation, the available power of the renewable unit increases again such that the storage unit can be charged with the available renewable unit power. Note that the line power in the lower plot was within the given bounds of ± 1.3 pu at all times.

6.6 Conclusion

In this chapter, we presented a novel certainty model predictive control approach for the operation of islanded MG with very high share of renewable energy sources. To this aim, we modelled the conversion losses of storage units by quadratic functions to reduce the error in storage units state of charge prediction.

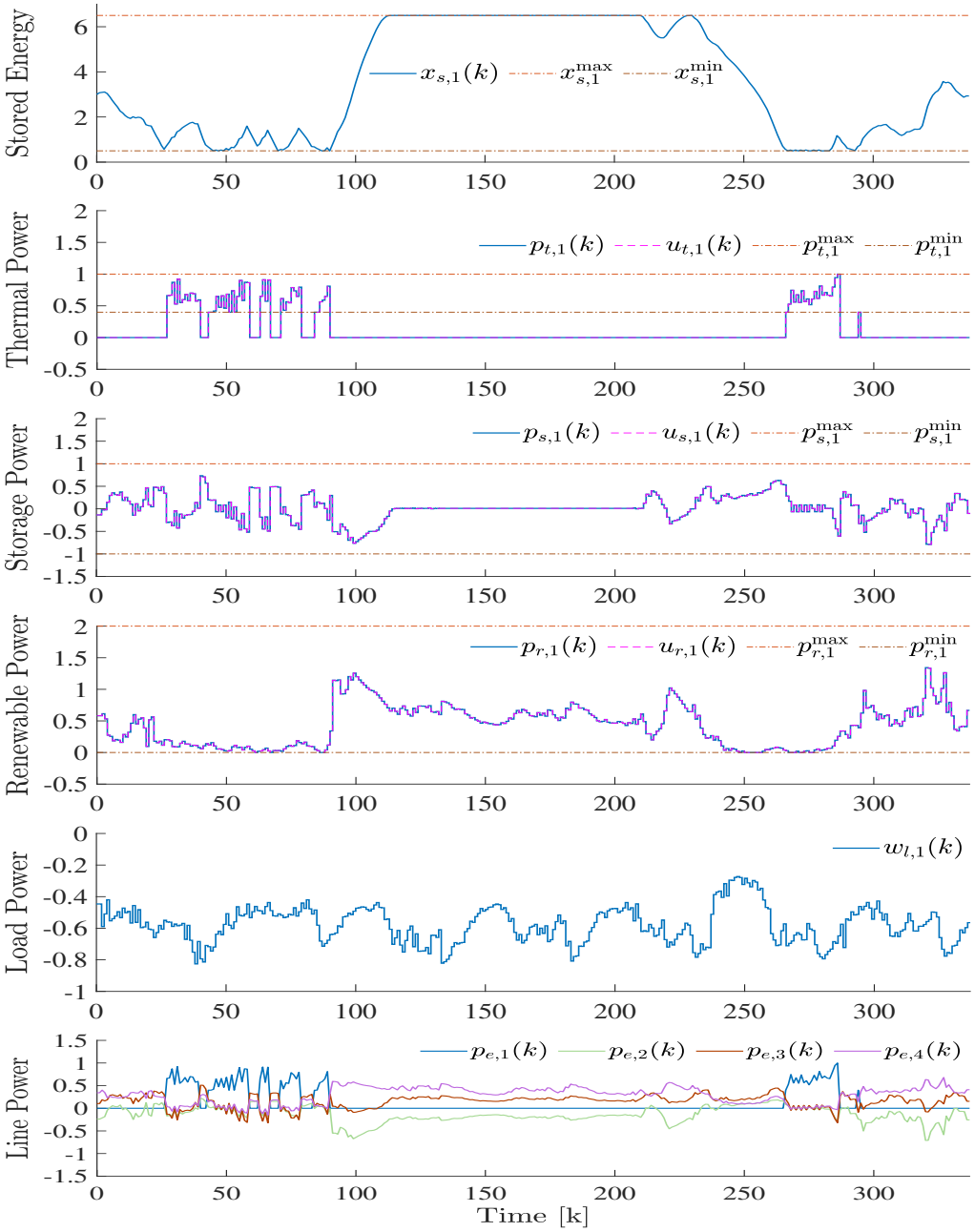

FIGURE 6.3: Power of units and load.

In the future, we would like to consider AC optimal power flow (OPF) problems which are more realistic than the widely used linearised DC power flow approximations. To solve the AC OPF problems, we intend to employ a convex relaxation of the original problem which led to a second-order cone program (SOCP) that can be solved by available commercial software.

Chapter 7

Conclusion

In what follows, a summary of this thesis is provided in Section 7.1. Moreover, future research directions are highlighted in Section 7.2.

7.1 Summary

This thesis deals with the problem of voltage and frequency restoration and optimization of AC MGs in some important challenges. To solve the problem, the concept of MGs and hierarchical control of them were provided in Chapter 1. Furthermore, the important challenges in controlling AC MGs such as (i) challenge in solving the problem of restoration in the presence of multiple non-uniform time-varying communication delays and nonlinear model uncertainties; (ii) challenge in solving the problem of restoration in finite-time under parameters uncertainties and unexpected load variations and (iii) challenge in optimising the operation of MGs in the presence of the power conversion losses terms have been reported in this chapter. A nonlinear islanded MG model, consisting of a set of DGs and loads was presented in Chapter 2 for designing SCs. Moreover, a mathematical model of an islanded MG was derived for providing operation control. In this model, the following components are considered: (a) energy storage units; (b) renewable energy sources, where the power infeed can be bounded, namely, if storage units are fully charged; and (c) conventional units that can be switched off, e.g., in times of high available renewable infeed.

In Chapter 3, to address challenge (i), two novel nonlinear robust distributed SC protocols were proposed, one for the frequency, and one for the voltage, capable of restoring, globally, and asymptotically, the DGs voltage and frequency to the desired value, and robust against multiple time-varying delays in the DGs's communications a class of parameter uncertainties and exogenous disturbances. Each SC consists of an integral sliding mode control term and a linear consensus scheme with adaptive gains. Robustness against model nonlinearities and uncertainties was achieved by means of the integral sliding mode control term embedded in both proposed SC protocols. Then, the global frequency and voltage restoration stability despite the communication delays were demonstrated through Lyapunov-Krasovskii analysis. Using Lyapunov-Krasovskii analysis led to derive the set of linear matrix inequalities that were a function of time-varying control gains. However, due to the construction of the adaptive control gains, it has been proven that there exists a constant control that ensures the asymptotic stability of the closed-loop system. Hence, a novel optimal distributed secondary voltage control was proposed in Chapter 4 to extend the proposed secondary voltage control in Chapter 3. Compared to the adaptive SC approach in Chapter 3, the local control gains Chapter in 4 were considered as constant values. Note that by considering the control gains as constant values, the LMIs obtained in the stability analysis, unlike Chapter 3, are not time-varying.

Therefore, given the delay bounds, and because of the stability conditions results that were a function of the controller gains, an optimization algorithm was proposed in order to find the optimal controller gains and estimate the maximal delay margin tolerated by the controlled system. Chapter 5 focussed on solving the frequency and voltage restoration problem in finite-time under the model uncertainties and disturbances. In this way, two novel distributed SC protocols for frequency and voltage were proposed based on the sliding-mode approach. Although this approach is not more realistic than the proposed SCs in Chapters 3 and 4 due to the absence of communication delays, it was proven that the DG's frequencies and voltages converge to the desired values in the finite time instead of asymptotic time under parameters uncertainties and unexpected load variations.

Using the mathematical model of an islanded MG in Chapter 2 and based on the generic MPC formulation and the nominal forecasts of load and available renewable infeed, in Chapter 6 a novel certainty equivalence operation control scheme with very high share of renewable energy sources was proposed to optimise the operation of MG systems. To make the MG model more realistic, the power conversion losses were considered by the quadratic functions in the dynamic of storage units. Moreover, to reduce the error in storage units state of charge prediction, the conversion losses functions was reformulated by the piecewise affine functions and included in the proposed controller.

7.2 Future research directions

The future research directions can be divided into two parts: (i) extension of sc approaches (ii) extension of operation schemes.

A possible extension for the current distributed SCs under commination delays is to remove the assumption of slowly varying delay. Another exciting extension will be targeted at relaxing the assumed restrictions on the communication topology by covering possibly switching gossip-based asynchronous communications. The next interesting extension would be to relax the non-convex optimization algorithm in Chapter 4 to convex ones and use traditional methods to solve the (convex) relaxed optimization problem. Another idea would be to design a distributed SC strategy that deals with both delays and finite time convergence. Other interesting lines of investigation that represents a natural continuation of this research are, the possibility to manage active loads, or exploit seamless distributed transfer strategies for the MG to switch from islanded to the grid-connected mode by means of local interactions among DGs.

One possible extension for the current operation control is to consider AC optimal power flow (OPF) problems which are more realistic than the widely used linearised DC power flow approximations. To solve the AC OPF problems, we intend to use a convex relaxation of the original problem which leads to a second-order cone program (SOCP) that can be solved by available commercial software. Different uncertainties could be included into the model. In the current operation control, only uncertain forecasts of load and available renewable infeed were considered. Hence, another possible step could be to extend the model by inducing uncertain storage dynamic and availability of power lines. Experimental validations are also one important future works, that will allow a performance assessment of the proposed techniques in a real scenario.

Bibliography

[1] Paul M Anderson and AA Fouad. *Power system control and stability*. John Wiley & Sons, 2003.

[2] Prabha Kundur, Neal J Balu, and Mark G Lauby. *Power system stability and control*. Vol. 7. McGraw-hill New York, 1994.

[3] Martin Pehnt. "Dynamic life cycle assessment (LCA) of renewable energy technologies". In: *Renewable energy* 31.1 (2006), pp. 55–71.

[4] Robert H Lasseter. "Microgrids". In: *2002 IEEE Power Engineering Society Winter Meeting. Conference Proceedings (Cat. No. 02CH37309)*. Vol. 1. IEEE. 2002, pp. 305–308.

[5] JA Peças Lopes, CL Moreira, and AG Madureira. "Defining control strategies for microgrids islanded operation". In: *IEEE Transactions on power systems* 21.2 (2006), pp. 916–924.

[6] N Hatziargyriou, H Asano, R Iravani, and C Marnay. *Microgrids. IEEE Power Energy Mag 5 (4): 78–94*. 2007.

[7] Faridaddin Katiraei, Mohammad Reza Iravani, and Peter W Lehn. "Microgrid autonomous operation during and subsequent to islanding process". In: *IEEE Transactions on power delivery* 20.1 (2005), pp. 248–257.

[8] Josep M Guerrero, Juan C Vasquez, José Matas, Luis García De Vicuña, and Miguel Castilla. "Hierarchical control of droop-controlled AC and DC microgrids—A general approach toward standardization". In: *IEEE Transactions on industrial electronics* 58.1 (2010), pp. 158–172.

[9] Josep M Guerrero, Mukul Chandorkar, Tzung-Lin Lee, and Poh Chiang Loh. "Advanced control architectures for intelligent microgrids—Part I: Decentralized and hierarchical control". In: *IEEE Transactions on Industrial Electronics* 60.4 (2012), pp. 1254–1262.

[10] Ali Bidram and Ali Davoudi. "Hierarchical structure of microgrids control system". In: *IEEE Transactions on Smart Grid* 3.4 (2012), pp. 1963–1976.

[11] Ali Mehrizi-Sani and Reza Iravani. "Potential-function based control of a microgrid in islanded and grid-connected modes". In: *IEEE Transactions on Power Systems* 25.4 (2010), pp. 1883–1891.

[12] Tine L Vandoorn, Juan C Vasquez, Jeroen De Kooning, Josep M Guerrero, and Lieven Vandevelde. "Microgrids: Hierarchical control and an overview of the control and reserve management strategies". In: *IEEE industrial electronics magazine* 7.4 (2013), pp. 42–55.

[13] Ali Bidram, Ali Davoudi, Frank L Lewis, and Shuzhi Sam Ge. "Distributed adaptive voltage control of inverter-based microgrids". In: *IEEE Transactions on Energy Conversion* 29.4 (2014), pp. 862–872.

[14] Alessandro Pilloni, Alessandro Pisano, and Elio Usai. "Robust finite-time frequency and voltage restoration of inverter-based microgrids via sliding-mode cooperative control". In: *IEEE Transactions on Industrial Electronics* 65.1 (2018), pp. 907–917.

[15] Joan Rocabert, Alvaro Luna, Frede Blaabjerg, and Pedro Rodriguez. "Control of power converters in AC microgrids". In: *IEEE transactions on power electronics* 27.11 (2012), pp. 4734–4749.

[16] Ajay Krishna, Christian A Hans, Johannes Schiffer, Jörg Raisch, and Thomas Kral. "Steady state evaluation of distributed secondary frequency control strategies for microgrids in the presence of clock drifts". In: *2017 25th Mediterranean Conference on Control and Automation (MED)*. IEEE. 2017, pp. 508–515.

[17] Fanghong Guo, Changyun Wen, Jianfeng Mao, and Yong-Duan Song. "Distributed economic dispatch for smart grids with random wind power". In: *IEEE Transactions on Smart Grid* 7.3 (2015), pp. 1572–1583.

[18] Farid Katiraei, Reza Iravani, Nikos Hatziargyriou, and Aris Dimeas. "Microgrids management". In: *IEEE power and energy magazine* 6.3 (2008), pp. 54–65.

[19] Dirk Lehmkuhl, Kurt Rohrig, Céline Trousseau, and Michel Vandenbergh. "Energy management system for Island grids". In: (2004).

[20] Alessandra Parisio, Evangelos Rikos, and Luigi Glielmo. "A model predictive control approach to microgrid operation optimization". In: *IEEE Transactions on Control Systems Technology* 22.5 (2014), pp. 1813–1827.

[21] Antonis G Tsikalakis and Nikos D Hatziargyriou. "Centralized control for optimizing microgrids operation". In: *2011 IEEE power and energy society general meeting*. IEEE. 2011, pp. 1–8.

[22] Ali Bidram and Ali Davoudi. "Hierarchical structure of microgrids control system". In: *IEEE Transactions on Smart Grid* 3.4 (2012), pp. 1963–1976.

[23] Josep M Guerrero, Mukul Chandorkar, Tzung-Lin Lee, and Poh Chiang Loh. "Advanced control architectures for intelligent microgrids—Part I: Decentralized and hierarchical control". In: *IEEE Transactions on Industrial Electronics* 60.4 (2012), pp. 1254–1262.

[24] JA Peças Lopes, CL Moreira, and AG Madureira. "Defining control strategies for microgrids islanded operation". In: *IEEE Transactions on power systems* 21.2 (2006), pp. 916–924.

[25] Gian Paolo Incremona, Michele Cucuzzella, Lalo Magni, and Antonella Ferrara. "MPC with sliding mode control for the energy management system of microgrids". In: *IFAC-PapersOnLine* 50.1 (2017), pp. 7397–7402.

[26] Michele Cucuzzella, Gian Paolo Incremona, and Antonella Ferrara. "Decentralized sliding mode control of islanded ac microgrids with arbitrary topology". In: *IEEE Transactions on Industrial Electronics* 64.8 (2017), pp. 6706–6713.

[27] Gian Paolo Incremona, Michele Cucuzzella, and Antonella Ferrara. "Adaptive suboptimal second-order sliding mode control for microgrids". In: *International Journal of Control* 89.9 (2016), pp. 1849–1867.

[28] Florian Dörfler, John W Simpson-Porco, and Francesco Bullo. "Breaking the hierarchy: Distributed control and economic optimality in microgrids". In: *IEEE Transactions on Control of Network Systems* 3.3 (2016), pp. 241–253.

[29] Sebastian Trip, Michele Cucuzzella, Claudio De Persis, Antonella Ferrara, and Jacquelien MA Scherpen. "Robust load frequency control of nonlinear power networks". In: *International Journal of Control* 93.2 (2020), pp. 346–359.

[30] Yousef Khayat, Mobin Naderi, Qobad Shafiee, Yazdan Batmani, Mohammad Fathi, Josep M Guerrero, and Hassan Bevrani. "Decentralized optimal frequency control in autonomous microgrids". In: *IEEE Transactions on Power Systems* 34.3 (2018), pp. 2345–2353.

[31] Juan M Rey, Pau Martí, Manel Velasco, Jaume Miret, and Miguel Castilla. "Secondary switched control with no communications for islanded microgrids". In: *IEEE Transactions on Industrial Electronics* 64.11 (2017), pp. 8534–8545.

[32] Yanbo Wang, Zhe Chen, Xiongfei Wang, Yanjun Tian, Yongdong Tan, and Chao Yang. "An estimator-based distributed voltage-predictive control strategy for AC islanded microgrids". In: *IEEE Transactions on Power Electronics* 30.7 (2015), pp. 3934–3951.

[33] Guannan Lou, Wei Gu, Liufang Wang, Bin Xu, Ming Wu, and Wanxing Sheng. "Decentralised secondary voltage and frequency control scheme for islanded microgrid based on adaptive state estimator". In: *IET Generation, Transmission & Distribution* 11.15 (2017), pp. 3683–3693.

[34] Wei Gu, Guannan Lou, Wen Tan, and Xiaodong Yuan. "A nonlinear state estimator-based decentralized secondary voltage control scheme for autonomous microgrids". In: *IEEE Transactions on Power Systems* 32.6 (2017), pp. 4794–4804.

[35] Martin Andreasson, Dimos V Dimarogonas, Henrik Sandberg, and Karl Henrik Johansson. "Distributed control of networked dynamical systems: Static feedback, integral action and consensus". In: *IEEE Transactions on Automatic Control* 59.7 (2014), pp. 1750–1764.

[36] Jiahu Qin, Qichao Ma, Yang Shi, and Long Wang. "Recent advances in consensus of multi-agent systems: A brief survey". In: *IEEE Transactions on Industrial Electronics* 64.6 (2016), pp. 4972–4983.

[37] Sebastian Trip, Michele Cucuzzella, Claudio De Persis, Arjan van der Schaft, and Antonella Ferrara. "Passivity-based design of sliding modes for optimal load frequency control". In: *IEEE Transactions on control systems technology* 27.5 (2018), pp. 1893–1906.

[38] Qobad Shafiee, Josep M Guerrero, and Juan C Vasquez. "Distributed secondary control for islanded microgrids—A novel approach". In: *IEEE Transactions on power electronics* 29.2 (2014), pp. 1018–1031.

[39] John W Simpson-Porco, Florian Dörfler, and Francesco Bullo. "Synchronization and power sharing for droop-controlled inverters in islanded microgrids". In: *Automatica* 49.9 (2013), pp. 2603–2611.

[40] Fanghong Guo, Changyun Wen, Jianfeng Mao, and Yong-Duan Song. "Distributed secondary voltage and frequency restoration control of droop-controlled inverter-based microgrids". In: *IEEE Transactions on industrial Electronics* 62.7 (2015), pp. 4355–4364.

[41] John W Simpson-Porco, Qobad Shafiee, Florian Dörfler, Juan C Vasquez, Josep M Guerrero, and Francesco Bullo. "Secondary frequency and voltage control of islanded microgrids via distributed averaging". In: *IEEE Transactions on Industrial Electronics* 62.11 (2015), pp. 7025–7038.

[42] Ali Bidram, Ali Davoudi, Frank L Lewis, and Zhihua Qu. "Secondary control of microgrids based on distributed cooperative control of multi-agent systems". In: *IET Generation, Transmission & Distribution* 7.8 (2013), pp. 822–831.

[43] Ali Bidram, Ali Davoudi, Frank L Lewis, and Josep M Guerrero. "Distributed cooperative secondary control of microgrids using feedback linearization". In: *IEEE Transactions on Power Systems* 28.3 (2013), pp. 3462–3470.

[44] Alberto Petrillo, Alessandro Salvi, Stefania Santini, and Antonio Saverio Valente. "Adaptive synchronization of linear multi-agent systems with time-varying multiple delays". In: *Journal of the Franklin Institute* 354.18 (2017), pp. 8586–8605.

[45] Ali Jadbabaie, Jie Lin, and A Stephen Morse. "Coordination of groups of mobile autonomous agents using nearest neighbor rules". In: *IEEE Transactions on automatic control* 48.6 (2003), pp. 988–1001.

[46] Fen Tang, Josep M Guerrero, Juan C Vasquez, Dan Wu, and Lexuan Meng. "Distributed active synchronization strategy for microgrid seamless reconnection to the grid under unbalance and harmonic distortion". In: *IEEE Transactions on Smart Grid* 6.6 (2015), pp. 2757–2769.

[47] John W Simpson-Porco, Florian Dörfler, and Francesco Bullo. "Voltage stabilization in microgrids via quadratic droop control". In: *IEEE Transactions on Automatic Control* 62.3 (2017), pp. 1239–1253.

[48] Qing-Chang Zhong. "Robust droop controller for accurate proportional load sharing among inverters operated in parallel". In: *IEEE Transactions on Industrial Electronics* 60.4 (2011), pp. 1281–1290.

[49] Johannes Schiffer, Thomas Seel, Jorg Raisch, and Tevfik Sezi. "Voltage stability and reactive power sharing in inverter-based microgrids with consensus-based distributed voltage control". In: *IEEE Transactions on Control Systems Technology* 24.1 (2016), pp. 96–109.

[50] Shichao Liu, Xiaoyu Wang, and Peter Xiaoping Liu. "Impact of communication delays on secondary frequency control in an islanded microgrid". In: *IEEE Transactions on Industrial Electronics* 62.4 (2015), pp. 2021–2031.

[51] Ernane Antonio Coelho, Dan Wu, Josep M Guerrero, Juan C Vasquez, Tomislav Dragicević, Cedomir Stefanović, and Petar Popovski. "Small-signal analysis of the microgrid secondary control considering a communication time delay". In: *IEEE Transactions on Industrial Electronics* 63.10 (2016), pp. 6257–6269.

[52] Jingang Lai, Xiaoqing Lu, and Xinghuo Yu. "Stochastic distributed frequency and load sharing control for microgrids with communication delays". In: *IEEE Systems Journal* 13.4 (2019), pp. 4269–4280.

[53] Yijing Xie and Zongli Lin. "Distributed event-triggered secondary voltage control for microgrids with time delay". In: *IEEE Transactions on Systems, Man, and Cybernetics: Systems* 49.8 (2019), pp. 1582–1591.

[54] Jingang Lai, Xiaoqing Lu, and Antonello Monti. "Distributed secondary voltage control for autonomous microgrids under additive measurement noises and time delays". In: *IET Generation, Transmission & Distribution* 13.14 (2019), pp. 2976–2985.

[55] Guannan Lou, Wei Gu, Xiaonan Lu, Yinliang Xu, and Haohao Hong. "Distributed Secondary Voltage Control in Islanded Microgrids With Consideration of Communication Network and Time Delays". In: *IEEE Transactions on Smart Grid* (2020).

[56] Amir Afshari, Mehdi Karrari, Hamid Reza Baghaee, and Gevork B Gharehpetian. "Resilient cooperative control of AC microgrids considering relative state-dependent noises and communication time-delays". In: *IET Renewable Power Generation* 14.8 (2020), pp. 1321–1331.

[57] Ali Bidram, Ali Davoudi, and Frank L Lewis. "Finite-time frequency synchronization in microgrids". In: *2014 IEEE Energy Conversion Congress and Exposition (ECCE)*. IEEE. 2014, pp. 2648–2654.

[58] Stanton T Cady, Alejandro D Domínguez-García, and Christoforos N Hadjicostis. "Finite-time approximate consensus and its application to distributed frequency regulation in islanded ac microgrids". In: *2015 48th Hawaii International Conference on System Sciences*. IEEE. 2015, pp. 2664–2670.

[59] Xiaoqing Lu, Xinghuo Yu, Jingang Lai, Yaonan Wang, and Josep M Guerrero. "A Novel Distributed Secondary Coordination Control Approach for Islanded Microgrids". In: *IEEE Transactions on Smart Grid* 9.4 (2018), pp. 2726–2740.

[60] Zicong Deng, Yinliang Xu, Hongbin Sun, and Xinwei Shen. "Distributed, bounded and finite-time convergence secondary frequency control in an autonomous microgrid". In: *IEEE Transactions on Smart Grid* 10.3 (2019), pp. 2776–2788.

[61] Xueqiang Shen, Haiqing Wang, Jian Li, Qingyu Su, and Lan Gao. "Distributed secondary voltage control of islanded microgrids based on RBF-neural-network sliding-mode technique". In: *IEEE Access* 7 (2019), pp. 65616–65623.

[62] Sonam Shrivastava and Bidyadhar Subudhi. "Robust Finite-Time Secondary Control Scheme for Islanded Microgrid with Nonlinear Dynamics and Uncertain Disturbances". In: *2019 IEEE 5th International Conference for Convergence in Technology (I2CT)*. IEEE. 2019, pp. 1–6.

[63] Makoto Kanagawa and Toshihiko Nakata. "Assessment of access to electricity and the socio-economic impacts in rural areas of developing countries". In: *Energy policy* 36.6 (2008), pp. 2016–2029.

[64] Changsong Chen, Shanxu Duan, Tong Cai, Bangyin Liu, and Gangwei Hu. "Smart energy management system for optimal microgrid economic operation". In: *IET renewable power generation* 5.3 (2011), pp. 258–267.

[65] E Barklund, Nagaraju Pogaku, Milan Prodanovic, C Hernandez-Aramburo, and Tim C Green. "Energy management in autonomous microgrid using stability-constrained droop control of inverters". In: *IEEE Transactions on Power Electronics* 23.5 (2008), pp. 2346–2352.

[66] Thillainathan Logenthiran and Dipti Srinivasan. "Short term generation scheduling of a microgrid". In: *TENCON 2009-2009 IEEE Region 10 Conference*. IEEE. 2009, pp. 1–6.

[67] Rodrigo Palma-Behnke, Carlos Benavides, Fernando Lanas, Bernardo Severino, Lorenzo Reyes, Jacqueline Llanos, and Doris Sáez. "A microgrid energy management system based on the rolling horizon strategy". In: *IEEE Transactions on smart grid* 4.2 (2013), pp. 996–1006.

[68] Benjamin Heymann, J Frédéric Bonnans, Pierre Martinon, Francisco J Silva, Fernando Lanas, and Guillermo Jiménez-Estévez. "Continuous optimal control approaches to microgrid energy management". In: *Energy Systems* 9.1 (2018), pp. 59–77.

[69] Ebony Mayhorn, Karanjit Kalsi, Marcelo Elizondo, Wei Zhang, Shuai Lu, Nader Samaan, and Karen Butler-Purry. "Optimal control of distributed energy resources using model predictive control". In: *2012 IEEE power and energy society general meeting*. IEEE. 2012, pp. 1–8.

[70] Daniel E Olivares, Claudio A Cañizares, and Mehrdad Kazerani. "A centralized energy management system for isolated microgrids". In: *IEEE Transactions on smart grid* 5.4 (2014), pp. 1864–1875.

[71] Christian A Hans, Vladislav Nenchev, Jörg Raisch, and Carsten Reincke-Collon. "Minimax model predictive operation control of microgrids". In: *IFAC Proceedings Volumes* 47.3 (2014), pp. 10287–10292.

[72] Christian A Hans, Pantelis Sopasakis, Jörg Raisch, Carsten Reincke-Collon, and Panagiotis Patrinos. "Risk-averse model predictive operation control of islanded microgrids". In: *IEEE Transactions on Control Systems Technology* (2019).

[73] Alessandro Pilloni, Mauro Franceschelli, Alessandro Pisano, and Elio Usai. "Sliding mode based robustification of consensus and distributed optimization control protocols". In: *IEEE Transactions on Automatic Control* (2020).

[74] Min Wu, Yong He, and Jin-Hua She. *Stability analysis and robust control of time-delay systems*. Vol. 22. Springer, 2010.

[75] Lin Shi, Hong Zhu, Shouming Zhong, Yong Zeng, and Jun Cheng. "Synchronization for time-varying complex networks based on control". In: *Journal of Computational and Applied Mathematics* 301 (2016), pp. 178–187.

[76] Jeremy G VanAntwerp and Richard D Braatz. "A tutorial on linear and bilinear matrix inequalities". In: *Journal of process control* 10.4 (2000), pp. 363–385.

[77] Sanjay P Bhat and Dennis S Bernstein. "Finite-time stability of homogeneous systems". In: *Proceedings of the 1997 American control conference (Cat. No. 97CH36041)*. Vol. 4. IEEE. 1997, pp. 2513–2514.

[78] Sanjay P Bhat and Dennis S Bernstein. "Finite-time stability of continuous autonomous systems". In: *SIAM Journal on Control and Optimization* 38.3 (2000), pp. 751–766.

[79] Haibo Du, Guanghui Wen, Guanrong Chen, Jinde Cao, and Fuad E Alsaadi. "A distributed finite-time consensus algorithm for higher-order leaderless and leader-following multiagent systems". In: *IEEE Transactions on Systems, Man, and Cybernetics: Systems* 47.7 (2017), pp. 1625–1634.

[80] Huanhai Xin, Zhihua Qu, John Seuss, and Ali Maknouninejad. "A self-organizing strategy for power flow control of photovoltaic generators in a distribution network". In: *IEEE Transactions on Power Systems* 26.3 (2010), pp. 1462–1473.

[81] Jianxing Liu, Sergio Vazquez, Ligang Wu, Abraham Marquez, Huijun Gao, and Leopoldo G Franquelo. "Extended state observer-based sliding-mode control for three-phase power converters". In: *IEEE Transactions on Industrial Electronics* 64.1 (2016), pp. 22–31.

[82] Alessandro Pilloni, Alessandro Pisano, and Elio Usai. "Voltage restoration of islanded microgrids via cooperative second-order sliding mode control". In: *IFAC-PapersOnLine* 50.1 (2017), pp. 9637–9642.

[83] Abdullah Bokhari, Ali Alkan, Rasim Dogan, Marc Diaz-Aguiló, Francisco De Leon, Dariusz Czarkowski, Zivan Zabar, Leo Birenbaum, Anthony Noel, and Resk Ebrahem Uosef. "Experimental determination of the ZIP coefficients for modern residential, commercial, and industrial loads". In: *IEEE Transactions on Power Delivery* 29.3 (2014), pp. 1372–1381.

[84] Kenan Hatipoglu, Ismail Fidan, and Ghadir Radman. "Investigating effect of voltage changes on static zip load model in a microgrid environment". In: *2012 North American Power Symposium (NAPS)*. IEEE. 2012, pp. 1–5.

[85] L. Powell. "Power system load flow analysis". In: *McGraw-Hill, New York*. 2005, pp. 1–5.

[86] He Renmu, Ma Jin, and David J Hill. "Composite load modeling via measurement approach". In: *IEEE Transactions on power systems* 21.2 (2006), pp. 663–672.

[87] José R Martí, Hamed Ahmadi, and Lincol Bashualdo. "Linear power-flow formulation based on a voltage-dependent load model". In: *IEEE Transactions on Power Delivery* 28.3 (2013), pp. 1682–1690.

[88] Zhiwen Yu, Qian Ai, Jinxia Gong, and Longjian Piao. "A novel secondary control for microgrid based on synergetic control of multi-agent system". In: *Energies* 9.4 (2016), p. 243.

[89] Xiaoqing Lu, Xinghuo Yu, Jingang Lai, Yaonan Wang, and Josep M Guerrero. "A novel distributed secondary coordination control approach for islanded microgrids". In: *IEEE Transactions on Smart Grid* 9.4 (2016), pp. 2726–2740.

[90] Tung-Lam Nguyen, Efren Guillo-Sansano, Mazheruddin H Syed, Van-Hoa Nguyen, Steven M Blair, Luis Reguera, Quoc-Tuan Tran, Raphael Caire, Graeme M Burt, Catalin Gavriluta, et al. "Multi-agent system with plug and play feature for distributed secondary control in microgrid—Controller and power hardware-in-the-loop Implementation". In: *Energies* 11.12 (2018), p. 3253.

[91] Ahmed S Alsafran and Malcolm W Daniels. "Consensus Control for Reactive Power Sharing Using an Adaptive Virtual Impedance Approach". In: *Energies* 13.8 (2020), p. 2026.

[92] Ali Bidram, Ali Davoudi, Frank L Lewis, and Josep M Guerrero. "Distributed cooperative secondary control of microgrids using feedback linearization". In: *IEEE Transactions on Power Systems* 28.3 (2013), pp. 3462–3470.

[93] Alberto Petrillo, Alessandro Salvi, Stefania Santini, and Antonio Saverio Valente. "Adaptive synchronization of linear multi-agent systems with time-varying multiple delays". In: *Journal of the Franklin Institute* 354.18 (2017), pp. 8586–8605.

[94] Alberto Petrillo, Alessandro Salvi, Stefania Santini, and Antonio Saverio Valente. "Adaptive multi-agents synchronization for collaborative driving of autonomous vehicles with multiple communication delays". In: *Transportation research part C: emerging technologies* 86 (2018), pp. 372–392.

[95] Martin Andreasson, Dimos V Dimarogonas, Henrik Sandberg, and Karl Henrik Johansson. "Distributed control of networked dynamical systems: Static feedback, integral action and consensus". In: *IEEE Transactions on Automatic Control* 59.7 (2014), pp. 1750–1764.

[96] F. Luo Y.; Effenberger. "Timestamp Provisioning in IEEE 802.3. IEEE 802 LAN/MAN Standards Committee". In: *www.ieee802.org/3/timeadhoc/* (2009).

[97] Vadim Utkin and Jingxin Shi. "Integral sliding mode in systems operating under uncertainty conditions". In: *Proceedings of 35th IEEE conference on decision and control*. Vol. 4. IEEE. 1996, pp. 4591–4596.

[98] Vladimir Kharitonov. *Time-delay systems: Lyapunov functionals and matrices*. Springer Science & Business Media, 2012.

[99] Emilia Fridman and Yury Orlov. "Exponential stability of linear distributed parameter systems with time-varying delays". In: *Automatica* 45.1 (2009), pp. 194–201.

[100] Arie Levant. "Higher-order sliding modes, differentiation and output-feedback control". In: *International journal of Control* 76.9-10 (2003), pp. 924–941.

[101] Hassan Saadaoui, Noureddine Manamanni, Mohamed Djemai, Jean-Pierre Barbot, and Thierry Floquet. "Exact differentiation and sliding mode observers for switched Lagrangian systems". In: *Nonlinear Analysis: Theory, Methods & Applications* 65.5 (2006), pp. 1050–1069.

[102] Thierry Floquet and Jean-Pierre Barbot. "Super twisting algorithm-based step-by-step sliding mode observers for nonlinear systems with unknown inputs". In: *International journal of systems science* 38.10 (2007), pp. 803–815.

[103] Arie Levant. "Robust exact differentiation via sliding mode technique". In: *automatica* 34.3 (1998), pp. 379–384.

[104] Giorgio Bartolini, Alessandro Pisano, and Elio Usai. "First and second derivative estimation by sliding mode technique". In: *J. of Signal Processing* 4.2 (2000), pp. 167–176.

[105] Milad Gholami, Alessandro Pilloni, Alessandro Pisano, Zohreh Alzahra Sanai Dashti, and Elio Usai. "Robust consensus-based secondary voltage restoration of inverter-based islanded microgrids with delayed communications". In: *2018 IEEE Conference on Decision and Control (CDC)*. IEEE. 2018, pp. 811–816.

[106] Milad Gholami, Alessandro Pilloni, Alessandro Pisano, and Elio Usai. "Robust Distributed Secondary Voltage Restoration Control of AC Microgrids under Multiple Communication Delays". In: *Energies* 14.4 (2021), p. 1165.

[107] Milad Gholami, Alessandro Pisano, and Elio Usai. "Robust Distributed Optimal Secondary Voltage Control in Islanded Microgrids with Time-Varying Multiple Delays". In: *2020 IEEE 21st Workshop on Control and Modeling for Power Electronics (COMPEL)*. IEEE. 2020, pp. 1–8.

[108] Yong Feng, Fengling Han, and Xinghuo Yu. "Chattering free full-order sliding-mode control". In: *Automatica* 50.4 (2014), pp. 1310–1314.

[109] Johannes Schiffer, Romeo Ortega, Alessandro Astolfi, Jörg Raisch, and Tevfik Sezi. "Conditions for stability of droop-controlled inverter-based microgrids". In: *Automatica* 50.10 (2014), pp. 2457–2469.

[110] Yongcan Cao, Wei Ren, and Ziyang Meng. "Decentralized finite-time sliding mode estimators and their applications in decentralized finite-time formation tracking". In: *Systems & Control Letters* 59.9 (2010), pp. 522–529.

[111] Milad Gholami, Alessandro Pisano, Seyed Mohsen Hosseini, and Elio Usai. "Distributed finite-time secondary control of islanded microgrids by coupled sliding-mode technique". In: *2020 25th IEEE International Conference on Emerging Technologies and Factory Automation (ETFA)*. Vol. 1. IEEE. 2020, pp. 454–461.

[112] Milad Gholami, Masoud Hajimani, Zohreh Al Zahra Sanai Dashti, and Alessandro Pisano. "Distributed Robust Finite-time Non-linear Consensus Protocol for High-order Multi-agent Systems via Coupled Sliding Mode Control". In: *2019 6th International Conference on Control, Instrumentation and Automation (ICCIA)*. IEEE. 2019, pp. 1–6.

[113] Francesco Borrelli, Alberto Bemporad, and Manfred Morari. *Predictive control for linear and hybrid systems*. Cambridge University Press, 2017.

[114] Carlos E Garcia, David M Prett, and Manfred Morari. "Model predictive control: theory and practice—a survey". In: *Automatica* 25.3 (1989), pp. 335–348.

[115] Manfred Morari and Jay H Lee. "Model predictive control: past, present and future". In: *Computers & Chemical Engineering* 23.4-5 (1999), pp. 667–682.

[116] S Joe Qin and Thomas A Badgwell. "A survey of industrial model predictive control technology". In: *Control engineering practice* 11.7 (2003), pp. 733–764.

[117] Frank Allgöwer, Thomas A Badgwell, Joe S Qin, James B Rawlings, and Steven J Wright. "Nonlinear predictive control and moving horizon estimation—an introductory overview". In: *Advances in control*. Springer, 1999, pp. 391–449.

[118] Frank Allgöwer and Alex Zheng. *Nonlinear model predictive control*. Vol. 26. Birkhäuser, 2012.

[119] Jan Marian Maciejowski. *Predictive control: with constraints*. Pearson education, 2002.

[120] DQ Mayne. *Model Predictive Control Theory and Design*. 1999.

[121] Ionela Prodan and Enrico Zio. "A model predictive control framework for reliable microgrid energy management". In: *International Journal of Electrical Power & Energy Systems* 61 (2014), pp. 399–409.

[122] Christian A Hans, Pantelis Sopasakis, Alberto Bemporad, Jörg Raisch, and Carsten Reincke-Collon. "Scenario-based model predictive operation control of islanded microgrids". In: *2015 54th IEEE conference on decision and control (CDC)*. IEEE. 2015, pp. 3272–3277.

[123] Ajay Krishna, Christian A Hans, Johannes Schiffer, Jörg Raisch, and Thomas Kral. "Steady state evaluation of distributed secondary frequency control strategies for microgrids in the presence of clock drifts". In: *MED*. 2017.

[124] Johannes Schiffer, Christian A Hans, Thomas Kral, Romeo Ortega, and Jorg Raisch. "Modelling, analysis and experimental validation of clock drift effects in low-inertia power systems". In: *IEEE Trans. Ind. Electron.* 64.7 (2017), pp. 5942–5951.

[125] C. A. Hans, P. Sopasakis, J. Raisch, C. Reincke-Collon, and P. Patrinos. "Risk-Averse Model Predictive Operation Control of Islanded Microgrids". In: *IEEE Transactions on Control Systems Technology* (2019), pp. 1–16.

[126] A. Bemporad and M. Morari. "Control of systems integrating logic, dynamics, and constraints". In: *Automatica* 35.3 (1999), pp. 407–427.

[127] Konrad Purchala, Leonardo Meeus, Daniel Van Dommelen, and Ronnie Belmans. "Usefulness of DC power flow for active power flow analysis". In: *IEEE Power Engineering Society General Meeting, 2005*. IEEE. 2005, pp. 454–459.

[128] Christian A Hans, Philipp Braun, Jörg Raisch, Lars Grüne, and Carsten Reincke-Collon. "Hierarchical distributed model predictive control of interconnected microgrids". In: *IEEE Transactions on Sustainable Energy* 10.1 (2018), pp. 407–416.

[129] C. A. Hans, P. Sopasakis, A. Bemporad, J. Raisch, and C. Reincke-Collon. "Scenario-Based Model Predictive Operation Control of Islanded Microgrids". In: *IEEE CDC*. 2015.

[130] Marijana Živić Đurović, Aleksandar Milačić, and Marko Kršulja. "A Simplified Model of Quadratic Cost Function for Thermal Generators". In: *Ann. DAAAM 2012 Proc. 23 Int. DAAAM Symp.* 23.1 (2012), pp. 25–28.